Masters Theses   Graduate School

5-2013

Conductive Textiles and their use in Combat Wound Detection, Sensing, and Localization Applications

Stephen A. Holland
shollan6@utk.edu

Recommended Citation

To the Graduate Council:

I am submitting herewith a thesis written by Stephen A. Holland entitled "Conductive Textiles and their use in Combat Wound Detection, Sensing, and Localization Applications." I have examined the final electronic copy of this thesis for form and content and recommend that it be accepted in partial fulfillment of the requirements for the degree of Master of Science, with a major in Electrical Engineering.

<div align="right">

Aly E. Fathy, Major Professor

</div>

We have read this thesis and recommend its acceptance:

Benjamin J. Blalock, Jeremy H. Holleman

<div align="right">

Accepted for the Council:
<u>Dixie L. Thompson</u>

Vice Provost and Dean of the Graduate School

</div>

(Original signatures are on file with official student records.)

CONDUCTIVE TEXTILES AND THEIR USE IN COMBAT WOUND DETECTION, SENSING, AND LOCALIZATION APPLICATIONS

A Thesis Presented for the
Master of Science
Degree
The University of Tennessee, Knoxville

Stephen A. Holland
May 2013

ACKNOWLEDGMENTS

I would like to extend my deepest gratitude to my advisor, Dr. Aly Fathy, who began working with me as an undergraduate and helped transform me into a researcher. He willingly brought me into the exciting realm of microwave technologies and allowed me to combine his area of expertise with other exciting advancements in electrical engineering. He has helped me understand the importance of balance, not only in work but also in life. He helped me maintain my focus while I juggled the completion of numerous, concurrent research activities.

The Safeguards and Security Technology Group at Oak Ridge National Laboratory (ORNL) provided the original motivation and opportunity for me to pursue this work for my graduate studies through a project setup with the University of Tennessee, Knoxville. Through ORNL, I was given the opportunity of leading a research effort to develop systems that utilize conductive fabrics for nuclear safeguards and security applications. I would like to thank Chris Pickett, group leader of the Safeguards and Security Technology Group, for his guidance and direction. Chris and Jim Radle worked closely with our government sponsor, the National Nuclear Security Administration's Office of Nuclear Verification (NA-243), to ensure our research efforts met the expectations and mission of NA-243. Additionally, I would like to thank my mentor, Dr. Michael Kuhn, and Nathan Rowe for guiding me as I worked to develop a sensing method for conductive textiles that allows the distributed resistance to be measured and the location of tamper or penetration determined. They worked with me to ensure we developed a robust sensing system and obtained useful, real-time

experimental results. I would also like to thank Cody Mahan for his assistance while he completed a summer internship at ORNL.

Additionally, I extend sincere appreciation to the microwave and antenna group at the University of Tennessee, Knoxville. My thanks go to Dounia Baiya for helping with the textile antenna designs and to Essam Elkhouly for agreeing to test the completed antennas on his indoor localization system. I would also like to thank to the group's graduate researchers for their support and encouragement. The ideas and challenges presented by each of my mentors and peers throughout this research have allowed me to develop useful research for various applications including combat wound detection and localization.

ABSTRACT

Conductive textiles, originally used for electromagnetic shielding purposes, have recently been utilized in body area network applications as fabric antennas and distributed sensors used to document and analyze kinematic movement, health vital signs, or haptic interactions. This thesis investigates the potential for using conductive textiles as a distributed sensor and integrated communication system component for use in combat wound detection, sensing, and localization applications. The goal of these proof-of-concept experiments is to provide a basis for robust system development which can expedite and direct the medical response team in the field. The combat wound detection system would have the capability of predicting the presence and location of cuts or tears within the conductive fabric as a realization of bullet or shrapnel penetration. Collected data, along with health vitals gathered from additional sensors, will then be wirelessly transmitted via integrated communication system components, to the appropriate medical response team.

A distributed sensing method is developed to accurately predict the location and presence of textile penetrations. This method employs a Wheatstone bridge and multiplexing circuitry to probe a resistor network. Localized changes in resistance illustrate the presence and approximate location of cuts within the conductive textile. Additionally, this thesis builds upon manually defined textile antennas presented in literature by employing a laser cutting system to accurately define antenna dimensions. With this technique, a variety of antennas are developed for various purposes including large data transmission as would be expected from multi-sensor system integration. The

fabrication technique also illustrates multilayer antenna development. To confirm simulation results, electrical parameters are extracted using a single-frequency resonance method. These parameters are used in the simulation and design of single-element and two-element wideband slot antennas as well as the design of a wideband monopole antenna. The monopole antenna is introduced to an indoor ultra-wideband (UWB) localization system to illustrate the capability of pinpointing the wearer of textile antennas for localization applications. A cavity-backed dog-bone slot antenna is developed to establish the ability to incorporate conductive vias by sewing conductive thread. This technique can be easily extrapolated to the development of textile substrate integrated waveguide (SIW) technologies.

TABLE OF CONTENTS

LIST OF TABLES

LIST OF FIGURES

CHAPTER I: Introduction and Motivation

Security is a vital part of today's world. Oak Ridge National Laboratory, the largest Department of Energy laboratory, is charged with enhancing global, national, and homeland security. Within this charge lies the Nuclear Security and Isotope Technology Division under the leadership of Dr. Alan Icenhour. The purpose of this division is to design and implement science and technology solutions for numerous areas, including but not limited to nonproliferation, safeguards and threat reduction. Within this division lies the Safeguards and Security Technology Group in which the research in this thesis was conducted in collaboration with the University of Tennessee, Knoxville. This group, headed by Chris Pickett, is focused on developing and applying safeguards and security technologies to improve the effectiveness and efficiency of proliferation prevention systems to enhance U.S. national security.

The Safeguards and Security Technology Group possesses a number of state-of-the-art laboratories geared towards accomplishing the goals mentioned above. These include the Containment and Surveillance Systems Laboratory, the Safeguards Laboratory, the Radiation Inspection Laboratory and the Security Science Field Laboratory. Each of these labs meets the goals of the group in different ways. The Containment and Surveillance Systems Laboratory, for example, implements tracking systems, develops and deploys security systems, creates active tamper indicating devices and performs vulnerability analysis on these devices, works with unattended remote monitoring systems employing both wired and wireless sensors. The Safeguards Laboratory has programs with training and international outreach which

teach nondestructive assay measurement techniques, equipment evaluation standards, and integrated safeguards methodologies. The research performed in the Radiation Inspection laboratory is geared towards the detection of radiation at ports and roadways with advanced portal monitoring systems. Lastly, the Security Science Field Laboratory evaluates various security technologies in both indoor and outdoor environments in addition to system design, test and evaluation.

My work at Oak Ridge National Laboratory was focused within the Containment and Surveillance Systems Laboratory. This lab has many capabilities as mentioned above and conducts various research and development projects to meet missions within the Department of Energy. Some notable recent advancements made in this regard under the direction of Chris Pickett and other personnel within the Safeguards and Security Technology group (e.g., Michael Kuhn, Nathan Rowe, Brad Stinson, Jim Younkin) include: an analysis of radio-frequency devices for safeguards [1], employment of ultra wideband systems for active tagging and tracking in secure environments [2], use of inductive communication technology as a means to inventory and manage weapons and related assets [3], and development of an automated vault inventory system for special assets which can be continuously monitored [4]. Each of these research solutions stems from the overarching charge of the Safeguards and Security Technology Group. My research as a graduate student within this group dealt with evaluating conductive textile materials for novel applications including nuclear safeguards, containment and surveillance, and combat wound detection systems.

Introduction to Combat Wound Detection

Combat wound detection systems are of paramount importance in ensuring maximal safety and minimized medical response time for deployed soldiers. The development of these systems, ideally, will integrate traditional health vital measurements with bullet penetration localization schemes to provide the maximum amount of useful information to medical staff. This information can be appropriately characterized to ensure a quick, effective medical response. A number of crucial requirements surround the development of combat wound detection systems. First, they must be lightweight, flexible and durable so that they do not hamper the field deployed soldiers. Second, they must combine multiple metrics to provide, with reasonable certainty, information as to the health and safety of the soldier. Lastly, these systems must reliably transmit the collected data to the appropriate medical staff.

Numerous options exist for the development of such systems. Each has its own attributes that make it worthy of selection. However, key components also rule out the use of some technologies. The most obvious solution is to employ a variety of off-the-shelf wireless sensors to measure vital signs such as pH, blood pressure, heart rate, temperature and respiration rate as well as accelerometers and pressure sensors to measure motion, proximity and haptic interactions. The drawback to this solution is the difficulty in combining each of these different platforms to a single, easy-to-implement solution for field deployment. It would be a nuisance to require a soldier to wear a number of different sensors to measure each of these vital signs mentioned.

Instead, integration into a unified platform promises success. A potential medium to harbor this integration is the use of conductive textiles. These textiles offer a flexible, lightweight and durable solution to combat wound detection systems as they allow for easy incorporation of fabric-based sensors as well as discrete sensors. Numerous sensor topologies have been previously developed and can be implemented within these textile systems to measure a number of biometrics. These include a wireless blood pressure monitoring system [5], a wireless oximeter 6], an integrated cardiac, tilt, respiratory, and temperature monitoring system [7], a wireless electroencephalography (EEG) system [8], a wireless electrocardiography (ECG) system [9], and a wireless gamma radiation detector [10]. System development for sensor integration has also been an area of recent development. FIT system is a wearable armband that includes a 3-D accelerometer, temperature sensor, sweat sensor, and radiated heat sensor [11] while the Basis Band is a wearable watch that includes a heart rate sensor, a galvanic sweat sensor, a 3-D accelerometer, and temperature sensor [12]. A visualization of some sensors being incorporated into a soldier's standard issue protective vest is illustrated in Figure 1. The electrical connections established between each of these sensors and a data acquisition unit can be achieved through the conductive textile.

In addition to measuring and tracking a number of health vital signs, combat wound detection systems are also required to accurately detect the presence of bullet penetration. Knowing the time of impact, the number of penetrations and the location of penetrations in addition to numerous vital signs will allow medical staff to quickly and accurately respond to field deployed soldiers. This response may come in to form of
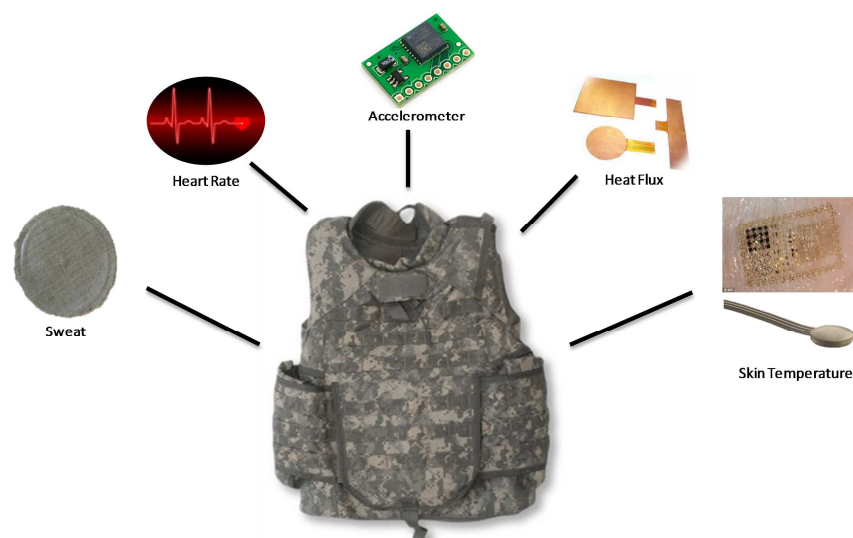
Figure 1: A variety of sensors for integration into a combat wound detection system.

accurate instructions for field dressing a wound or by sending a rapid response medical team to perform injury countermeasures. Conductive textiles can also be implemented to meet this requirement of combat wound detection systems. Using these textiles, a fabric-based sensor can be developed to accurately detect and localize the penetration. An example of this sensing capability is illustrated in Figure 2.

Conductive Textile Fabrication

A wide variety of conductive textiles exist for a number of different applications. Among these are the use of conductive textiles for shielding, sensing, communication systems and computation applications. Each of these applications poses different requirements for the conductive textile. Shielding, for example, requires the textile to be flexible, durable and easily configurable to enclose various shapes. Additionally, these textiles
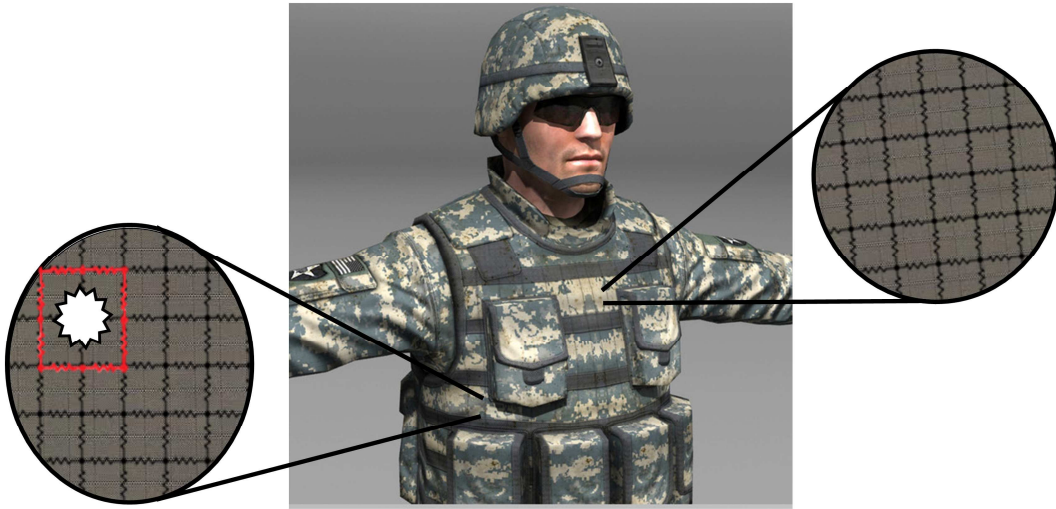
Figure 2: Illustration of fabric-based sensor to detect and localize cuts and tears achieved with conductive textile material.

must offer sufficient radio frequency shielding so as to block the penetration of unwanted electromagnetic interference. Sensing methods, on the other hand, require conductive textiles capable of producing detectable data for specific uses. In other cases, such as in communication systems, highly conductive textiles are necessary to ensure accurate data transmission is achieved with minimal losses. Computation, too, requires conductive textile properties to provide accurate methods for performed the computation analysis.

In each of the applications listed, different conductive textile properties are required for successful implementation. These various textiles can be created through a variety of methods stemming from two distinct ideologies. Conductive textiles can be made of woven metal threads or can be formed through a process known as metallization. In comparison, the metallized textiles are much more durable and flexible

than their metal thread counterparts. Depending on the weave pattern, the metal thread in non-metallized textiles can sever and render the entire system useless. This would likely occur if the same thread was run throughout the entire cloth. Zysset [13] presents a technique whereby individual metal threads can be woven in specific patterns such that electronic functionality can be achieved at the yarn level. Conductive thread is woven in the warp direction and plastic fibers in the weft direction of an existing fabric. The intersection of conductive thread and plastic fibers represents contact points that can be used as the insertion point for sensors and other integrated circuits. Depending on the type of conductive thread and plastic fibers used, the circuits can be attached with conductive epoxy or solder. An example of Zysset's fabric structure is shown in Figure 3.
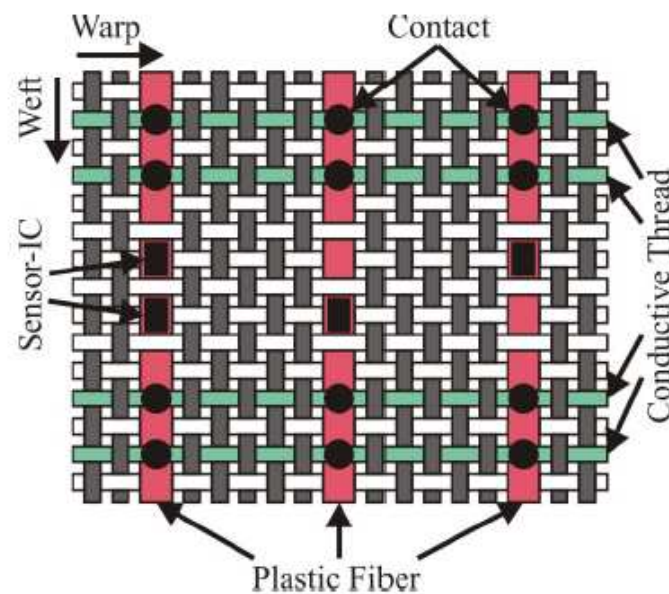
Figure 3: Fabric structure with woven conductive threads for body area network applications [13].

Metallization Process

In addition to weaving individual threads into a fabric, conductive textiles can be created through a process known as metallization. Metallization is a process in which a fabric or some other solid can be coated with a thin layer of metal. Different materials can be coated through various metallization techniques. Metallization of fabric can occur on two scales; either the individual thread can be metallized prior to being woven or a finished fabric can be metalized to coat the entire surface as one.

Four metallization techniques are common: vacuum deposition, ion plating, electroplating, and electroless plating. The most common techniques used to create conductive textiles are electroplating, also known as electrodeposition, and electroless plating. Electroplating is a process that utilizes electrical current to deposit a layer of metal particles on a material. Metals such as alloys, chromium, copper, gold, nickel and silver can be deposited on fabric surfaces by using the electroplating process. An example electroplating system is shown in Figure 4. In this system, the sample material is connected to the cathode while the anode contains the metal to be deposited on the fabric. In the presence of an electrical current, metallic ions travel through the plating solution and are deposited on the fabric material. [14]

A thorough description of the other common metallization technique, electroless plating, is presented in [14]. Electroless plating is "a non-galvanic technique that involves several simultaneous chemical reactions in an aqueous solution occurring without the use of external electric current" [14]. Ionization occurs when hydrogen is released by a reducing agent and produces a negative charge on the surface of the

material following oxidization. This method enables the metal coating of non-conductive textile materials. A uniform metallic layer can be achieved with this method due to the lack of an electric field. This technique is commonly used to bond a metallic nickel base layer to a textile prior to recoating with a more conductive metal such as silver or gold. Little and his team [15] show the capability of metallizing Kevlar fibers with gold using an electroplating method as well as an electroless method. They encountered inconsistencies when comparing these two methods. These differences are determined to be likely results of challenges arising from the original nickel coating achieved with the electroless plating technique rather than the electroplating method. [15] Many commercially available conductive textiles are created through this or a similar metallization process.

One challenge with conductive textile fabrication is ensuring an even coating of
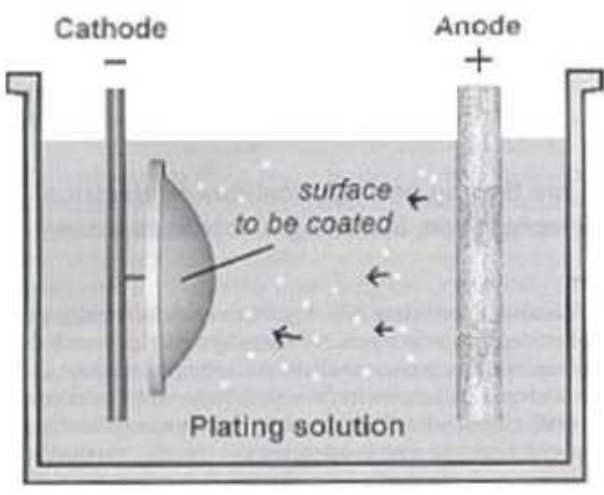
Figure 4: Electroplating (electrodeposition) technique that could be used to metallize a fabric [4].

the fabric. This is a crucial parameter as uniformity of the metallization becomes paramount in sensor and communication system component design. Figure 5 depicts a conductive textile sample under intense magnification. This image shows the capability of the metallization process to evenly coat all parts of the textile providing uniform conductivity throughout.

Many vendors market conductive textiles. A few of these vendors include LessEMF.com, Swift Textile Metalizing, LLC, Marktek, Inc., Shieldex, and Metal Textiles Corporation. Each of these companies mainly advertises the use of conductive textiles for shielding applications. A number of potential conductive textiles can be found in the conductive textile tables in the Appendix of this thesis. These tables compare various properties of conductive textiles based on vendor such as, fabric type, fabric thickness, metallic coating and shielding effectiveness. Figure 6 illustrates a wide variety of conductive textiles that can be purchased.
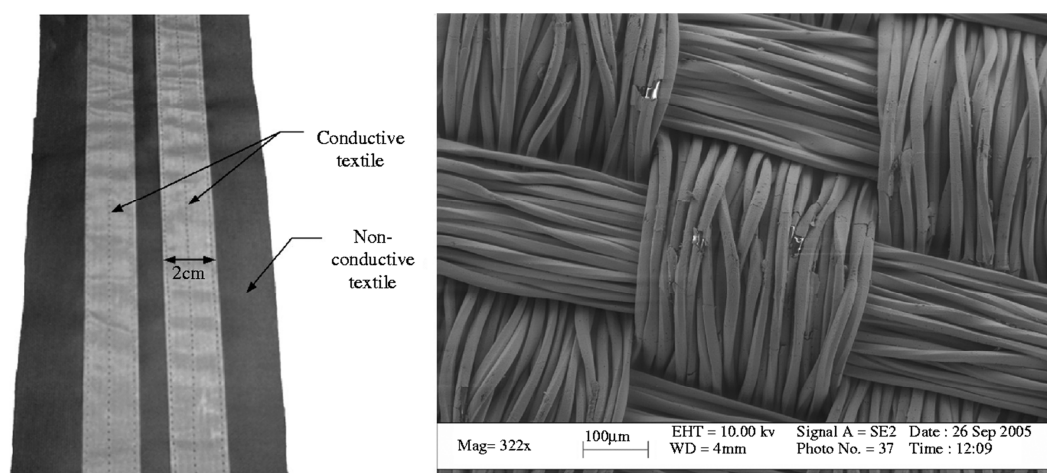
Figure 5: 322x Magnification of Conductive Textile. [16]

Figure 6: Numerous varieties of conductive textiles. [17]

Organization of the Thesis

Combat wound detection systems rely on two main pillars for success. First, data must be accurately and quickly obtained to discern whether medical staff should be alerted to a situation. Second, in the event of a situation, the appropriate health vital data needs to be accurately transmitted to medical staff so they can make an educated decision on how to proceed. To meet these requirements, this thesis further investigates the implementation of conductive textiles in both sensing and communication systems. Chapter II discusses the current state-of-the-art in the use of conductive textiles for both sensing and communication applications. The subsequent sections of this thesis combat the challenges determined by the literature review of Chapter II. Chapter III discusses the materials used during the completion of this research. This includes the

textile samples as well as the electrical characterization of the samples and subsequent details of the fabrication process. Chapter IV follows the development of accurate simulation models and experimental testing of fabric-based sensors for use in combat wound detection scenarios. This application looks for changes in localized resistance of the conductive fabric to determine the location of penetration within a textile sample. Simulation models were developed using MATLAB to aid in the characterization of penetration indicating events due to a change in resistance. These models portray the conductive fabric as a large grid of discrete resistors. Penetration is detectable by measuring and recording the change in point-to-point resistance of this grid. The location of penetration is indicated through a graphical representation of the textile surface. The results of the simulation models are discussed in detail and compared with measured results from two generations of the distributed fabric-based sensing system. The first-generation sensing system verifies the accuracy of the simulation model by collecting experimental data using a LabView data acquisition system. The results suggest good agreement and show cause for further, more robust development of this sensing technique. A second-generation penetration detection system is developed and presented with experimental verification.

Chapter V analyzes the alternate applications for conductive textiles presented in this thesis; a medium for discrete sensor integration as well as employment as a component in a communication system. A number of sensors are described which can be easily implemented using the capabilities of conductive textiles. RF characterization of fabric samples is performed using resonance techniques at a single frequency to

determine the electrical properties. Using this characterization, antennas are designed, fabricated using laser-precision and tested based on design specifications. Via implementation in textiles is explored and the potential for textile substrate integrated waveguides is discussed. The accuracy and potential use for the textile antennas is verified through experimentation. Chapter VI discusses the potential for future work entailing the use of conductive textiles for combat wound detection and localization systems and Chapter VII offers conclusions.

CHAPTER II: Literature Review

The applications of conductive textiles have traditionally been in the areas of shielding, sensing, communication and computation. For use in combat wound detection systems, this thesis investigates the potential for using conductive textiles as both a sensing device as well as a communication system component. This chapter attempts to corral the copious research performed in this expanding area and delineate between research utilizing the textiles as a sensing device and that which employs them as a signal transmission medium through the development of textile antennas. These antenna components can be connected to a larger communication system to transmit various sensor data to a storage hub or to a medical team for review.

Conductive Textile Sensor Development

Sensing applications using conductive textiles have been an area of great research in recent years as sensor technology and the electronics industry moves towards flexible, low-cost and lightweight products. Wearable electronics make up a significant and growing segment of the world-wide electronics industry. As such, these wearable systems are increasingly being employed in biomedical research environments to constantly and accurately measure the vital signs of patients. Various sensors integrated into a common unit are commonly referred to as body area networks. The early advancements in the developments of body area networks through 2005 are thoroughly discussed in [18]. Carpi and De Rossi describe the early advancements made in electroactive polymer (EAP)-based sensors, actuators,

electronic components, and power sources. Each of these components is designed with the intention of integration into wearable devices such as a body area network. The goal of body area networks is to improve the overall quality of life by maintaining supervision of health and fitness levels through applications such as bio-monitoring, rehabilitation, telemedicine, ergonomics and sports medicine [19-24]. In many cases, sensors to track the status of these metrics can be directly integrated into the garments. These sensors, as mentioned above, include heart rate monitors, accelerometers, and communication devices. Kifayat [25] employs body area network technology to assist therapists in physiotherapy exercises. A data acquisition logger constantly uploads data during the exercise, which allows the therapist to better mold the recovery program to the individual patient. Other sensor networks make use of telemonitoring to alert personnel when drugs are to be administrated [26]. Conductive textiles can also be employed to detect and measure deformation [27], proximity and haptic interactions [28] and motion [18, 29].

There are many opportunities in which conductive textiles can be applied to other body area network research. Carpi [18] points out that garments capable of detecting strain and stress, such as piezoresistive materials, would enable the tracking of posture and gestures. This would allow for precise analysis of kinematic movements. Similarly, these e-textiles would permit real-time monitoring of health vitals for patients. This strive towards disease prevention is critical in the diagnosis and treatment of cardiovascular diseases [20, 24]. Rehabilitation requirements can also be assessed and met through the use of body area network technology. As suggested by Binkley [20], body area

networks could be equipped with actuators in addition to sensors. These actuators would allow for successful monitoring and completion of rehabilitation programs.

In a similar application of conductive textiles, Tognetti [27] characterizes a novel data glove that makes use of conductive elastomers to detect hand movement. The glove, pictured in Figure 7, has the ability to sense these kinematic movements through the piezoresistive effect engaged by the conductive elastomer under deformation. Piezoresistivity is an inherent property in certain materials that forces the electrical resistance of a material to change when an external force is applied. Twenty sensors are distributed over the hand in each conductive elastomer thread. The respective piezoresistive changes in each of these sensors allowed Tognetti [27] to formulate algorithms to help localize sensor deformation thereby mapping the movement of the hand.

Figure 7: Sensing glove created by Tognetti et al. [27]

The uniqueness in Tognetti's approach [27] is that the sensors are printed directly to the fabric glove using the original glove material. This technique, however, can also be a disadvantage. Wijesiriwardana [28] comments on the potential disadvantages of a similar printing technique. He investigates a printing technique to print electro-conductive materials onto textiles using piezoresistive coatings and sewing conductive thread directly on the textile substrate. They claim that:

> the disadvantages involving these approaches are the aging effects of the electrodes constructed with piezoresistive materials [polypyrrole (PPY)/metal-loaded rubber, such carbon-loaded rubber (CLR)], damage with washing and variable performance with deformation (due to time dependencies of these materials and poor repeatability), false alarms due to capacitance change caused by parasitic deformations, and calibration difficulties where absolute readings are necessary (change of capacitance due to humidity temperature, aging, and washing. [28]

This suggests that, over time, the sensing effectiveness of the glove may deteriorate due to the aging effects of the conductive material. Instead of using these techniques, Wijesiriwardana [28] integrates the electrodes directly in to the substrate textile by utilizing electrodes with inherent conductivity. This conductivity derives from "inherently conductive polymers and multifilament metallic fibers" [28]. To detect proximity and touch, Wijesiriwardana et al. employ both capacitive and resistive measurement techniques. In their sensor example, shown in Figure 8, you can see that the conductive fibers are sewn directly in to the nonconductive dielectric textile. Using two layers of electrodes allows for sensing as a result of the variations in displacement. Utilizing the piezoresistive coatings described in [30], touch sensing is also achieved.

Wade and Asada [29] created a cable-free wearable sensor system using DC powerline technology in a conductive fabric vest. They envision their vest to be applied
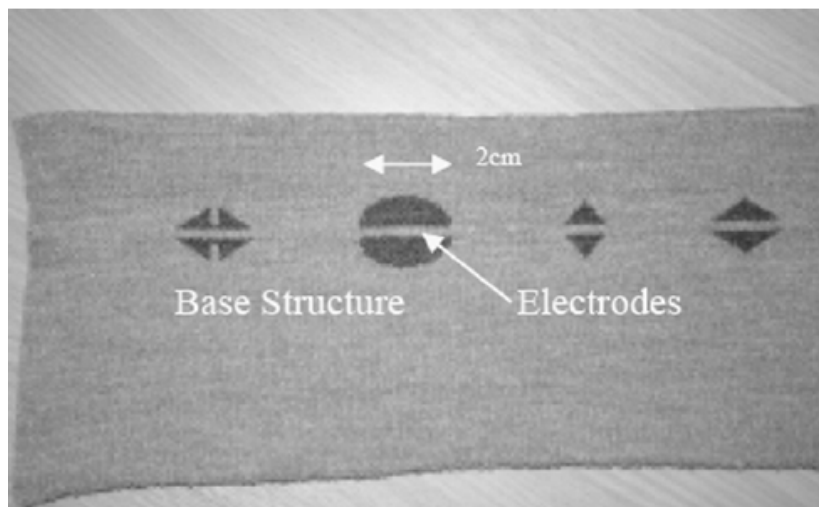
Figure 8: Conductive electrodes used by Wijesiriwardana et al. for touch and proximity-sensing applications [28].

to health monitoring and rehabilitation applications. To reduce the bulkiness of wearable networks, Wade combines DC powerline communication (PLC) technology with intelligent sensors. This combination offers a "comfortable, flexible and washable monitoring network" [29]. Their sensor vest consists of three primary components. These are the sensor nodes, the 'central' node which constitutes for power and information processing, and two conductive sheets which act as a medium for power and data transmission. To test the reliability of signal transmission across their vest, Wade connected an accelerometer to the upper arm of the vest. The output of the accelerometer was modulated and transmitted along the vest to the opposite shoulder. The signal received agrees well with the transmitted signal. This suggests reliability in data transmission and therefore allows for investigation of textile antenna development with these sensing systems.

Body area networks (BAN) are among the leading applications for utilizing conductive textiles as a sensing and communicating mechanism. Many products have been developed to monitor health and fitness levels of wearers as well as other information. Some of the early advances in this field came through the advances of systems such as the MIThril system [31], the Georgia Tech Vest [32], and the VivoMetrics Shirt [33]. These first generation systems appear bulky and inflexible. Before these preliminary systems can become useful for many BAN applications, comfort, durability and flexibility must be addressed.

In order for these body area network prototypes to be successfully realized and implemented in combat wound detection schemes, a few key elements must be characterized and improved. The main shortcomings that fall out of the sensing systems discussed above are their durability and size. In order for sensing systems employing these materials to be viable options, the incorporation of sensors needs to be enacted in such a way as to avoid bulkiness and rigidity in the final product. Additionally, harsh environments such as those presented to deployed soldiers, will require durable, efficient products. For these applications, power consumption must also be considered. If soldiers are to constantly wear these networks to monitor health, fitness and security, they must be comfortable and lightweight. Second, the accuracy of the data must be guaranteed to be collected, received and transmitted reliably. This calls for investigation into using these conductive textiles in communication systems in addition to their use in sensing systems. Wade's previous work [29] shows that signals can travel through the fabric largely unimpaired. Many researchers have investigated using these textile

materials for antenna development as is discussed in the following section. Further development of low-power, lightweight, flexible, durable communication systems will allow for the success of these body area networks to propagate into other fields and applications.

Conductive Textile Antenna Development

In addition to being used as a sensing device, conductive textiles can also be employed as a component in communication system development applications. There has been much research geared towards developing both on-body and off-body communication systems which utilize conductive textiles to implement textile antennas for the purpose of transmitting or receiving signals collected from or sent to sensors or detectors [34-43]. These antennas generally offer low-cost, lightweight, flexible alternatives when compared with their rigid counterparts. The key to textile antenna development is two-fold. First, thorough characterization of the various fabric layers much be performed so that accurate simulation can be achieved. Additionally, fabrication requirements must be determined and prescribed so that precise structures can be manufactured and incorporated into antenna designs. Antennas, like the sensing mechanisms discussed above, can be developed using metallized textiles or by sewing conductive thread. In lower-frequency applications, many choose to incorporate the metallized textiles due to the larger size of the antenna. However, for high frequency applications, the antenna size is much smaller and conductive thread can be tightly woven together with accurate antenna dimensions.

Numerous configurations of textile antennas such as monopoles, patches, and slots have long been sought for body area network applications and could easily be incorporated in combat wound detection systems. Sensors connected within the body area network can, ideally, send their information wirelessly via textile antennas incorporated directly into the clothing. Sugiyama et al. [36] describe this very idea in their development of a wearable, dual-band antenna. This antenna is unique to most in that it is designed to be placed on the ring finger. This alone restricts the maximum dimensions of antenna fabrication. They propose feeding their T-shaped monopole antenna with a 50 Ω coaxial cable. The dual-band nature of this antenna also enhances its operation as there is resonance between 2.4 GHz and 2.5 GHz as well as resonance from 4.5 GHz to 10 GHz. [36]

A wide variety of flexible, lightweight antenna configurations have been developed at lower frequencies other than those mentioned in [36]. These configurations include patch designs, spirals, slots, and monopoles. For example, Galehdar [37] presents a linearly polarized rectangular patch antenna for incorporation into athletic uniforms and clothing. The draw for incorporating antennas into athlete clothing is substantial and can easily be extrapolated to militaristic avenues. Galehdar mentions the desire for coaches to have information useful in making tactical changes during a sporting event. With knowledge of how an athlete is performing biomechanically and physiologically, these changes can be accurately made. Gain is also an important characteristic for these antenna designs so that the battery size can be decreased while the range can be large enough for the event. Galehdar designs a

patch antenna operating at 2.45 GHz with thickness 1.6 mm and relative permittivity of 1.63. He investigates the effects of bending in both the E and H planes. Determined experimentally, increasing the radius of bend decreases the resonant frequency in the E plane of the patch antenna. Similarly, the resonant frequency increases for positive bending angles and decreases for negative bending angles in the H plane. The maximum change in frequency for both planes is 8%. [37] For wideband antenna design, this change in resonant frequency is largely negligible. However, for narrow-band resonance, special care must be taken in the design of flexible, textile antennas to ensure the changes in frequency of operation are acceptable throughout the bending and maneuvering of the antennas. Depending on its use in combat wound detection systems, antenna design may need to account for these bending effects. For localization applications demonstrated in this thesis, wideband antennas are used and will be less susceptible to bending as a result of their wideband nature. However, wireless transmission at Wi-Fi frequencies could be affected by this property.

Shimasaki [38, 39] also investigates the effects of bending on conductive textile antennas. He performs studies on a cavity-backed slot antenna bent along a spherical surface. The antenna developed to complete these studies has thickness of 2.5 mm and area of 95 mm x 90 mm and is created from conductive threads. The slot is realized by removing the conductive threads in the appropriate areas. The operation frequency of this antenna is around 2.3 GHz. Instead of reporting the effects of cylindrical bending as discussed in [37, 39], Shimasaki reports the effects of bending along a spherical surface. The radius of bending along the spherical surface of this antenna is 200 mm.

For the planar antenna, the bandwidth of the designed cavity-backed slot is 230 MHz as compared to a decreased bandwidth of 162 MHz for the bent case. The center resonance frequency also decreases by 84 MHz. [38] This down-shift in frequency is similar to the results presented by Galehdar. The radiation patterns differ slightly from the planar and bending scenario. The shape of the pattern remains similar though a slight decrease in directivity amplitude is visible. One potential source of inaccuracies in this design comes from the repeated bending and flexing of the cavity-backed slot antenna. This repeated motion could affect the dimensions of the cavity by producing thickness fluctuations over time.

In addition to the metallized fabric used for many antenna applications, some designers choose to, instead, weave metallized fibers into fabrics in the appropriate antenna shape. Morris et al. [40] proposes the use of metallized, high-strength Kevlar for conformal load-bearing antenna applications. These antennas can be of use for applications involving unmanned aerial vehicles (UAVs) due to their conformal, lightweight, and damage-resistant (high-strength) properties. Morris points out that, in some cases, the frequency of communication coupled with the small size of some UAV models forces the entire chassis to be used as the antenna. This places even more importance on a lightweight, durable antenna design. To meet these design requirements, Morris metallized Kevlar fibers and wove them into broadband antenna designs. This manual weaving of metallic thread is risky; if the thread were to break, the antenna would prove useless. Morris designed and fabricated a broadband spiral antenna on a polymer-ceramic composite meant for RF applications. This dielectric,

polydimethylsiloxane (PDMS), has the flexibility required to meet the antenna design specifications (thickness of 4mm) while offering a tunable permittivity up to 20 and a loss tangent less than 0.01. Its electrical properties are similar to those of the Rogers TMM4. The broadband spiral antenna is designed to work from 200 MHz to 1000 MHz and can be seen in Figure 9. The substrate was drilled using a 50 W laser to etch patterns for the fiber to be woven. The metallized yarn was then manually woven through the substrate using a sewing needle. They found that weaving the yarns created a gradual increase in the wire resistance and attribute this to the "deterioration of the metal film under cyclic flexing and torsion" [40]. It is possible that, due to consistent flexing over time, antennas created by this technique will not continue to function correctly. While it is not the Kevlar that is suspect to fail, the metalized coating
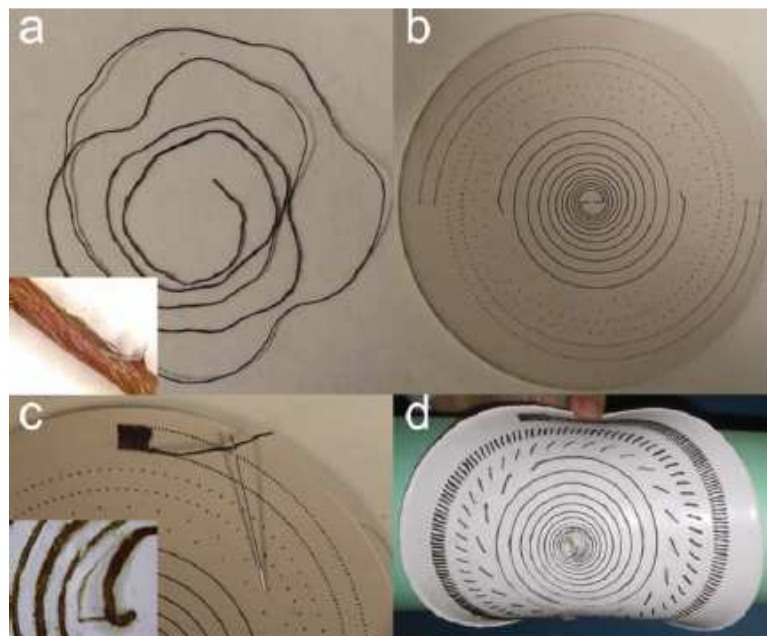
Figure 9: Broadband Spiral Antenna Implemented by Morris et al. Using Metalized Kevlar Yarn [40].

could wear off under repetitive stress. This is the primary challenge that faces the development of textile antennas using singular conductive threads. Further analysis would be necessary to determine the expected lifespan of an antenna created by weaving metallized threads. While the return loss matches decently with the test antenna printed on Rogers TMM4 at frequencies greater than 600 MHz, the realized gain measurements are dissimilar until approximately 750 MHz. At lower frequencies, the realized gain of the woven antenna is far inferior to the realized gain produced by the traditionally fabricated antenna. They attribute these inconsistencies to improper input matching at lower frequencies.

As mentioned above, conformal, load bearing antennas are an attractive option for UAV applications. These antennas are critical for low frequency communication applications in these scenarios. To ensure durability while maintaining beneficial characteristics such as flexibility and low weight, Wang et al. chose to adapt a multilayer approach to antenna fabrication. This approach utilizes lightweight, low-loss materials such as polymers as a dielectric for the textile antennas. Like the work completed by Morris et al., Wang chooses PDMS as the flexible dielectric for his patch antenna designs. Also like Morris, Wang [41] employs conductive thread to weave a patch antenna on his multilayer surface. Amberstrand silver-coated Zylon fibers with resistance of 0.8 Ω/m were used as this conductive thread. This envisioned multilayer surface is depicted in Figure 10. To test this new conductive fiber, a 31 mm x 31 mm probe fed patch was developed and placed on the PDMS substrate. This antenna was designed to resonate at 2.2 GHz. Compared to a simulated version of the same design,
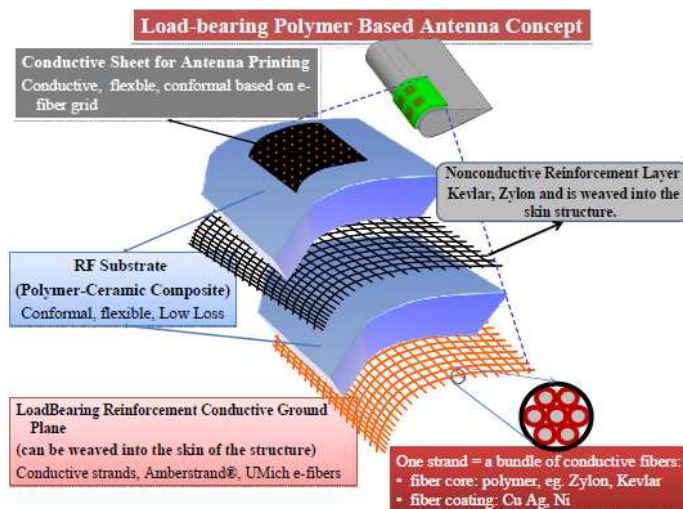
Figure 10: Multilayer Textile Antenna for Integration into UAV Body Envisioned by Wang et al. [41]

the fabricated textile patch antenna gain was only 0.2 dB lower. This corresponded to a textile antenna gain of 5.7 dB. It is evident that these textiles can be implemented in antenna design to provide a reliable, flexible solution to the UAV communication application.

In addition to their aforementioned use in wireless body area networks as well as load-bearing applications, textile antennas are also a popular alternative in ultra-wideband (UWB) applications. Klemm and Troester [42] develop a textile UWB antenna for wireless body area networks. They claim that their antennas offer direct integration into clothing due to their thinness and flexibility. They realize two different types of textile antennas: a coplanar-waveguide-fed disc monopole and an annular slot antenna. These designs operate in the entire UWB band, 3.1 GHz to 10.6 GHz, approved by the Federal Communications Commission. Each utilizes conductive textiles with very high

conductivity. This metallized Nylon fabric created by Shieldex has surface resistivity of 0.03 Ω/sq. As the dielectric substrate, they use an acrylic fabric with thickness of 0.5 mm. The permittivity of this dielectric was found to be 2.6 ± 0.1 over the frequency band of interest. As important as the fabric selection is the antenna fabrication. The antenna must be fabricated in such a way as to retain the correct antenna dimensions while also preventing a change of the electrical properties. Klemm uses adhesive iron-on sheets to achieve this goal. These sheets merely deposit a thin adhesive layer on the textiles such that the sheet resistance and permittivity parameters are not altered. An SMA connector was attached to the antenna using a two-part conductive glue. [42]

Difficulties exist in using textiles to implement antennas. As Klemm points out, it is difficult to implement CPW technology through manual means. They use a scalpel to realize the small widths between the ground plane and the signal. This is a very difficult task. In their fabrication process, they achieved a characteristic impedance of 59 Ω. As you can see, this is not a perfect match to a 50 Ω system. For textile antennas to become more accurate, the fabrication process must be addressed and higher accuracy be achieved. At low frequencies, up to 8 GHz, the textile antennas agree well with traditional printed circuit board (PCB) antennas. Above 8 GHz, however, the losses of the textiles outweigh those of traditional PCB antennas. However, it is evident that these antennas are a viable option for UWB systems. The received pulses of a two-antenna system with textile antennas match near perfectly with the PCB antennas. Klemm also investigates the influence of the body on the UWB antennas. As the antenna moves closer to the body, the normalized amplitude of the transmitted pulse decreases.

Interestingly, when the antenna is 6 mm from the body, the transmitted pulses are higher in amplitude than the transmitted pulses in free space. Klemm and Troester [38] attribute these results to indication that the body constructively reflects electromagnetic waves at frequencies greater than 4.5 GHz.

Giddens [43] investigated the influence of the body on wearable antenna efficiency. With this information, it is hopeful that more efficient antennas could be developed for use in body area network applications. This study analyzes the reflection coefficient of the antenna at different distances away from the body. They confirm through simulation and measurement that no significant detuning occurs as a result of proximity to the phantom. While increasing the ground plane of the patch antenna did not alter efficiency, their study shows that a 75% increase in efficiency can be obtained by spacing the antenna away from the body. In Table 1, data was reproduced from their presentation to describe the increase in efficiency seen as the distance between the body and patch antenna was increased. Similar results were obtained through other studies performed by Zhu [44], Klemm [45], and Thompson [46]. Instead of increasing the distance from the body to improve efficiency, Zhu [44] incorporates the antenna over an electromagnetic band gap structure. Klemm [45] illustrates the differences between on-body and off-body communication, while Thompson [46] focuses his efforts on the antenna mounting method and how that can be altered

Table 1: Effect of Increasing Distance between Body and Textile Antenna on Antenna Efficiency as Shown by Giddens, et al. [43]

Number of felt layers	Measured Efficiency (±5) (%)	Maximum Measured Radiated Power (dB)
0	29	-2.3
1	33	-2.6
3	34	-1.5
5	46	-1.1
7	51	0

to improve the "correlation coefficient of body worn antennas' reflection coefficients on and off the body" [46].

Substrate integrated waveguide technology has also been introduced to textile antenna development to improve the bandwidth and input matching characteristics of the antenna and eventually can be used for long low loss transmission lines embedded on the fabric. Moro [47] designs a cavity-backed dog-bone slot antenna in substrate integrated waveguide technology. There are numerous benefits for utilizing the cavity for textile antennas to be used in on-body communication applications. These include a suppression of surface waves, lower sensitivity to body proximity, and high front-to-back ratio [48]. The substrate used to fabricate this antenna is protective foam typically incorporated into firefighter uniforms. It has a thickness of 3.94 mm, permittivity of 1.575 and a loss tangent of 0.0238 at 2.45 GHz. The top and bottom conductive textile layers employ Flectron with surface resistivity of 0.18 Ω/sq at 2.45 GHz. The substrate integrated waveguide technology is realized by perforating the antenna and placing metal eyelets in each of the holes. These eyelets are 7 mm in diameter and are spaced

14 mm apart. The complete antenna fabricated by Moro is shown in Figure 11. The Flectron sheets are the copper colored sheets in Figure 11. This antenna was tested stand-alone and resonates at 2.45 GHz with broadside gain of 3.9 dBi measured (compared to 3.21 dBi simulated). It was again tested after integration into the backside of a firefighter uniform between the waterproof and moisture/thermal barrier layers. The body proximity does not affect this antenna as the resonant frequency is negligibly decreased and the radiation patterns generate the same approximate shape. It is worthwhile to note, however, that Moro reports a measured broadside gain of 4.9 dBi during the on-body test. This increase is "attributed to the wider ground plane caused by the presence of the body" [47]. The use of substrate integrated waveguide technology in textile antenna design could be useful to improve the on-body characteristics as compared to antenna development neglecting the effects of body proximity.
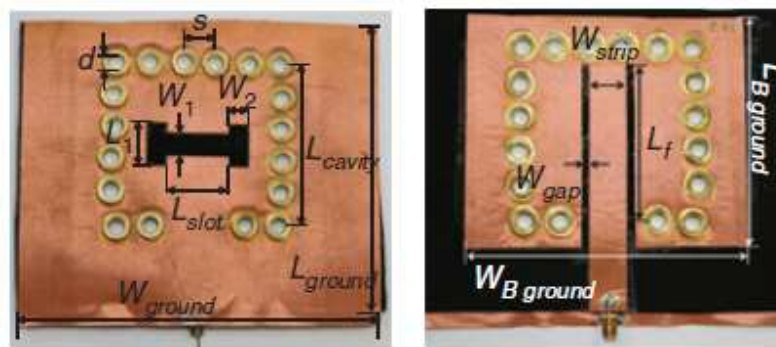
Figure 11: Substrate Integrated Waveguide Cavity-Backed Dog-Bone Slot Antenna Fabricated by Moro et al. [47]

Some important challenges still face the development of textile antennas. The fabrication process must be thoroughly addressed before textile antennas can become a major success. The manual fabrication aspect of these antennas generates inconsistencies in design and disallows for repeatability in measurement. The design of each of the antennas presented manually defines the antenna patterns using a sharp knife or scalpel. This introduces many sources of error and creates difficulty in ensuring a good match. Automating sections of the process, if not the entire process, would allow much more accurate textile antennas to be developed. This would lend the ability to develop precise textile arrays fed with microstrip or coplanar waveguide transmission lines. Until this automation can allow for this precision, however, alternative feeding methods should be investigated. Additionally, there is great difficulty in ensuring the multiple layers, after they have been cut, are properly aligned on either side of the dielectric material. Without this alignment, the antenna cannot be expected to function according to simulation. If either of these challenges can be overcome, the development of textile antennas can be revolutionized and be implemented into many applications.

CHAPTER III: Materials

Combat wound detection applications require that the used materials meet a number of specifications including that they be durable, reliable, lightweight, and thin. These requirements are in addition to electrical requirements such as conductivity for data transmission and resistivity for distributed textile sensing. Numerous materials were used create a sensing system as well as communication system components which met each of these requirements. This chapter investigates the selection of these materials and their purpose in their respective combat wound detection system uses. Among the materials investigated are conductive textiles, dielectric textiles, fabric-based sensor materials, and adhesive materials.

Conductive Textiles

Swift Textile Metalizing provided our team with a fabric sample portfolio that allowed an accurate decision to be made regarding the conductive textile selection. These fabrics varied in thickness, weave, electrical resistance, and metal coating. While the electrical properties of these samples would allow the material to be used in a variety of applications, its physical parameters must also be evaluated. In some cases, the sample was a mesh as opposed to a fabric sheet. This mesh does not provide the durability and security required for some applications. For comparison, Table 2 lists the properties of the various samples. Specifications for both the remote sensing and antenna development applications garner different material considerations. For example, to develop a fabric-based sensor, it is desirable to have a textile with greater

Table 2: Fabric samples provided for consideration by Swift Textile Metalizing, LLC

Material Base Fabric	Metal Coating	Thickness (mm)	Electrical Resistivity (Ω/sq)
Continuous Nylon Loop	Ag	0.86	< 1.5
Nylon Knit 48×21	Ag	0.18	< 1.0
Nylon Tricot Knit 55×40-2	Ag	0.23	< 0.5
Nylon Knit 55×40	Ag	0.18	< 1.0
Nylon Knit 13×26	Ag	0.15	< 5.0
Non-Woven Point Bonded 10	NiAg	0.23	< 1.0
Non-Woven Point Bonded 20	NiAg	0.38	< 0.1
Nylon Rip Stop	NiAg	0.10	< 0.1
Nylon Rip Stop	**3NiAg**	**0.10**	**< 0.05**
Nylon Rip Stop	Ag	0.10	< 1.0
Nylon Heavy Rip Stop	Ag	0.18	< 1.0
Nylon Taffeta	NiAg	0.13	< 0.1
Spandex	**Ag**	**0.57**	**< 1.5**

surface resistivity. This characteristic allows for more accurate sensing to determine touch and intrusion. Alternately, signal transmission requirements prevent the use of resistive textiles and, instead, promote the use of highly conductive ones. In each of these cases, however, metallization uniformity is paramount.

To meet the requirements of a distributed textile sensor, the spandex fabric with electrical resistance less than 1.5 Ω/sq was selected. Alternatively, the 3NiAg Nylon Rip Stop was selected to meet the high conductivity requirements associated with antenna development and signal transmission methods. The material's small thickness as well as its low resistivity is ideal for this application. Additionally, the 3NiAg Nylon Rip Stop is a similar textile to those implemented in previous textile antennas as discussed in Chapter II (e.g., Shieldex Nora) and is more conductive than the copper Flectron textile.

The conductivity of these materials can be determined by knowing the material thickness and sheet resistivity and by using the relationship in Equation (7) where σ is the fabric conductivity in S/m, ρ_s is the sheet resistivity in Ω/sq, and t is the fabric thickness in meters [49].

$$\sigma = {}^{\mathbf{1}}\!/_{(\boldsymbol{\rho}_s * \boldsymbol{t})} \qquad (7)$$

Dielectric Materials

Another key component to textile antenna development is the selection of an appropriate dielectric material. This material must successfully balance all application requirements such as flexibility, durability, thickness, and dielectric loss. For example, wireless body area networks require the antenna to be lightweight, conformal, easily integrated into clothing, flexible, and inexpensive. For these applications, a lightweight, inexpensive dielectric textile is preferred. Contrasting with this would be lightweight textile antenna development for a more rugged scenario such as deployment on UAVs. UAV textile antennas must offer the same specifications as the wireless body area networks while also committing to be highly durable and tear resistant. In these applications, a higher strength fabric is desirable. This fabric, however, must still provide sufficient electrical characteristics to complement its physical properties. Investigation into an acceptable dielectric returned a number of potential solutions. These candidates are presented in Table 3. The permittivity and loss tangent values for these textile materials are taken from 40, 44, 47, 50, 51]. PDMS, polydimethylsiloxane, is a flexible

Table 3: Dielectric fabrics for consideration by Morris [40], Zhu [44], Moro [47], Ouyang [50] and Sankaralingam [51]

Material Base Fabric	Thickness (mm)	Relative Permittivity	Loss tangent – tan(δ)
PDMS	4.0	Tunable to 20	< 0.01
Silk	0.58	1.75	0.012
Moleskin	1.17	1.45	0.05
Felt	1.1	1.38	0.023
Fleece	2.55	1.17	0.0035
Firefighter Protective Foam	3.94	1.575	0.0238
Cordura	0.57	1.90	0.0098
Cotton	0.145	1.60	0.04
100% Polyester	-	1.90	0.0045
Quartzel Fabric	-	1.95	0.0004
Jeans Cotton	2.84	1.67	-

polymer composite and not a textile material, but is included for dielectric material comparison.

Durability is an important parameter when selecting textile materials. The denier rating of textiles corresponds directly to the textile strength; a higher denier rating implies higher strength. Due to its high denier rating of 1000, just shy of some Kevlar fabrics with a denier rating around 1200, as well as its relatively low loss and small thickness, the Cordura fabric was selected as a dielectric and insulating material. This fabric can be used for both applications in this thesis as it is strong enough to provide durability to a distributed textile sensor network as well as a sufficient dielectric for use in antenna development.

All three selected textiles are shown in Figure 12; the high resistivity spandex in Figure 12(a), the high conductivity 3NiAg Nylon Rip Stop in Figure 12b), and the Cordura dielectric in Figure 12(c).

Fabric-Based Sensor Materials

Creating a large-scale distributed fabric-based sensor utilizes a number of different materials in addition to the textile layers. To ensure a good electrical connection, adhesive snap electrodes and electrode cables were purchased from bio-medical.com and placed on the fabric sample in a desired pattern. These electrodes and electrode cables can be found in Figure 13 and Figure 14.

Adhesive Materials

An iron-on adhesive was used to secure multiple textile layers together. The adhesion process was fairly straightforward. After preparing the textile layers and cutting the

| (a) | (b) | (c) |
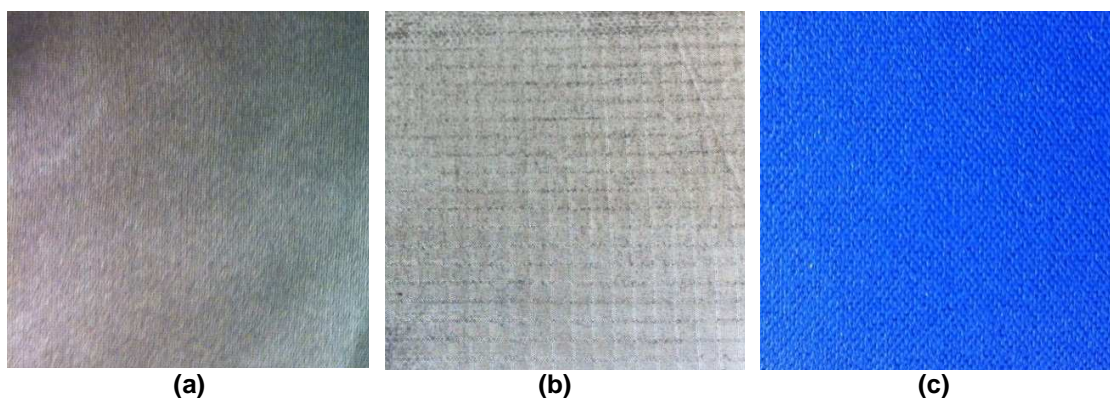
Figure 12: Textiles selected for our applications: (a) conductive spandex, (b) conductive 3NiAg nylon rip stop, (c) Cordura dielectric.
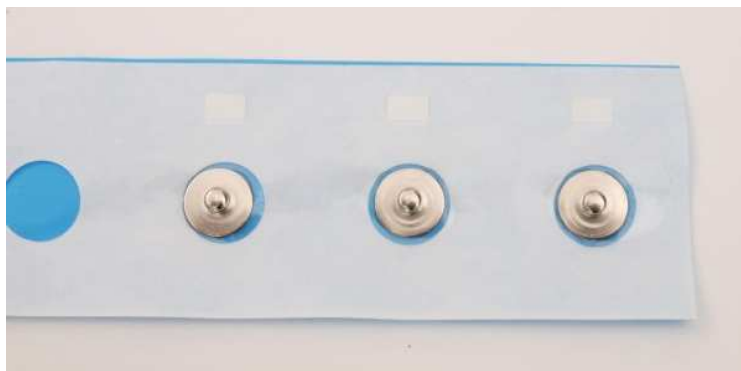
Figure 13: Adhesive snap electrodes for large fabric samples.

Figure 14: Electrode cables for connection between fabric and sensing hardware.

paper-backed adhesion material to the appropriate dimensions, the adhesive layer

could be laid on one of the textile layers. Applying heat causes the glue to bond with the

textile layer and allows for removal of the original paper backing. Then the second

textile layer is aligned with the first layer in the desired location. Applying heat to this

second layer, once it is in position, bonds the two textile layers to one another. A

diagram of this process is presented in Figure 15. The bonding is strong and durable,

even permitting machine washing without losing its adhesiveness. Once the multiple layers have been secured together, the various designs can be electrically connected to external equipment. This connection has been achieved in this thesis through the use of a two-part conductive epoxy, shown in Figure 16. The selected epoxy was AI Technology's EG8028 High Strength Two Component Electrically Conductive Epoxy Paste Adhesive. After mixing equal parts of the epoxy components, a layer can be applied to the textiles, allowing for mating between the connector and textile design. This connection can be left to dry and secured using hot glue if added durability is desired.
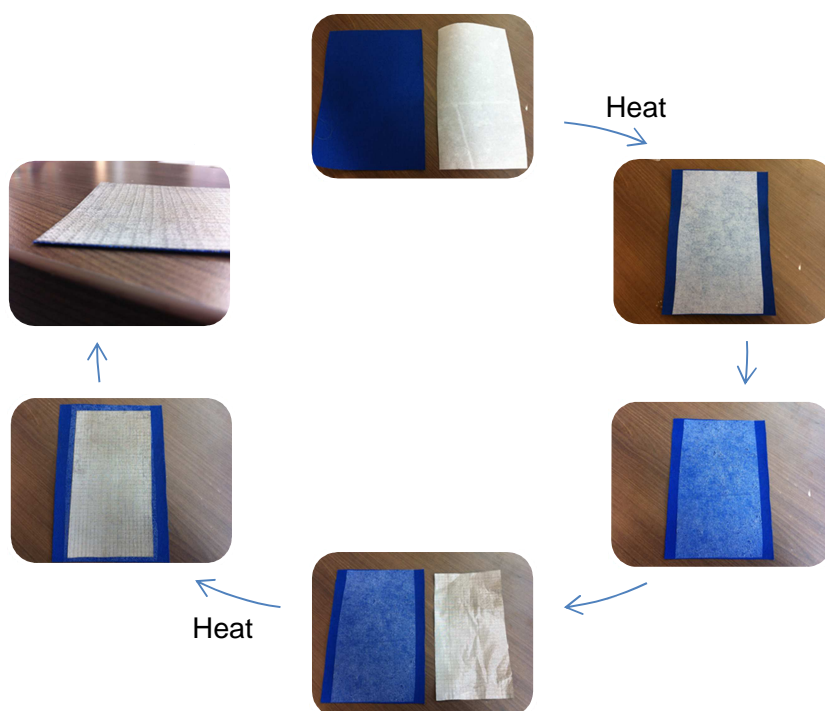
Figure 15: Multilayer textile adhesion process.

An additional solution to electrically connecting multiple layers is by using conductive thread shown in Figure 17. Though resistive in large lengths, <100 Ω/cm, this thread can be overlapped and used over short distances very effectively. The process of overlapping the conductive thread forms parallel combinations of the resistances, thereby reducing the overall effective resistance. These threads can be utilized to emulate the metal walls of the SIW technology for signal transmission.

Figure 16: Two-part conductive epoxy.

Figure 17: Electrically conductive thread.

CHAPTER IV: Using Conductive Textiles as Fabric-Based Sensors

Combat wound detection systems require combination and incorporation of distributed sensing capabilities coupled with data transmission techniques. Chapter IV focuses on utilizing conductive textiles as a sensing device to detect the presence and location of cuts and tears in the conductive textile. These discontinuities can be seen as a realization of bullet holes and wounds to the field-deployed soldier. The sensing method presented in this chapter couples with a data acquisition system to sense discrete changes in resistance at various points along the conductive textile. Incorporation of additional medical sensors, as mentioned in Chapter I, allows for medical personnel to not only measure the external safety of the deployed soldier but also the internal safety stemming from changing sweat levels, respiration rate, heart rate/pulse, blood pressure, etc.

Distributed Fabric-Based Sensor Development

One application using conductive textiles calls for textile implementation as a distributed sensor. For these textiles to produce readily detectable data, high resistivity conductive fabric can be used. Generally, a textile resistivity greater than 1.0 Ω/sq produces detectable changes in resistance. Spandex metalized by Swift Textile Metalizing was chosen to implement this sensor technology. This chapter analyzes the potential to utilize metalized spandex as a distributed sensor for combat wound detection by employing simple sensing to detect penetration and intrusion into conductive-textile-lined clothing. The form-fitting capability of spandex yields greater

certainty in fully covering a soldier in the desired areas such as over a bulletproof vest or field uniform.

Resistance Network Theory

By probing the textile surface at discrete locations and measuring the change in resistance over time, the integrity and safety of the soldier can be ascertained. For simplicity in data analysis and visualization, the resistance is probed at discrete locations over a grid pattern by measuring the corresponding analog voltages using a data acquisition system. If the resistive changes between successive acquisition times are large, damage to the fabric, whether accidental or intentional, becomes evident. With this knowledge, creating a resistive network between the probing points and measuring resistive perturbations can accurately determine if penetration by cutting or tearing holes in the textile has occurred.

To provide certainty in the event of unwarranted penetration, simulation profiles to model the effect of penetration through the conductive textiles were developed and analyzed. With proper analysis, the comparison between simulation and measurement indicates evidence of penetration. The development of this simulation model requires knowledge of resistance network theory. The mathematical theory behind resistance matrices has been studied in great detail [52-57]. From this mathematical theory, a numerical technique was developed in MATLAB to simulate the properties of conductive fabric for cut detection. Implementation of the mathematical theory provides a solid theoretical base from which to model conductive textiles. Wu [52] describes a closed form expression, given in Equations (8) and (9), to analyze resistive grids of size *M* x *N*.

This expression determines the resistance between two nodes, r_1 and r_2, where $r_1 = (x_1, y1)$ and $r_2 = (x_2, y2)$ are defined.

$$R^{free}_{\{MxN\}}(r_1, r_2)$$

$$= \frac{r}{N}|x_1 - x_2| + \frac{s}{M}|y_1 - y_2| + \frac{2}{MN}$$

$$* \sum_{m=1}^{M-1} \sum_{n=1}^{N-1} \frac{\left[\cos\left(x_1 + \frac{1}{2}\right)\theta_m \cos\left(y_1 + \frac{1}{2}\right)\phi_n - \cos\left(x_2 + \frac{1}{2}\right)\theta_m \cos\left(y_2 + \frac{1}{2}\right)\phi_n\right]^2}{r^{-1}(1 - \cos\theta_m) + s^{-1}(1 - \cos\phi_n)}$$

(8)

where *r* and *s* denote the value of the resistances in the two principal directions and

$$\theta_m = \frac{m\pi}{M} \quad \text{and} \quad \phi_n = \frac{n\pi}{N} \; . \tag{9}$$

This closed-form expression does not easily allow for the simulation of holes within the grid. To implement this capability, the methods presented by Grothmann [53] were adapted to a resistor grid network. Modeling conductive fabric as a large grid of resistors entails working under the assumption that the interior resistor matrix follows the mathematical theory of an infinite resistor grid. The conductive fabric, however, has finite boundaries. In this, the conductive textiles cannot be modeled as an infinite grid of resistors. Through the mathematical device known as an incidence matrix, these boundary limitations can be correctly accounted for. The incidence matrix is a mathematical body that maps the relationship between all nodes in a larger network. For this application, each row and column in the incidence matrix enumerates the direct electrical connections corresponding with that node in the resistor network. An example resistor network is illustrated in Figure 18.
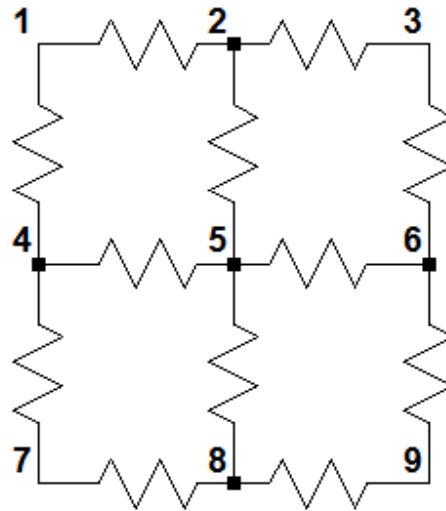
Figure 18: Example resistor network.

To populate an incidence matrix based on the resistor network, the direct electrical connections must be established with each node in the matrix. This matrix is of square size with each dimension equivalent to the number of nodes in the network. The example in Figure 18, with nine nodes, carries an incidence matrix of size 9 × 9. To populate the matrix, the computer model cycles through each node determining the appropriate electrical connections and placing a "1" in the corresponding location in the incidence matrix. This value of "1" corresponds to a resistor value of 1 Ω between each node in the example resistor network. For example, node 1 in Figure 18 has a direct electrical connection with nodes 2 and 4. So, the first row of the incidence matrix, corresponding with node 1, will be populated with a "1" in columns 2 and 4. This process is carried out for each node and presents an incidence matrix as seen in Equation (10).

$$A_I = \begin{matrix} 0 & 1 & 0 & 1 & 0 & 0 & 0 & 0 & 0 \\ 1 & 0 & 1 & 0 & 1 & 0 & 0 & 0 & 0 \\ 0 & 1 & 0 & 0 & 0 & 1 & 0 & 0 & 0 \\ 1 & 0 & 0 & 0 & 1 & 0 & 1 & 0 & 0 \\ 0 & 1 & 0 & 1 & 0 & 1 & 0 & 1 & 0 \\ 0 & 0 & 1 & 0 & 1 & 0 & 0 & 0 & 1 \\ 0 & 0 & 0 & 1 & 0 & 0 & 0 & 1 & 0 \\ 0 & 0 & 0 & 0 & 1 & 0 & 1 & 0 & 1 \\ 0 & 0 & 0 & 0 & 0 & 1 & 0 & 1 & 0 \end{matrix} \qquad (10)$$

After development of this incidence matrix, mathematical operations are performed to institute a test voltage at one corner of the sample textile. Matrix calculations are then executed to find the voltage and current at each node in the network. With this data, a resistance matrix can be formed which details the point-to-point resistance from the test node to each other node in the resistor network. This resistance matrix can be plotted to observe the discrete changes in resistance between successive data acquisition times. As expected, the point-to-point resistance increases as nodes further away from the test node are probed. In Figure 19, the resistance grid is plotted as a surface of size 65 × 65. The increasing trend in resistance is obvious.

Nonlinearities can be observed as the resistances are plotted near the edges. This is the result of having a finite boundary along the edge of the resistor network. These boundaries have fewer network connections and fewer paths for current flow and therefore do not increase uniformly as compared to the interior points. The rapid growth is even more dominant in the corners of the fabric and can be explained by an even larger reduction in potential current paths than in edge nodes. These nonlinearities would not be noticeable if an infinite resistor grid could be observed. The nonlinearities within a finite resistor network are better illustrated in the image in Figure 20 where the *x*

and *y* axes are the resistor grid locations and the *z* axis is the normalized resistance. This resistance matrix is also of size 65 × 65.
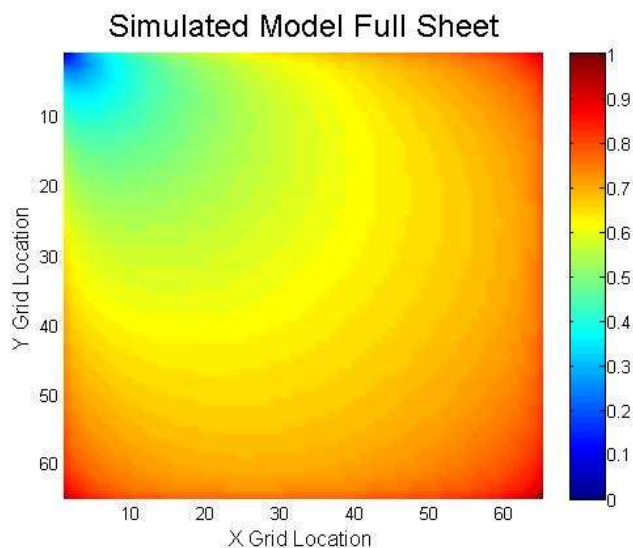
Figure 19: Resistance grid illustrating the gradual increase in resistance as the second probe location extends further away from the origin (top left).
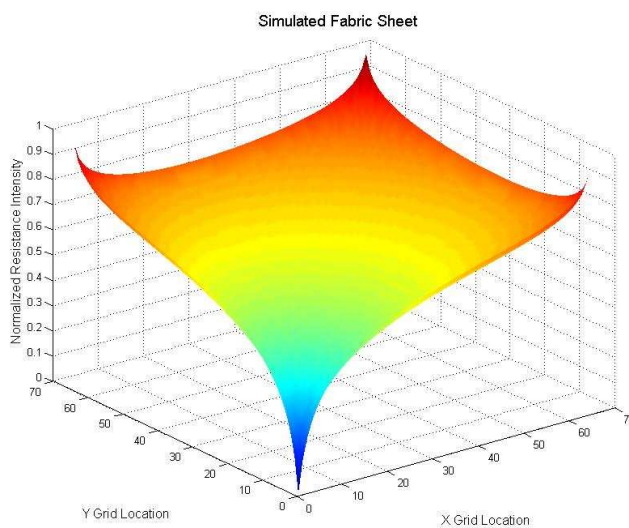
Figure 20: Resistance grid plotted as a surface to better visual the edge and corner nonlinearities.

The resistance grid simulation model provides identical results when compared to the closed-form mathematical expression provided by Wu in Equations (8) and (9). The accuracy of the model is, therefore, ascertained. In addition to providing an accurate representation of a conductive textile sheet, as will be further detailed below in the experiment review, the computer model also has the ability to predict the outcome of introducing cuts and holes within the fabric. Figure 21 illustrates a vertical cut being introduced along the top edge of the fabric. The increase in resistance as a direct result of this action can be attributed to a drastic change in current path length when compared to the uncut scenario in Figure 19. The model is capable of predicting the change in resistance from a variety of cuts as will be discussed later.

After validating the accuracy of the model and performing successful simulations and experiments with the fabric sheet, the model was extended to predict the outcome
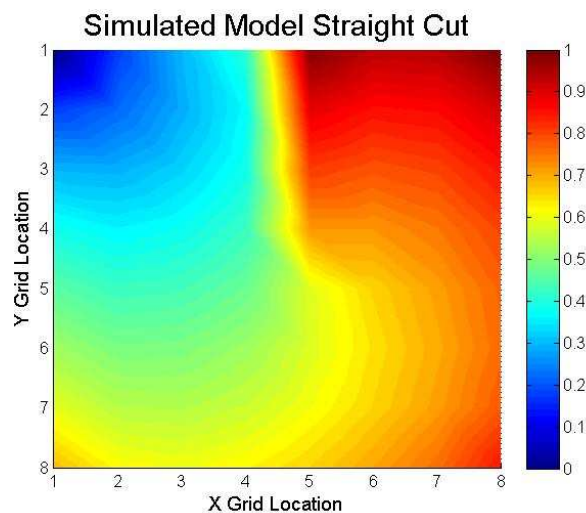
Figure 21: Simulated vertical cut originating from the top edge and extending to the center node.

of a textile sheet wrapped around a three-dimensional structure such as a cylinder. Figure 22 illustrates a cylindrical structure with open top and bottom. This cylinder models a resistor grid similar to that seen in Figure 18. However, to achieve the cylinder effect, node 1 is electrically connected to node 3, node 4 is electrically connected to node 6, and node 7 is electrically connected to node 9. Again, the color mapping intensity suggests that the resistance increases as the distance between probing points increases. The edge effects associated with this model, however, are only seen on the top and bottom.

As with the textile sheet, the cylindrical structure is capable of predicting the resistance changes associated with cuts and holes being introduced to the model. However, due to the size of the cylinder, change in resistance is not as evident when the secondary probe locations are far away from the origin. As such, it would be more
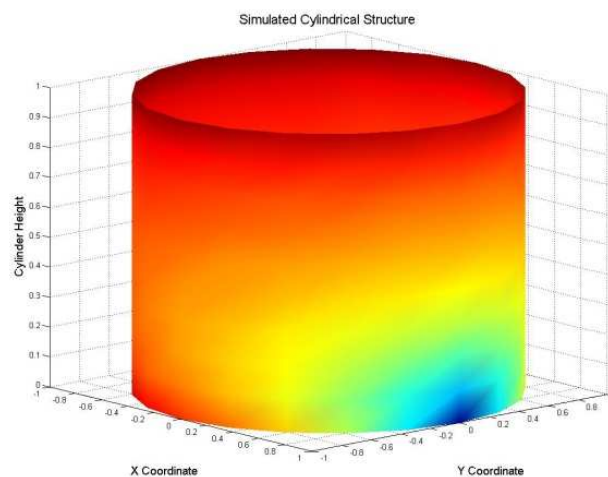
Figure 22: Computer model of cylindrical resistor network.

difficult to determine the presence and location of a cut. Changes in resistance far away from the origin promote the need for redundancy and multiple origins within the distributed sensing network. By fixing multiple locations and probing to every other point, greater resolution can be obtained. The robustness of the model allows other shapes to be developed in addition to cylinders. If the electrical resistor network can be accurately modeled, the incidence matrix can be computed and the resistance matrix can be determined. However, more complex structures may require additional visualization techniques to properly visualize the presence of cuts and tears.

First Generation Fabric-Based Sensing System

To verify the accuracy of the computer simulation model for conductive textiles, experimental data were collected and analyzed. Initial manual measurement testing was performed to investigate the plausibility of conductive textiles following a resistor network construct. This was performed by manually probing marked grid locations with a digital multi-meter while maintaining one probe location constant in the corner. Manual measurements provided preliminary validation of this model. However, for added certainty, a more automated system for data acquisition was developed. Automation allowed for the reduction of error and experiment time compared to the initial manual method.

The first step in designing the test circuitry was to choose a method for effectively and precisely measuring electrical resistance and small variations in electrical resistance. With some consideration, it was evident that the use of a Wheatstone bridge, reproduced in Figure 23, would be the most effective design choice as a

compromise between measurement precision, ease of integration, and relatively low power consumption. The Wheatstone bridge is a simple circuit that is easily implemented on any testing printed circuit board designs. In order to develop a printed circuit board capable of probing multiple locations, multiplexing circuitry was implemented. The use of multiplexing circuitry also saves on expensive analog-to-digital converters. This printed circuit board was employed to measure the analog signal and compute the resistance from a simple mathematical formula shown in Equations (11)–(13). When the bridge is balanced and the voltage V_G is equivalent to zero, the resistance, R_X, can be determined from Equation (11). However, if the bridge is unbalanced, the voltage V_G must be accounted for. This variation on the bridge produces an R_X value as shown in Equation (12) and simplified in Equation (13). If the resistances R_1, R_2, and R_3 are known to high precision, then the resistance R_x can be
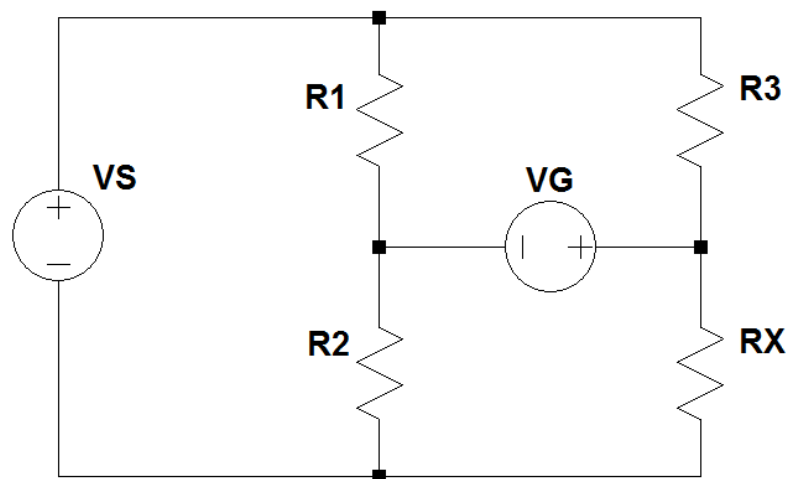
Figure 23: Wheatstone bridge circuit.

determined to high precision. Variations in the source voltage, V_S, will produce fluctuations in the measured voltage, V_G, which results in lower precision in the determination of R_x.

$$\frac{R_2}{R_1} = \frac{R_X}{R_3} \tag{11}$$

$$V_G = \left(\frac{R_X}{R_3 + R_X} - \frac{R_2}{R_1 + R_2}\right) V_S \tag{12}$$

$$R_X = \frac{R_3}{\dfrac{V_S(R_1 + R_2)}{V_G(R_1 + R_2) + V_S R_2} - 1} \tag{13}$$

For ease of system development, National Instruments' NI-6212 Data Acquisition System was selected with accompanying software package, the LabView Development Suite. The specifications regarding the analog input capabilities for this data acquisition system provide a 16-bit analog-to-digital converter with a sample rate adjustable to 400 kS/s, which allows for very fine resolution of the Wheatstone bridge when a voltage range of ±0.2 V was used. This voltage range provided a voltage range sensitivity of 5.2 µV and a voltage range accuracy of 0.089 mV. A system diagram for this first-generation experiment can be found in Figure 24. The resistors R_1 and R_3, corresponding to Figure 23, were chosen to be 150 Ω while the resistor R_2 was chosen to be 10 Ω as this is similar in size to the resistance received by the data acquisition system. Resistor R_1 was chosen as a larger resistance to reduce current flow in the
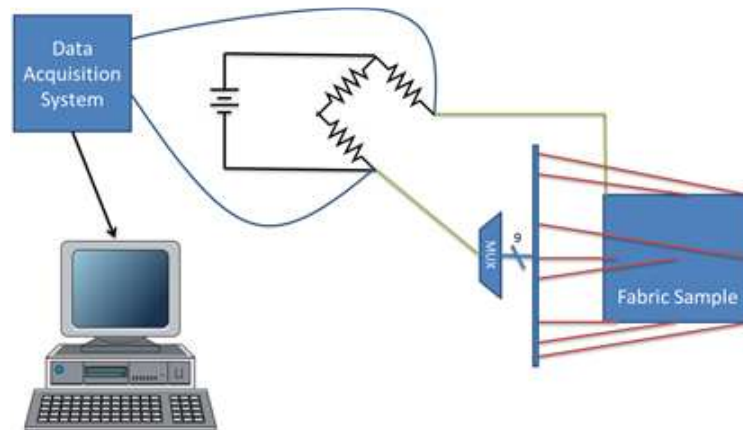
Figure 24: System diagram for first-generation fabric-based sensor testing.

bridge, while R_2 was chosen to be 10 Ω as an approximate match to the measured resistances of the textiles. This match forces V_G to be a lower voltage, which allows the data acquisition program to more accurately sense changes.

A printed circuit board was developed which allowed for inclusion of a small conductive fabric sample for discrete resistance grid sensing. The board and data acquisition system, developed as a proof-of-concept experiment for modeling conductive textiles as a large resistor grid, are shown in Figure 25. To ensure sufficient electrical connection between the circuit board and textiles, the textile samples were pressed against the exposed pads on the printed circuit board. These pads represented each discrete location to be probed through the multiplexing circuitry. The developed board contained four 16:1 multiplexers from Analog Devices, part number ADG706BRUZ, to accommodate the probing of 64 discrete locations on a 3.5 in. × 3.5 in. textile sample. These 64 locations would provide measurements for an 8 × 8
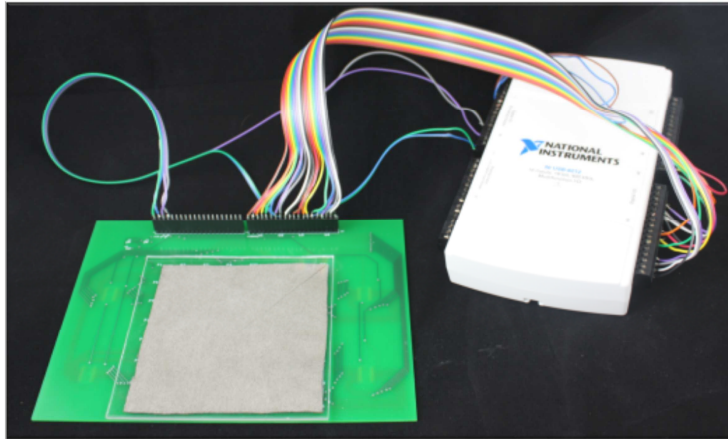
Figure 25: Multiplexing circuit board connected to NI-6212.

resistor grid. The Wheatstone bridge circuitry incorporated into the board design allows for measurement of various point-to-point resistances. Switching circuit control lines, as well as analog output measurements and DC power connections, were linked to the DAQ and a stable external power supply.

By use of this setup, a point-to-point resistance matrix is developed by measuring the resistance between port 1 and each additional port (ports 2–64). The density of resistance points taken over the fabric sample allows for an accurate representation of the fabric sample as a resistive network. Analysis of the preliminary results showed the necessity for a more robust method of ensuring optimum electrical connectivity between printed circuit board pads and the conductive textile sample. The initial method was to place the fabric beneath a piece of Plexiglas so that the application of firm pressure would provide the electrical connection. This method seemed effective initially. However, the results varied between different experiments depending on both the magnitude and uniformity of force applied to the Plexiglas. These inconsistencies led to

the requirement of a more effective means of ensuring conductivity between the board and fabric. AI Technology's EG8020 High Strength Two Component Electrically Conductive Epoxy Paste Adhesive, discussed in Chapter III, was placed on each pad and then adhered to the fabric samples to guarantee proper connection. Providing stable, accurate results, this technique was used for the collection of the data.

Comparison between First-Generation Fabric-Based Sensor Experimental Results and Computer Model Expectations

Experiments were carried out in the manner suggested above to validate the modeling of conductive textiles as a large resistor grid. For comparison, the graphs illustrated below were normalized to their maximum values. Care was taken to reduce experimental error by factoring in trace and multiplexer component on-resistances from the data acquisition circuit boards. The resistance between port 1 and the data acquisition system was taken as this value. This resistance, assumed to be approximately equivalent for each of the ports, was subtracted from the overall resistance value calculated from the Wheatstone bridge equations.

Three data sets were recorded for model validation. Each of these sets corresponds to different fabric configurations. These configurations were selected as a full fabric sheet, a sheet with a vertical cut extending from the center of the textile to the top edge, and a diagonal cut extending from the center to the top right corner of the sample. Samples were arranged so that incisions never directly encountered a contact pad on the data acquisition boards. This ensured that sound data was achievable through all 64 ports. For convenience, sectors of the plots in the discussion below will

be referred to as quadrants of a Cartesian coordinate system (i.e., the top right quadrant is quadrant 1 with quadrants increasing in a counterclockwise direction). This naming technique is clarified in Figure 26.

Simulated (a) and measured (b) uncut conductive textile sheets are illustrated below in Figure 27. Since the measurement takes a total of 64 points creating an 8×8 matrix, the simulation model was adapted to correspond to the same size resistor grid. Visibly, the difference between simulation and modeling is small. The main inconsistencies between the computer model and measurements reside along the boundary. The model predicts higher resistances along the outer boundary of quadrants 1, 3, and 4. These minute differences can be attributed to the placement of the sample on the probing points. In simulation, the sample is probed at the outermost edge, whereas measurement probes the sample as close to the edge as possible. This subtle difference can increase the number of paths current can flow and thereby can slightly reduce the measurement resistance values.
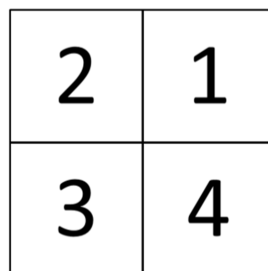
Figure 26: Quadrant naming convention for conductive textile samples.
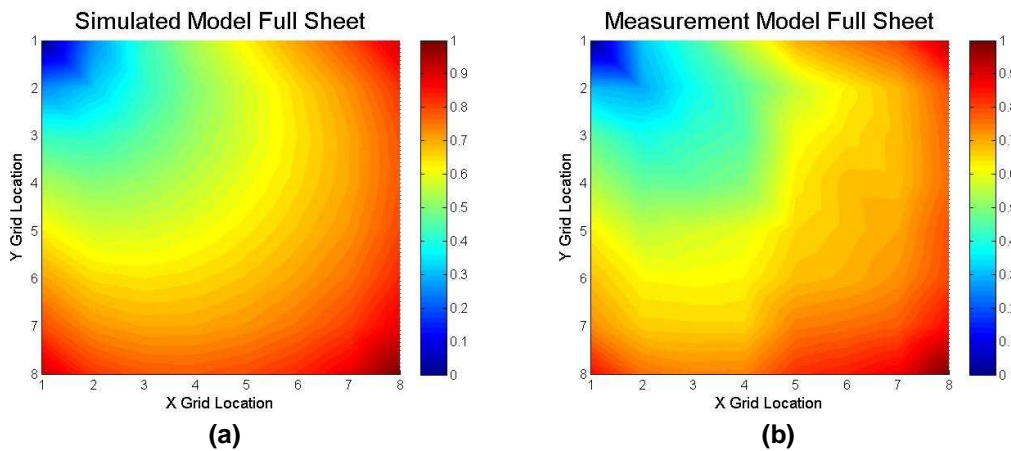
Figure 27: (a) Simulated and (b) measured conductive textile sheet.

The introduction of cuts and holes in the textile samples further tests the validity of the fabric resistivity model presented. Figure 28 compares the results modeled and verified through the introduction of a vertical cut between quadrants 1 and 2. As expected, there is a distinct increase in resistance along the edge of the cut opposite the first measurement location. As with the uncut sheet, error still exists along the boundary of quadrants 1 and 4. Additional error is present in quadrant 4 as seen from the differences in the gradient as the resistance sweeps in a clockwise motion from quadrant 3 to quadrant 1.

The final scenario presented for validation of the computer model illustrates a diagonal cut just shy of bisecting the first quadrant. This cut was chosen to be just shy of 45° to avoid removing any measurement points. Th is scenario provided the largest discrepancy between simulation and measurement. The presence of a diagonal cut is much harder to ascertain from the measurement data presented in Figure 29. A faint
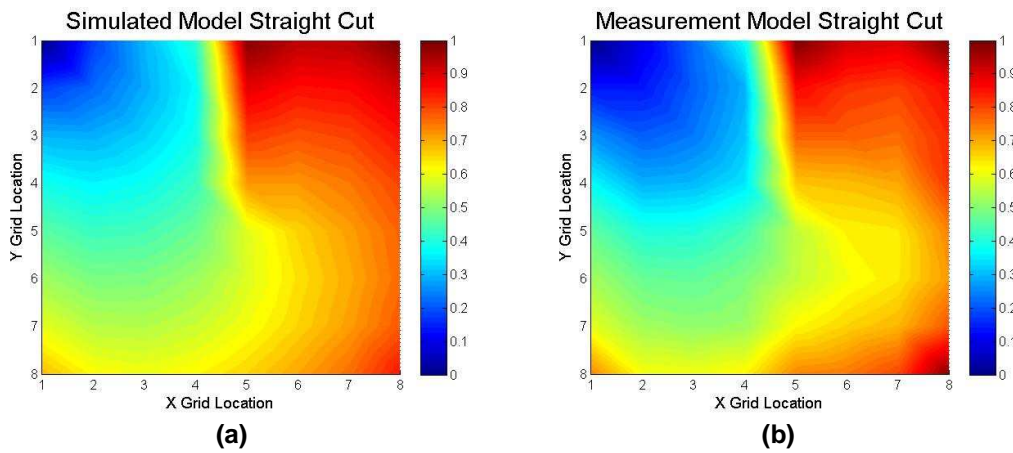
Figure 28: (a) Simulated and (b) measured conductive textile sheet illustrating the presence of a vertical cut.
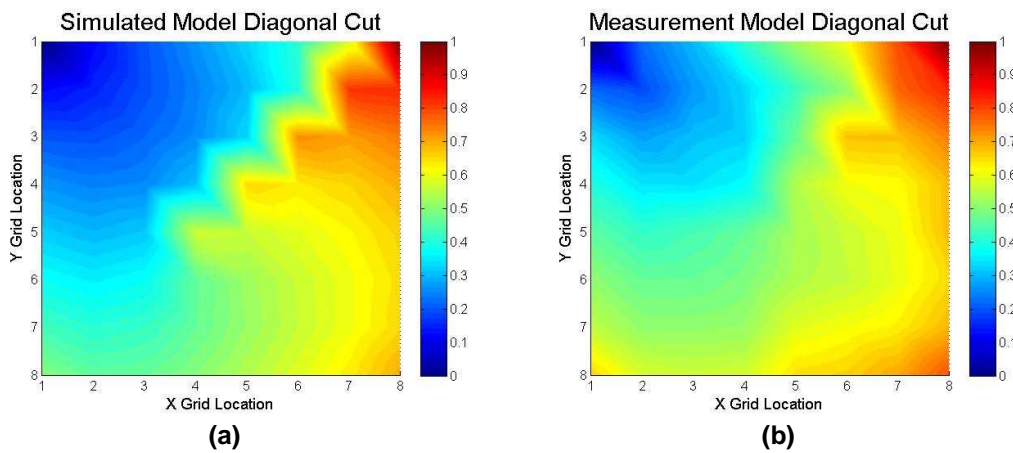
Figure 29: (a) Simulated and (b) measured conductive textile sheet illustrating the presence of a diagonal cut.

stair-stepped pattern resulting from the diagonal cut can be seen in the measurement, a pattern far more visible in simulation.

A comparison between simulation and measurement supplements the theory posed above: conductive textile samples do follow the mathematical relationship of a large grid of resistors. The most favorable comparison between the simulation model and the measurements was evident in the full textile sheet case. There were very few discrepancies between the simulation and measurement. Similarly, the vertical cut scenario provided clear evidence of a cut in the conductive fabric sample. However, the diagonal cut scenario returned inconclusive results when compared with simulation. The differences between simulation and measurement are more attributed to the experiment than to a fault in the computer modeling software. The data generated by the cutting experiments by no means discredit the model but must take into account that more avenues for error are available in these measurements. Sustaining a good electrical connection throughout the experiment is difficult due to the motion of the fabric as it is being cut. The act of making an incision in the textile sample could have altered the electrical connection between the sample and the probing points. It is noteworthy to mention, however, that even in the worst case, a percent difference calculation between simulation and measurement points yielded 76% accuracy in the diagonal cut scenario. Comparatively, the uncut textile sheet displayed over 95% agreement with the model, while the vertical cut scenario displayed over 90% accuracy. Combat wound detection systems require knowledge of the location and size of the penetration. Application of this technology in such a system requires more reliable data collection and verification techniques.

The results gathered through this experiment validate the developed computer model. In future work, a few questions need to be answered. Chief among these is providing a secure electrical connection that can withstand the act of penetration and return reliable evidence as to the certainty of penetration. Additionally, a system that permits the analysis of larger textile samples must be created. This technology cannot be applied if its size restricts applications to a 3.5 in. × 3.5 in. textile sample. To the untrained eye, it may be difficult to understand the presence of a cut based on the visualization methods presented. It would be helpful to implement a weighting function or masking function that would help to normalize the graph and illustrate only the evidence of cutting or tearing instead of plotting the case-by-case resistance grid. Implementation of such a weighting function calls for real-time updates of the data acquisition software to ensure that resistance perturbations are not overlooked through periodic data acquisition runs. The masking function implemented to solve these problems as well as the physical limitations surrounding this technology is discussed in the following section and compared with experimental results.

Second-Order Discrete Laplacian Mask

In order to present the resistance grid in such a way as to emphasize the presence of cuts and tears in the conductive textile, a masking method must be implemented. A second-order partial differential equation can be applied to distinctly illustrate these resistive changes. Specifically, the resistance grid results can be normalized through the use of Laplace's equation. Being a second-order equation, the discrete Laplacian can be used as a smoothing filter while enunciating the highest

gradient changes. The derivation of the solution to Laplace's equation is credited to Mitra [58]. A typical Laplace problem follows Equation (14).

$$\nabla^2 \phi = \frac{\partial^2 \phi}{\partial x^2} + \frac{\partial^2 \phi}{\partial y^2} = 0 \qquad (14)$$

Based on this equation, an accurate second-order finite difference approximation can be made for both the *x* and *y* directions. Three points on each axis separated by a distance *h* are labeled *i − 1*, *i*, and *i + 1*. This is depicted in Figure 30. The second-order finite difference approximations are given in Equations (15) and (16) and follow from the Taylor expansion of a function $\varphi(x, y)$ at three points φ_{i-1}, φ_i and φ_{i+1}. These approximations are exhibited graphically and mathematically below. The superposition of the *x* and *y* direction stencils creates a second order, five point stencil shown in Figure 31. Ignoring the higher order terms allows for Equation (17) to be composed.
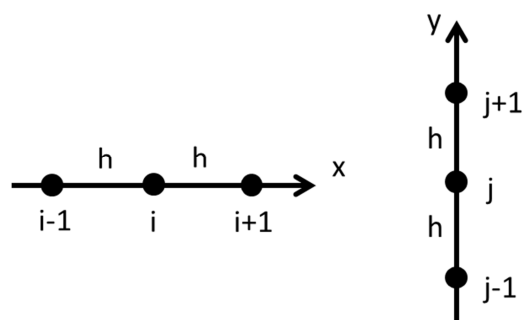
Figure 30: Finite difference along the *x* and *y* directions.
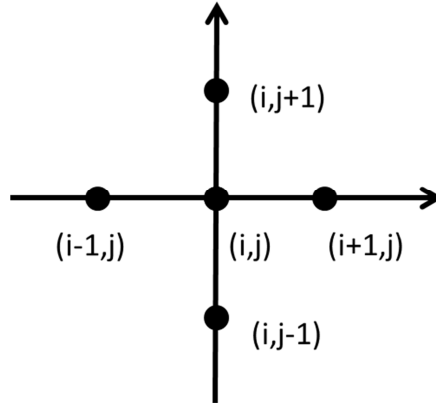
Figure 31: Five-point stencil for the two-dimensional Laplace equation.

$$\frac{\partial^2 \phi}{\partial x^2}\big|_i = \frac{\phi_{i+1} - 2\phi_i + \phi_{i-1}}{h^2} + O\left(h^2\right) \tag{15}$$

$$\frac{\partial^2 \phi}{\partial y^2}\big|_j = \frac{\phi_{j+1} - 2\phi_j + \phi_{j-1}}{h^2} + O\left(h^2\right) \tag{16}$$

$$\left(\frac{\partial^2 \phi}{\partial y^2} + \frac{\partial^2 \phi}{\partial y^2}\right)\big|_{i,j} = \frac{\phi_{i+1,j} - 2\phi_{i,j} + \phi_{i-1,j}}{h^2} + \frac{\phi_{i,j+1} - 2\phi_{i,j} + \phi_{i,j-1}}{h^2} \tag{17}$$

By substituting the result of Equation (17) into Laplace's equation, given in Equation (14), we find:

$$\phi_{i,j} = \frac{1}{4}\left(\phi_{i+1,j} + \phi_{i-1,j} + \phi_{i,j+1} + \phi_{i,j-1}\right). \tag{18}$$

Equation (18) suggests that applying the two-dimensional discrete Laplacian operator to the resistance matrix will have an overall smoothing effect on the resistance grid. The value of each point, *(i, j)*, will reduce to the average of the four surrounding points. The

smoothing effect is dictated by the fact that Laplace's equation is a second-order partial differential equation as described above. The presence of cuts and penetrations, however, will be enunciated by this mask due to the large gradient changes in adjacent resistive measurements. Figure 32(b) illustrates the effect of performing the discrete Laplacian on the resistance grid. It is depicted as a surface to enable visualization of the smoothing effect that the discrete Laplacian operator provides. The corners and edges still exhibit the upward turn due to the decrease in potential current paths. However, the overall shape is much flatter than that seen in Figure 32(a).

Applying this Laplacian operator to the same simulated experiments discussed above yields promising results. The goal of this operation is to illustrate only where penetration of the fabric has occurred and ignore the other areas. In effect, places that experience the most change in resistance will be highly recognizable compared to those places that are unaffected by resistance change. This is evident in the images below. Figure 33 shows a simulated conductive textile sheet with no cuts both with and without applying the Laplacian. Figure 34 depicts this relationship when a vertical cut is applied, and Figure 35 with a diagonal cut applied. In addition to these cuts, Figure 36 shows the simulation results when a single point is affected by a cut or penetration. In Figure 36(a) there is no evidence that this penetration has occurred; however, by performing the discrete Laplacian operator, the location of this penetration becomes evident as shown in Figure 36(b). The gradient changes are made more apparent through application of the discrete Laplacian operator as is evident in the results presented below.
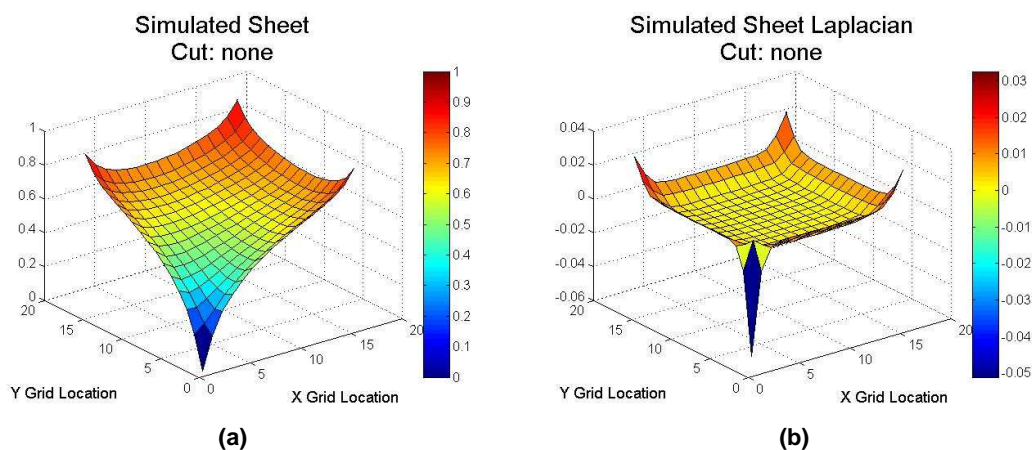
Figure 32: Simulated conductive textile sheet without (a) and with (b) application of the discrete Laplacian operator.
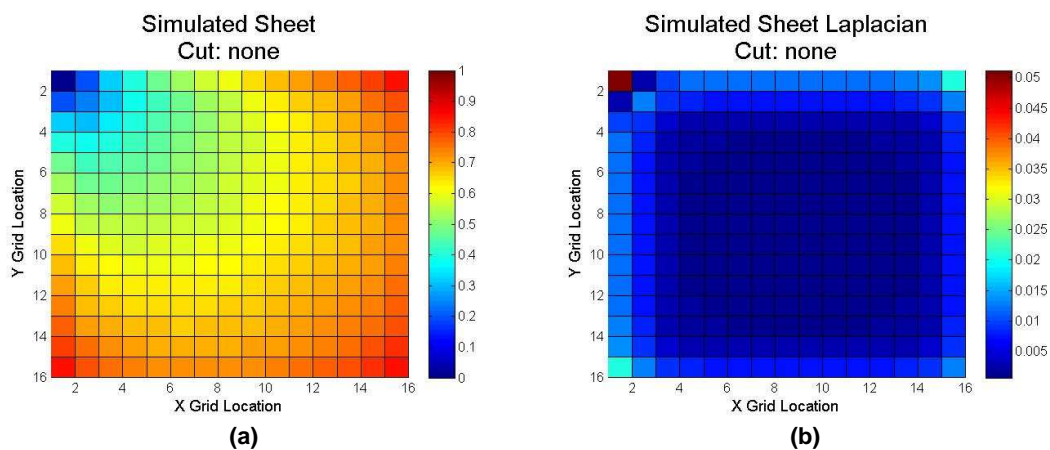
Figure 33: Simulated conductive textile sheet without (a) and with (b) application of the discrete Laplacian operator.
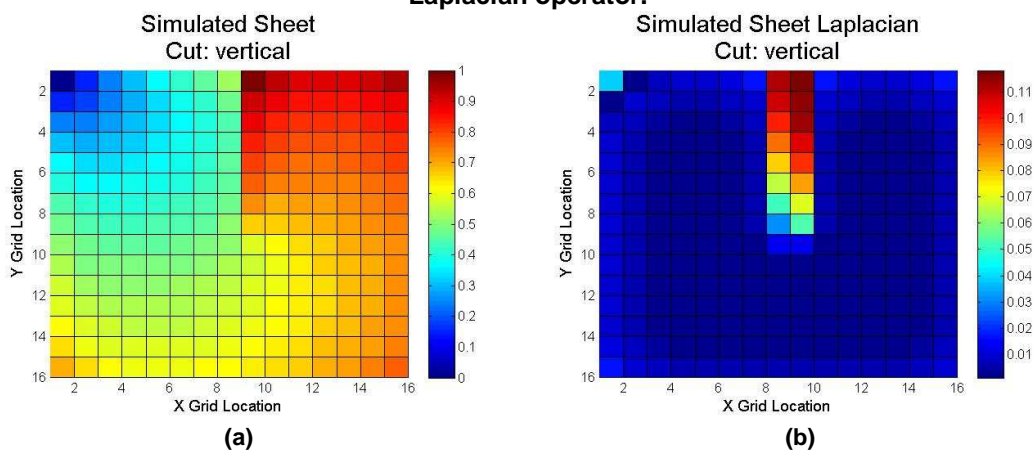
Figure 34: Simulated conductive textile sheet exhibiting a vertical cut without (a) and with (b) application of the discrete Laplacian operator.
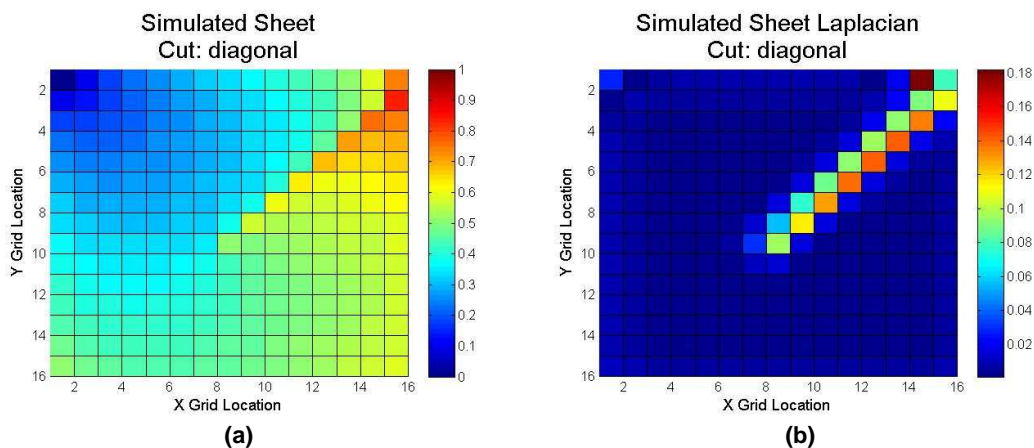
Figure 35: Simulated conductive textile sheet exhibiting a diagonal cut without (a) and with (b) application of the discrete Laplacian operator.
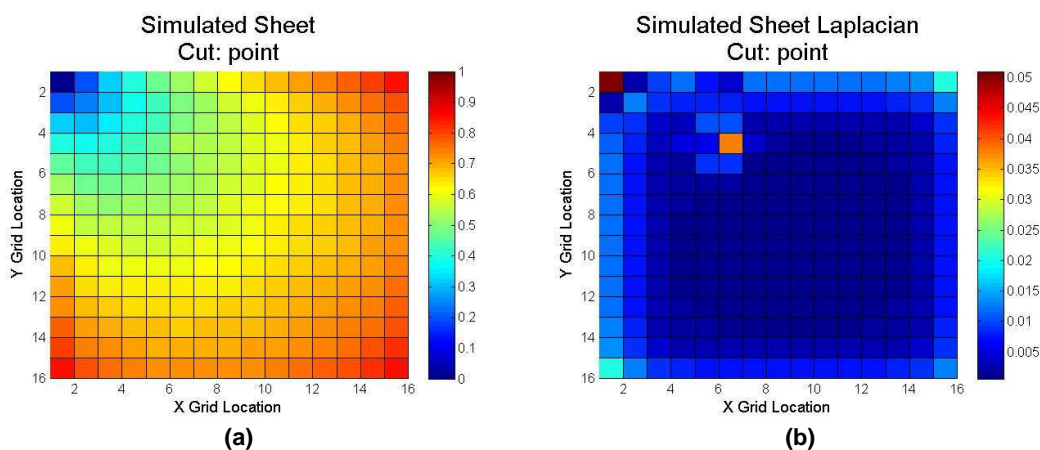
Figure 36: Simulated conductive textile sheet exhibiting the effect of a penetration or cut on a single point without (a) and with (b) application of the discrete Laplacian operator.

To implement the discrete Laplacian for our measurement systems, a second-generation printed circuit board was developed. This board also altered the probing method to produce more reliable electrical connections throughout the experiment. With an adapted version of the data acquisition system and hardware, experimental data have been collected and processed with the discrete Laplacian operator. The inclusion of the discrete Laplacian provides more reliable, accurate evidence that the conductive

fabric has experienced a cut or penetration. Additionally, the use of this operator better allows for quick localization of the perturbation within the resistance grid.

To solve the other problems mentioned above regarding the experimental procedures and electrical connection between the probes and the textile sample, a new printed circuit board was developed. This board retains the use of multiplexing circuitry to cycle through the 64 ports but moves the ports to the outside of the board instead of constricting them to a 3.5 in. × 3.5 in. square. The pads on the outside of the circuit provide an area to which cables can be connected by soldering. The second-generation fabric-based sensor employs electrocardiogram (EKG) cables and snap-electrode connections to provide adequate electrical conductivity between the fabric sample and data acquisition hardware. Experimental results are obtained and analyzed in the forthcoming sections.

Second-Generation Fabric-Based Sensor

After the results of the first-generation proof-of-concept experiment validated the computer model, development of a more robust second-generation system began. The goal of this system was to alleviate some of the problems encountered in the first system. These corrections included a more secure electrical connection between the multiplexer probes and the conductive textile and the allowance for any size of fabric to be tested as opposed to a small square. Figure 37 depicts the second-generation printed circuit board developed to meet these requirements. As shown, the probe locations line the edge of the board, allowing for external probing. This board meets the
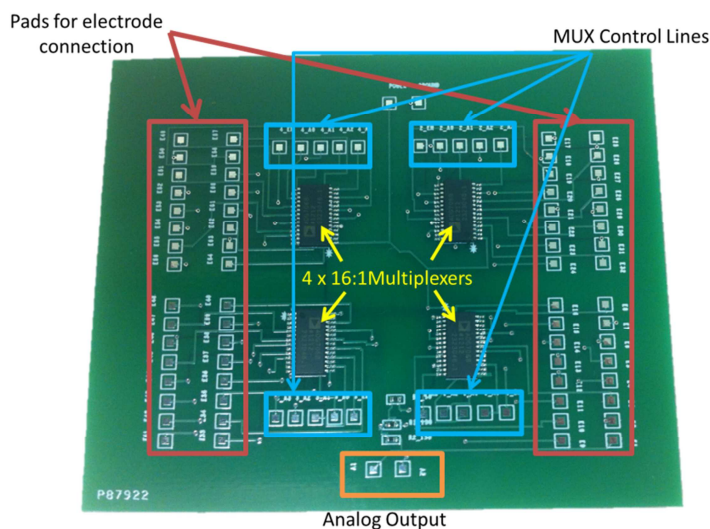
Figure 37: Second-generation fabric-based sensor board.

same specifications as the previous board by implementing four 16:1 multiplexers for switching and a Wheatstone bridge for precise resistance measurements.

EKG cables are placed on the fabric through a connection between the fabric and an adhesive snap electrode. These snap electrodes and electrode cables are detailed in Chapter III. Attaching these electrodes and cables to the fabric results in a system as depicted in Figure 38. As shown, the placement of these electrodes resembles a grid. This structure was chosen for visualization comparison between the simulation model and the results. In reality, the sensing points can be chosen randomly for a given application. They need not follow a distinct pattern so long as the visualization tools are capable of accurately depicting the electrode array. For example, heartbeat measurements may be calculable in addition to penetration detection if the electrodes are placed in close proximity to the heart as is performed by EKGs. The

second-generation sensing system with fabric connected to the sensing board and data acquisition system can be seen in Figure 39.

Experiments conducted with this system were similar to those from the first-generation validation. National Instruments' LabView was used to gather real-time samples of the fabric and process the data to return a plot of the textile resistance grid.

Figure 38: Large conductive textile sample with electrodes connected.
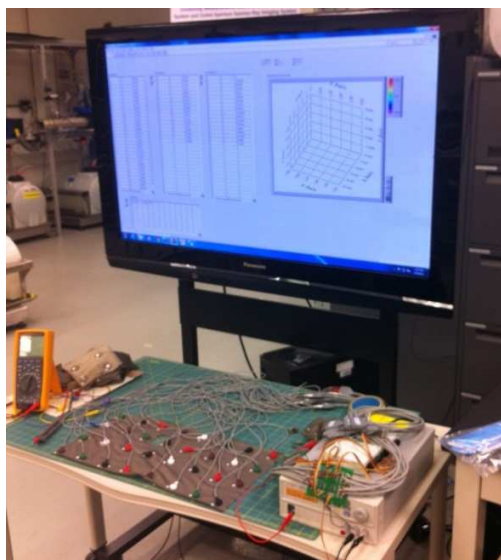
Figure 39: Second-generation sensing system.

The LabView block diagram from this data acquisition system is shown in Figure 40. The plots below examine the ability of the second-generation system to accurately detect and define penetration or resistive changes within the textile sample. The discrete Laplacian operator has been implemented to better visualize the collected data. Each image is compared with original resistance grid data prior to applying the discrete Laplacian for comparison.

Through experimentation, it was determined that a base calibration would be necessary to provide the most accurate results. Originally, the resistance variance between points, attributed to the varying on-resistance of the multiplexers, highlighted some areas not affected by a cut. To solve this inconsistency, a calibration was performed on the base fabric prior to cut implementation. The inclusion of a cut then became more pronounced as the results below suggest.
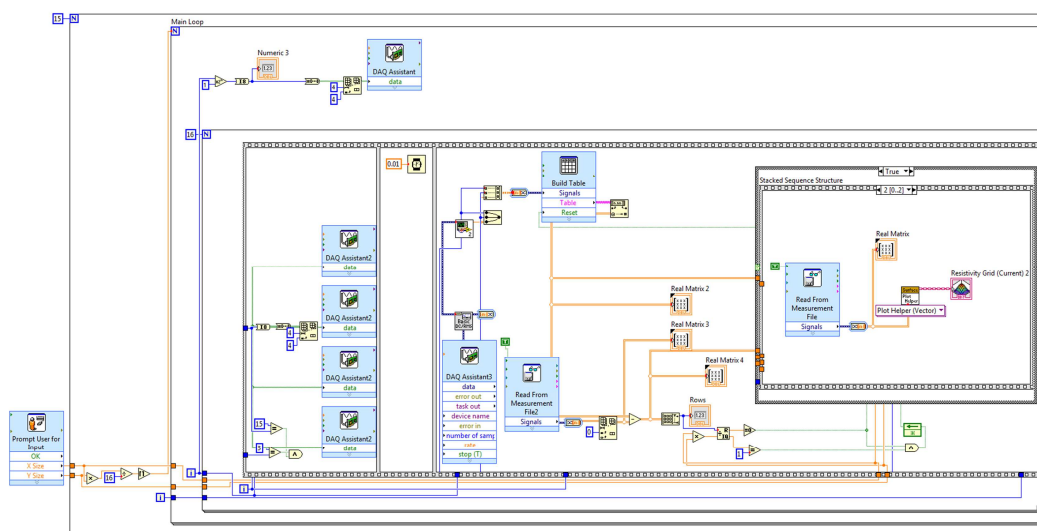
Figure 40: LabView block diagram for data acquisition.

The first experiment conducted with this method used a solid sheet. Figure 41 illustrates the results of this experiment. Figure 41(a) shows the solid sheet point-to-point resistances. Figure 41(b) depicts the result of applying the discrete Laplacian to the resistive grid of Figure 41(a). Figure 41(c) illustrates the resistive difference between the measurement and calibration results. In the case of a solid sheet, subtle differences are expected. Lastly, Figure 41(d) shows the result of applying the discrete Laplacian to the difference plot of Figure 41(c). This same format is applied for each of the experiments conducted below. For ease of comparison, the color mapping scales were equated for each experiment. The raising of the upper limit of the color map lowers the sensitivity of the image to detecting cuts. In comparison to the results of the discrete Laplacian being applied to resistance grid, the results of the same mask being applied to the calibrated difference results in values half the original magnitude. This means that the ability for the calibrated measurements to sense changes will be much greater than the uncalibrated measurements.

Following the solid sheet calibration measurements, a vertical incision was introduced to the textile, and the same experiment was conducted again. The physical cut can be seen in Figure 42. Figure 43(a)–(d) shows the results of this cut when compared with a solid sheet calibration measurement. As can be seen, the vertical cut is clearly defined in all the measurements shown in Figure 43. However, by applying the discrete Laplacian to the difference between the calibration and measurements, more information can be gleaned about the cut size and location. Figure 43(d) helps to
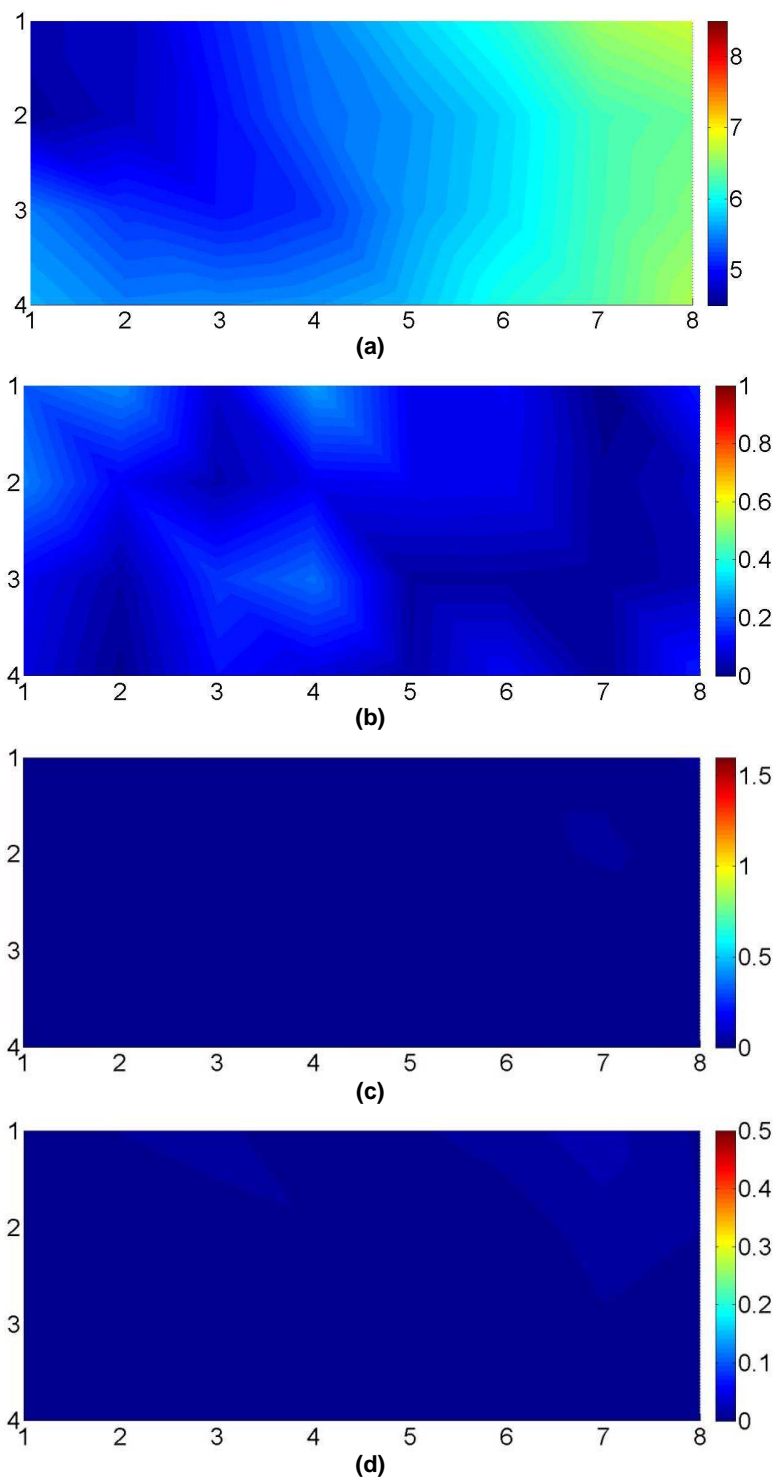
Figure 41: Solid sheet experimental results. (a) Resistance measurements, (b) discrete Laplacian of resistance measurements, (c) difference between measurements and calibration, (d) discrete Laplacian of difference between calibration and resistance measurements.

suggest the size of the cut shown in Figure 42 as well as the location. As expected, the changes in resistance are higher at the edge. This phenomenon is accurately depicted in all the measurements. Without applying the base calibration, inflection points are present in the measurement data as shown in Figure 43(b). Similar results can be found for each of the cuts discussed below.

Figure 42: Experiment with vertical cut introduced to textile.

Figure 43: Vertical cut experimental results. (a) Resistance measurements, (b) discrete Laplacian of resistance measurements, (c) difference between measurements and calibration, (d) discrete Laplacian of difference between calibration and resistance measurements.

After applying the vertical cut, the sample was replaced, and a calibration was again performed. Then, a diagonal cut was applied. The physical cut can be seen in Figure 44. Figure 45(a)–(d) shows the results of this cut when compared with a solid sheet calibration measurement. Each plot suggests an anomaly existing on the right edge of the textile sample. This corresponds accurately with the cut applied as shown in Figure 44. The greatest definition of the cut can be seen in Figure 45(d). This figure not only accurately predicts the presence of a cut but is also accurate in suggesting the location. The location can be determined by noting the area of highest intensity, shown by dark red in the figures. If a probing grid as shown in Figure 44 is superimposed on top of Figure 45(d), it makes sense that the rightmost point on the second row is affected the most when the resistance is measured between that point and the fixed point on the top left corner. With increased resolution, the length of this cut could be more accurately determined.

Figure 44: Experiment with diagonal cut introduced to the textile.

Figure 45: Diagonal cut experimental results. (a) Resistance measurements, (b) discrete Laplacian of resistance measurements, (c) difference between measurements and calibration, (d) discrete Laplacian of difference between calibration and resistance measurements.

With the same sheet, a second cut was applied in a vertical form along the lower edge of the sample. This cut tested the ability of the measurement algorithm to detect multiple cuts. The cuts are shown in Figure 46 with results presented in Figure 47(a)–(d). The detection algorithm is successful in detecting multiple cuts on the same sample of conductive fabric. In the resistance measurement plots there is little evidence of a perturbation existing on the lower edge as a result of a vertical cut between the third and fourth measurement probes. However, by performing the discrete Laplacian, this cut has now become evident. It is interesting to note the indication of a perturbation on the top edge of the sample directly above the cut. When MATLAB performs the discrete Laplacian, cubic interpolation is used to estimate the exterior edge resistances. This interpolation may create a source of error as shown on the top edge of Figure 47(b) and Figure 47(d). More measurements may prove to eliminate the case of false detection as is somewhat illustrated through this experiment.

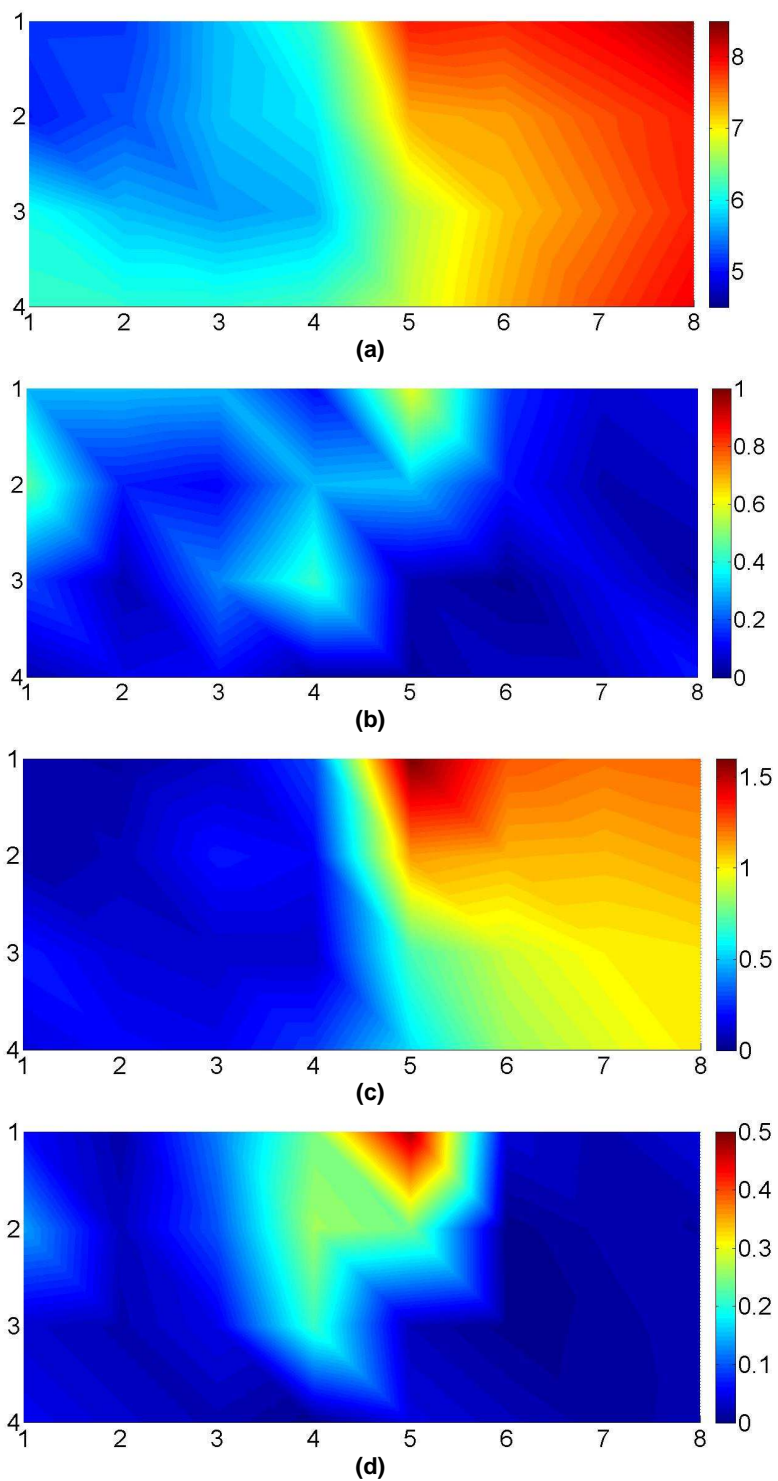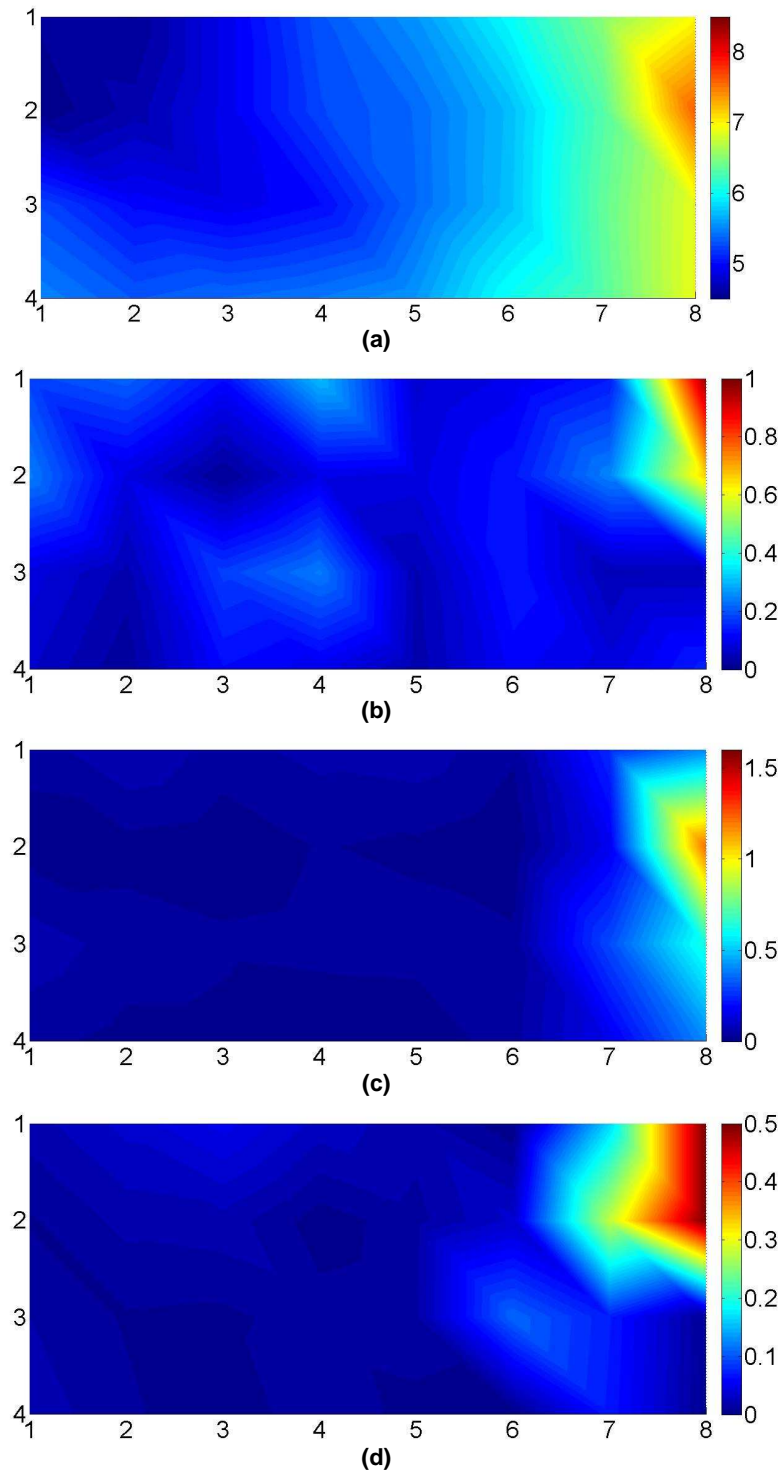**Figure 46: Experiment with multiple cuts introduced to the textile.**

Figure 47: Multi-cut experimental results. (a) Resistance measurements, (b) discrete Laplacian of resistance measurements, (c) difference between measurements and calibration, (d) discrete Laplacian of difference between calibration and resistance measurements.

The final experiment conducted was to analyze the presence of a hole in the fabric. This hole could be a result of a bullet wound if applied to combat wound detection applications. As visible in Figure 48, the size of this hole is large as related to the density of measurement probes. Figure 49(a)–(d) illustrates the results of a cut of this shape. It is interesting to note that the detection of a hole in this location is similar to the detection of a vertical cut but of far less intensity. This similarity is attributed to the probing point density. The resistance measurements affected by this cut are similar to those measurements affected by the presence of a vertical cut. By increasing the density of probing locations, it is believed that a smaller hole could be detected. The intensity of the hole shown in Figure 49(c) is far less than the high-intensity levels of the vertical cut in Figure 43(c). Further analysis and resolution could help to ascertain the difference between a vertical cut and a hole.
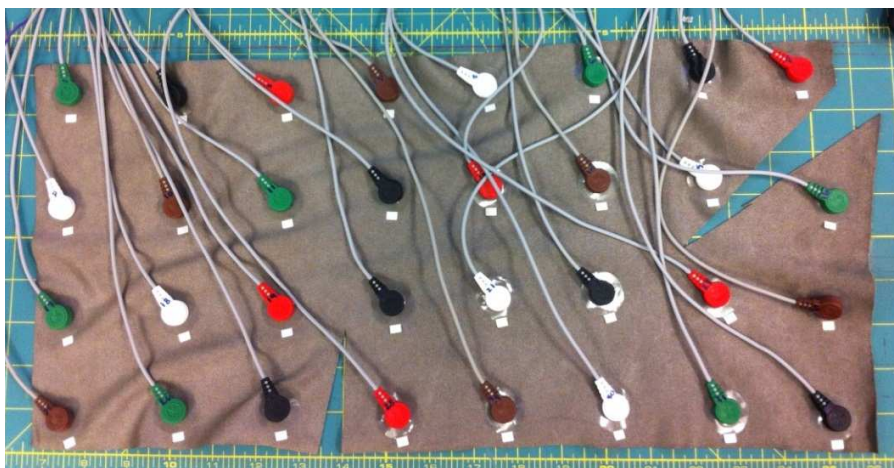

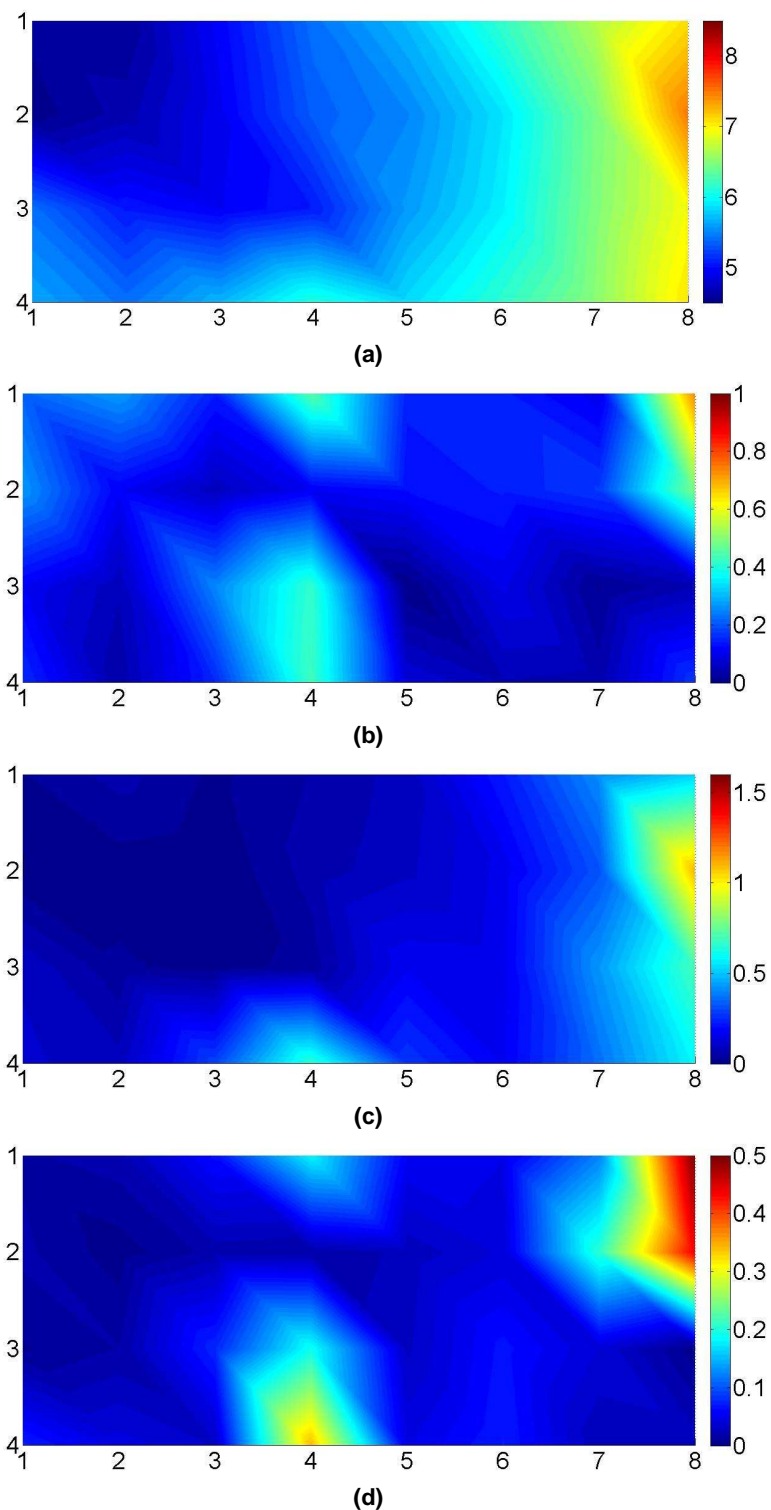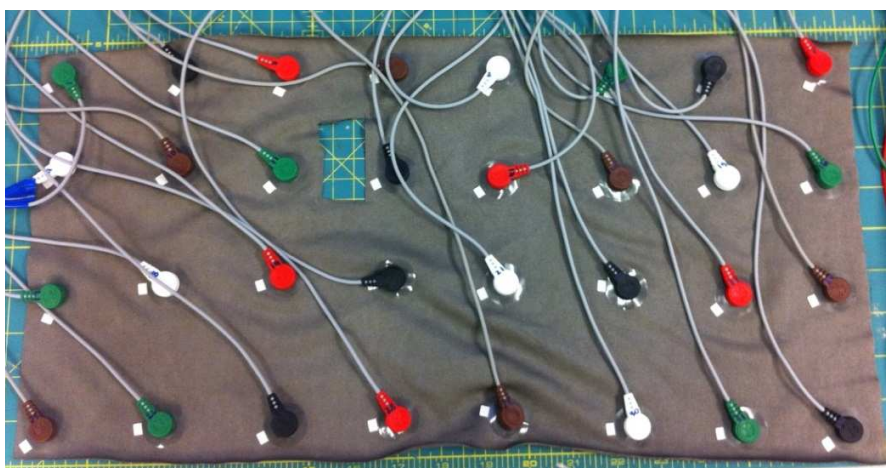
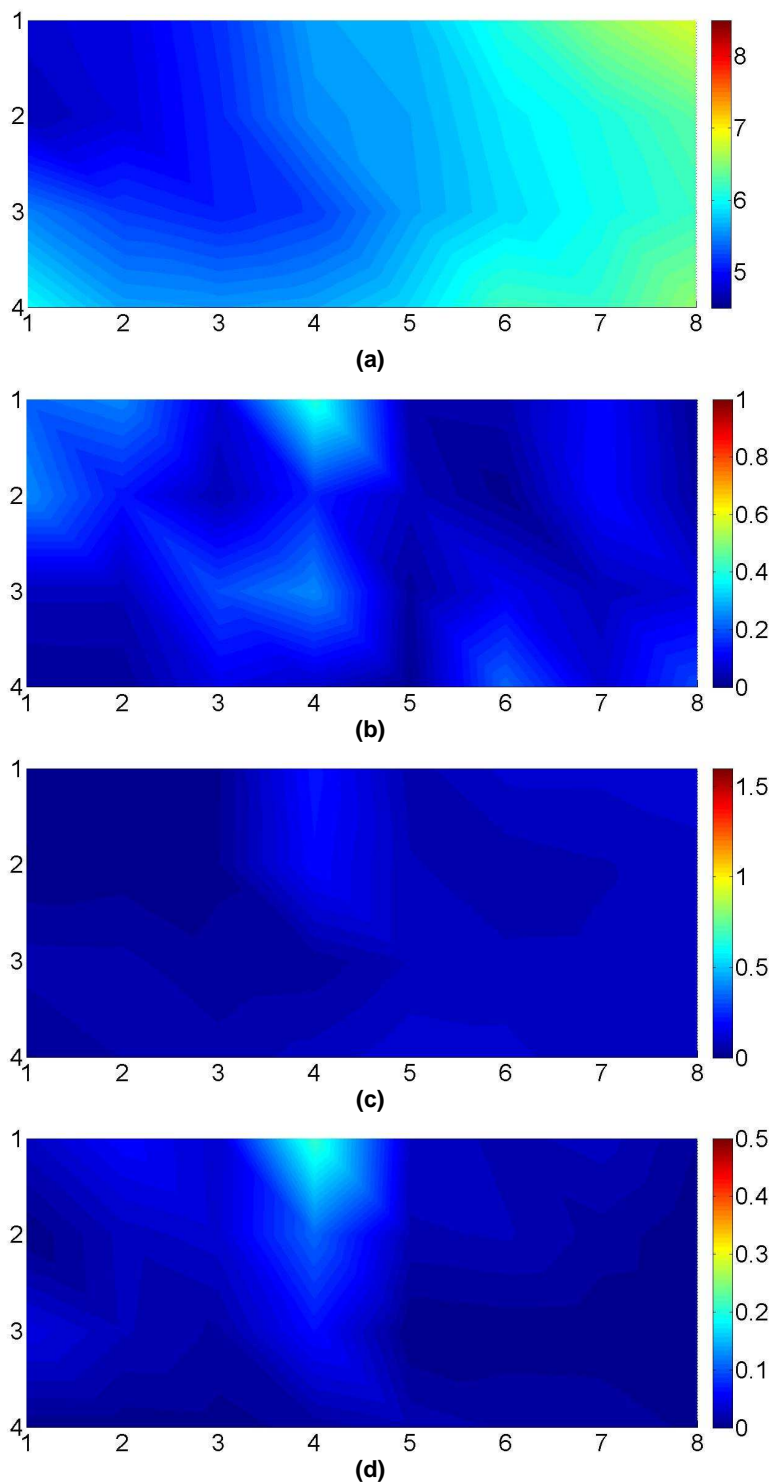**Figure 48: Experiment with a hole introduced to the textile.**

Figure 49: Hole experimental results. (a) Resistance measurements, (b) discrete Laplacian of resistance measurements, (c) difference between measurements and calibration, (d) discrete Laplacian of difference between calibration and resistance measurements.

Overall, it is evident that this detection method is accurate for detecting the presence of cuts and holes within a fabric sample. Localization of these cuts is predictable through simple visual analysis. This capability is evident in the case of the diagonal cut and the multi-cut scenario. In many applications, this level of sensitivity is acceptable. For example, if incorporated into combat wound detection; the approximate location of a bullet wound could still provide myriad information to medical staff. This approximation can allow for a faster response time to treat the affected area as opposed to full diagnosis of the injury upon arrival of the medical staff. It is easy to imagine how this technology could be accurately employed in many applications.

Variability Assessment

For the application of this technology to become realistic, the data must be accurately validated and proven to provide consistent information. If a soldier had a more serious wound than was reported by the combat wound detection system, the effective medical response time could increase owing to a lack of preparation. To ensure that data collected in this second-generation sensing system are valid, a variability assessment was performed. This experiment compared collected data to a normal distribution to help evaluate the potential sources of error. The first experiment averaged 20,000 samples for each cycle and completed 1,000 cycles. As Figure 50 suggests, the data follow the trend of a normal distribution. Variation from this normal distribution can be seen in the outlying points. Figure 51 plots these same data as a histogram and compares the shape of the collected data to a Gaussian curve. Again, the general trend is approximately equivalent. The bars represent the number of

samples collected into each bin as represented by a range of resistance values. The variation in the location of each bin is minimal; with a standard deviation of only 0.0026Ω about a mean of 5.7277Ω and range of 0.0127Ω.
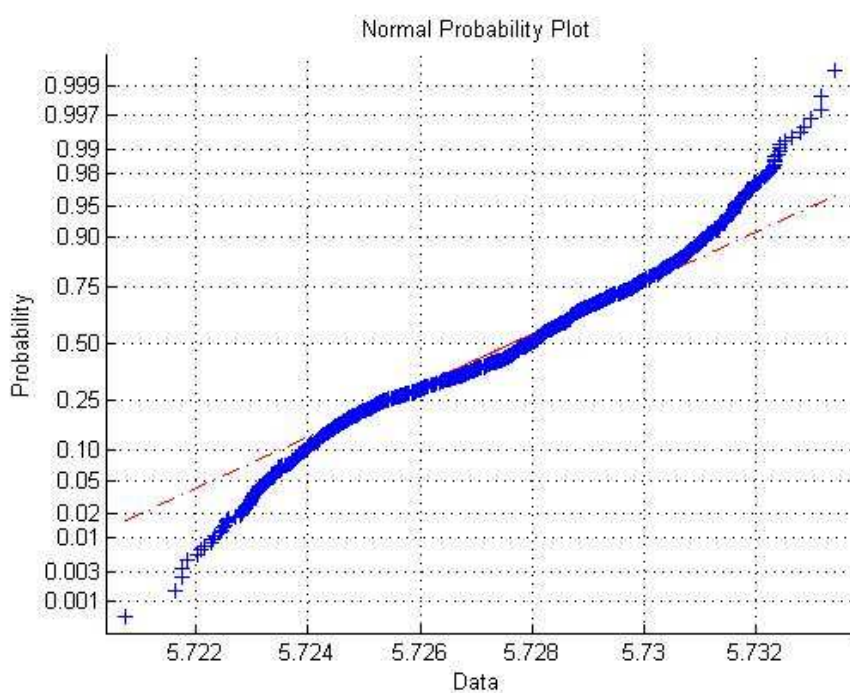
Figure 50: Comparing the collected data (blue) with a normal probability distribution (red) for 1,000 cycles.
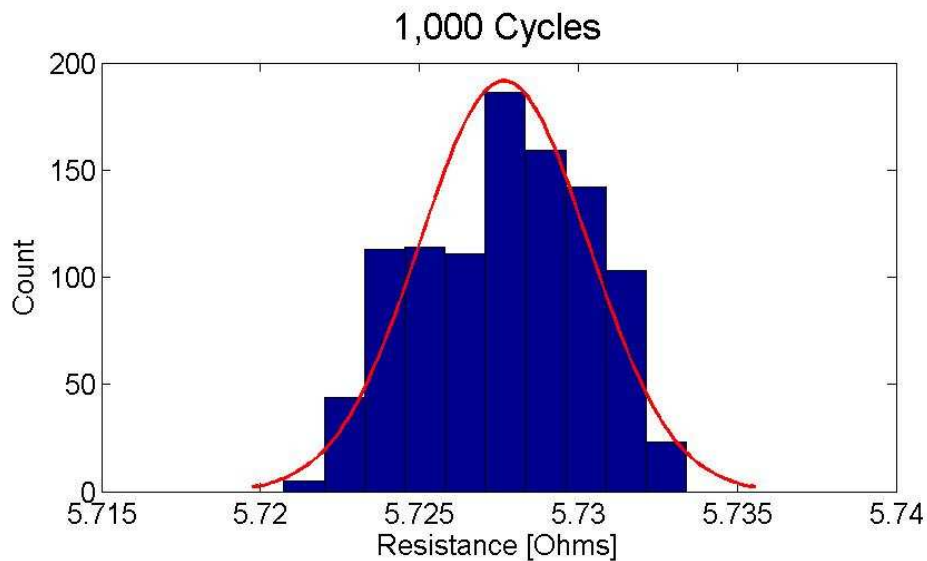
Figure 51: Histogram plot of collected resistance data (blue) versus a normal probability distribution (red) for 1,000 cycles.

With a goal to improve the accuracy of describing this data set as a normal distribution, a second, more extended experiment was conducted. This time, each data point was averaged over 20,000 samples for 10,000 cycles. The data collected throughout this experiment, ideally, becomes more accurately described by the normal probability distribution with allowance for some variation due to the inconsistencies of the conductive textile metallization process and the unfamiliarity with how the resistance of the textile varies with time. However, there is some fluctuation evident still on the high end of the resistance measurement data. The results of these experiments can be found in Figure 52 and Figure 53. The presented data follows the same outline as that presented for the condensed data set described above. For the case of 10,000 samples, the collected data had a standard deviation of 0.0057Ω about a mean of 5.6785Ω
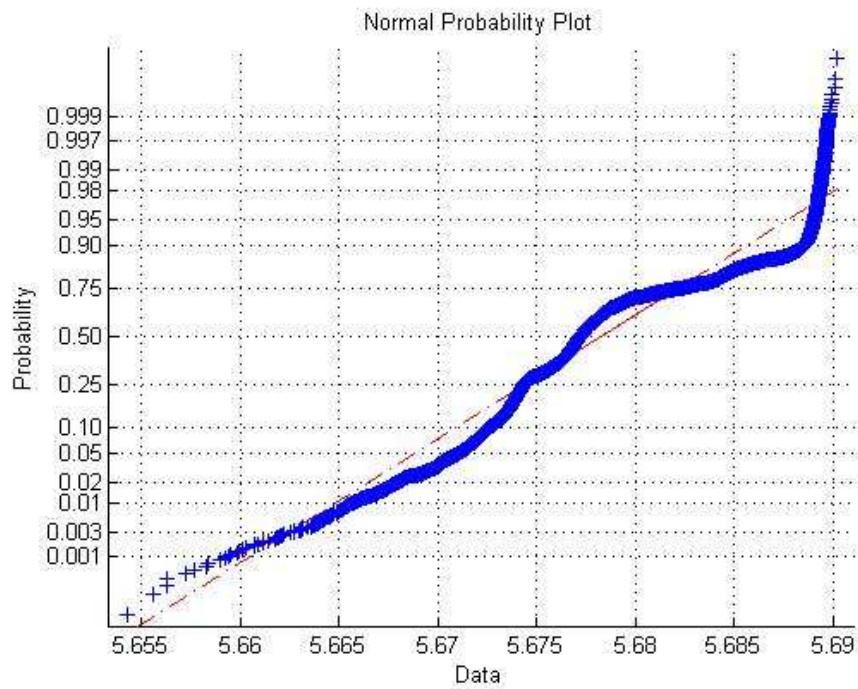
Figure 52: Comparing the collected data (blue) with a normal probability distribution (red) for 10,000 cycles.
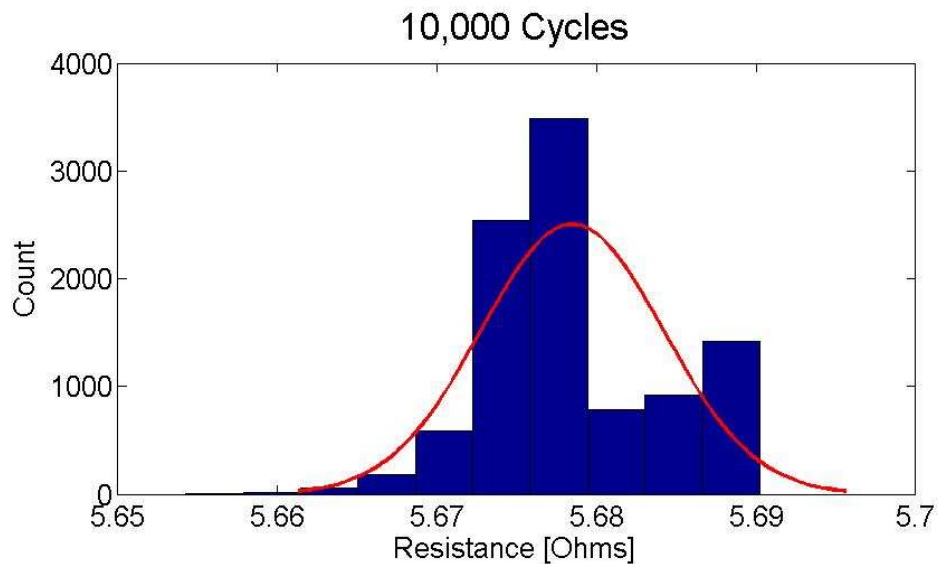
Figure 53: Histogram plot of collected resistance data (blue) versus a normal probability distribution (red) for 10,000 cycles.

and a range of 0.0360Ω. It is evident by looking at the comparison between the histogram data and the Gaussian fit curve that the data collected appears to less likely fit a normal distribution in this experiment. An attempt to understand this discrepancy resulted in measuring the drift in resistance over time.

The resistance data collected during the 10,000 cycle run is also plotted in Figure 54 versus sample count. This figure illustrates the drift over time of the measured resistance from point A to point B. These samples were taken over a time period of approximately 15 minutes. As the histogram in Figure 53 verifies, there is a drift to higher resistance over time. This drift results in a distribution that does not closely follow a normal curve. Without certainty in data collection, the false alarm rate in detecting the presence of penetrations based on resistive changes may be high. To eliminate the effects the time-based resistance variation may have on the false alarm rate, more frequent calibration is suggested. The calibration rate should be application specific; if the application is sensitive to 30mΩ changes in resistance, then the system should be recalibrated often so that the drift does not reach this level. Recalibrating too often will result in the hiding of true penetrations, however. For example, if a penetration occurs at time A but the system is recalibrated at times A-δ and A+δ, the results indicating penetration will only be visible for times A < t < A+δ. It is possible that this drift is a result of the data acquisition system's internal analog-to-digital converter or other electronic components used in the data acquisition process.
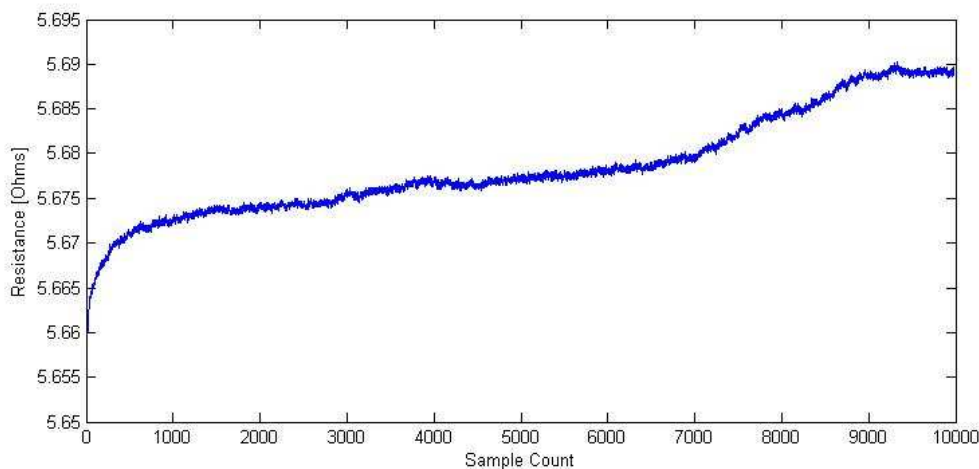
Figure 54: Resistance drift over time collected for one point-to-point resistance measurement.

Before combat wound detection and localization technology can be fully implemented into a prototype, some issues need to be addressed. First, the copious amount of wires extending from the electrodes would need to be replaced with traces printed on or created out of textiles materials. Similarly, the data acquisition system would need to be developed on a small scale using a microcontroller with adequate sampling speeds for real-time analysis and enough analog precision to not mask small perturbations in resistance. If these items are addressed, it would be possible to develop an accurate prototype to use in combat wound detection applications. Future work to improve this technology is discussed in Chapter VI.

CHAPTER V: Using Conductive Textiles for Microwave Applications

In addition to their employment as a distributed fabric-based sensor, conductive textiles can also be applied to microwave applications. In these applications, the textiles can operate as a wireless transmitting device. Numerous antennae can be developed through the adhesion of conductive textiles to a dielectric fabric using the iron-on process discussed in Chapter III. Alternately, printing methods can be used to directly print metal onto textile surface through ink-jet printing or screen printing. Additionally, this process can be applied to developed substrate integrated waveguides for signal transmission. In order for these antennas to correlate with the simulated designs, these textile materials must be accurately characterized and precisely defined through the fabrication process.

Precise Antenna Fabrication Using a Laser Cutter

This thesis presents a low-cost method for fabricating textile antennas which offers higher precision than those previously developed through manual means. Traditionally, the fabrication process involves manually cutting the antenna patterns with a sharp knife or scalpel as discussed in the literature review of Chapter II. The proposed process, however, employs a laser cutter to accurately realize the antenna dimensions. Then, the textile layers are glued together using an iron-on process defined in Chapter III. This process is similar to those mentioned in literature.

The laser cutter technique can achieve high precision line widths, down to 0.5 mm. After designing the antenna with Ansoft's High Frequency Structure Simulator

(HFSS), it is exported to the laser cutter, which systematically cuts each layer of the antenna. The layers can then be assembled as mentioned. To meet the antenna fabrication needs of this research, the Epilog Zing 24 Laser System was utilized. Figure 55 illustrates this machine cutting various monopole designs, which were developed and tested for ultra-wideband (UWB) applications as discussed below.

The Epilog Zing 24 laser cutter is capable of cutting a variety of materials such as textiles, wood, glass, and metal. Strict size limitations do exist with this machine, however. The maximum allowable continuous antenna design cannot exceed 24" x 12". Additionally, the maximum material thickness cannot exceed 7.75". Thickness limitations are irrelevant to this research since textiles are being laser defined layer by layer. This fabrication process offers a quick, effective solution for cutting textile antennas. Within a few minutes, a complicated design can be accurately defined and the system can be ready to prepare another prototype. User-defined parameters that allow for varying scales of precision include adjustable dot density (100 to 1000 dots per inch [dpi]) and adjustable speed and laser power (from 1 to 100 percent). Using this machine, an 8-element microstrip-fed patch array can be laser cut in approximately five minutes at a 500dpi setting with 40% power, and 25% speed. This design, due to its' complexity, was not able to be accurately glued to the dielectric material. In future antenna designs, support bars were incorporated to stabilize the design during transport and assembly. Settings of 500 dpi, 40% power, and 25% speed were used to define the antennas presented throughout this chapter.
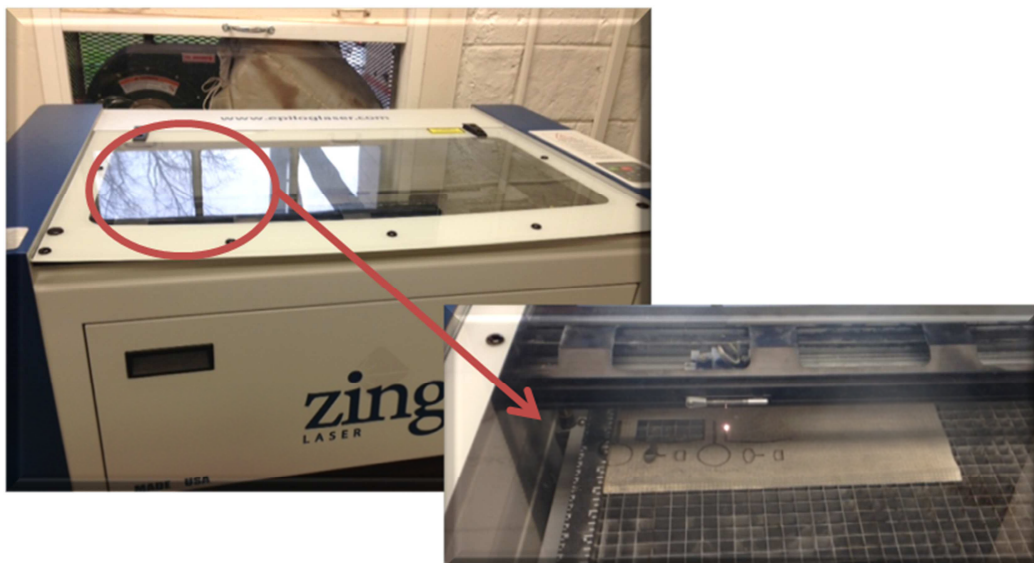
Figure 55: Epilog Zing 24 laser system used to accurately define antenna designs.

In addition to accurately defining antennas by using lasers, this thesis demonstrates the ability to sew conductive vias into the designs through the use of conductive thread and a simple sewing machine. The sewing machine allows for variations in stitch type, stitch length, and stitch width which promote the use of this automated technique for via implementation in the development of substrate integrated waveguide designs for signal transmission. After fabricating the antenna designs and assembling them using the iron-on process, an SMA connector is attached to the feeding point with the two-part conductive epoxy. As more antenna designs were tested, it became evident that this method of securing the connector would not suffice as the connectors could easily slip off the fabric during testing. Silicon hot-glue was layered onto the connector and textiles following the placement of the SMA connector

on the antenna design using the conductive epoxy. This technique provided enhanced stability for the SMA connector for handling and testing.

Fabric Characterization

To develop functional antenna designs from textile materials, the textiles need to be accurately characterized. Specifically, the dielectric permittivity and loss tangent must be known, as the value of these dictate the antenna designs. In order to characterize the textile materials, a patch antenna was developed. The experiment suggested by Sankaralingam and Gupta [51] was used to extract the permittivity of the cordura substrate. The proposed technique used the patch antenna design equations to back-calculate the effective permittivity given the return loss characteristics of a fabricated patch antenna. The loss tangent can be approximated similarly. It can be reasonably determined by matching the width of the return loss peak in simulation with the width of the measured results; i.e. comparing the Q's. This approach does produce some error, however. It assumes that the majority of the loss comes from the dielectric and that a limited amount comes from the metal conductive layers. If these layers attribute to the loss of the antenna significantly, then the loss tangent value derived from this experiment will be significantly skewed.

Based on the extracted permittivity and loss tangent results of various textile materials presented by Ouyang [50], the design of a patch antenna considered a loss tangent of 0.0098 and a relative permittivity of 1.90 as a starting point. Following the fabrication and testing of this antenna, it was shown that the relative permittivity is better

estimated as 2.05. Similarly, the loss is projected to be approximately 1.5× greater than that predicted by Ouyang. While the results generated by Ouyang may be accurate for cordura alone, they do not take into account the adhesive layers employed to secure the fabric layers together. These adhesive layers alter the electrical characteristics of the dielectric to produce the results of the patch experiment. Figure 56 illustrates these results. As shown, the simulated peak coordinates well with the measured values. The loss tangent is difficult to predict with this method because changing the loss tangent in simulation affects not only the width of the return loss peak but also the depth of the peak. A balance between the conductivity of the top and bottom textile layers, assumed to be 200,000 S/m based on manufacturer specifications, and the appropriate permittivity and loss tangent of the dielectric will yield the most precise results. Additionally, the connector losses and losses generated due to misalignment in the fabrication process were not considered in simulation.
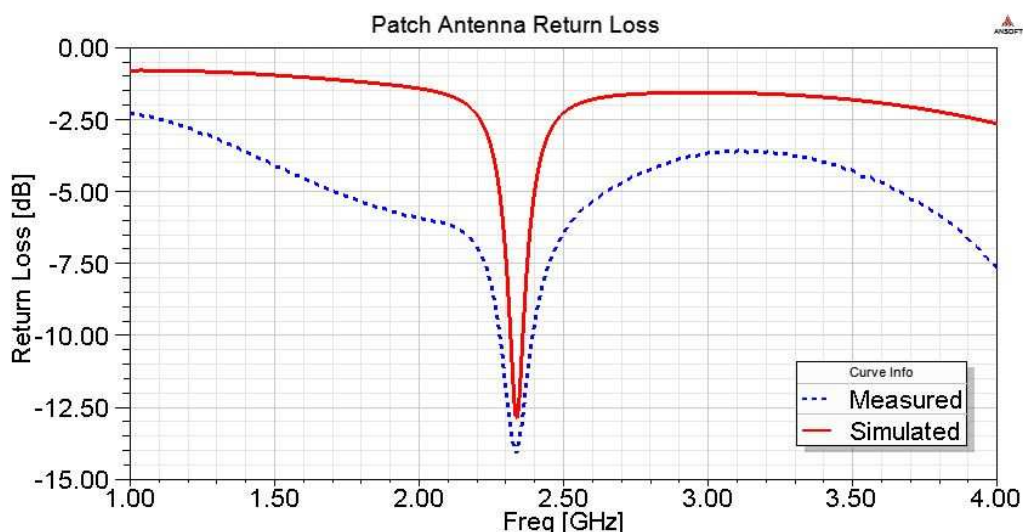
Figure 56: Patch antenna results for fabric characterization.

Demonstration of Multilayer Capability

Once the appropriate electrical parameters of the conductive textile and dielectric layers had been extracted, further antenna development ensued. Even though line widths of 0.5 mm can be achieved through the laser cutting process, the handling of these thin textiles becomes quite difficult. Instead, the designs presented use more conservative dimensions with minimum widths greater than 1 mm. To illustrate both the capability of the laser cutter as well as the ability for conductive textiles to be used to implement multilayer antenna arrays, a wideband slot antenna was developed. This antenna utilized a similarly shaped feeding structure to achieve wideband performance. This shaped feeding technique was previously described by Liu et al. [59]. This design requires double side definition.

The antenna was designed in Ansoft's HFSS and operates with a bandwidth of approximately 4.81:1. The simulation model of the single-element slot antenna is shown in Figure 57. The fabricated antenna is shown in Figure 58. Swift Textile Metalizing's conductive 3NiAg Nylon Rip Stop, along with nylon cordura dielectric, were used during fabrication of the slot antenna. Differences between simulation and measurement results could be caused by inaccuracies in the fabrication process. The fabrication of this slot antenna requires that the feed be placed directly in the center of the substrate while the feed structure clears the edge of the slot by just a few millimeters. In practice, ensuring spacing of only a few millimeters is difficult.
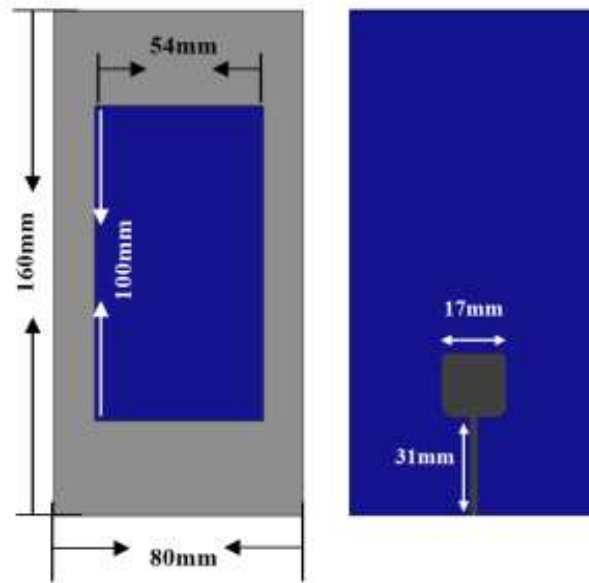
Figure 57: Simulation model of single-element wideband slot antenna.
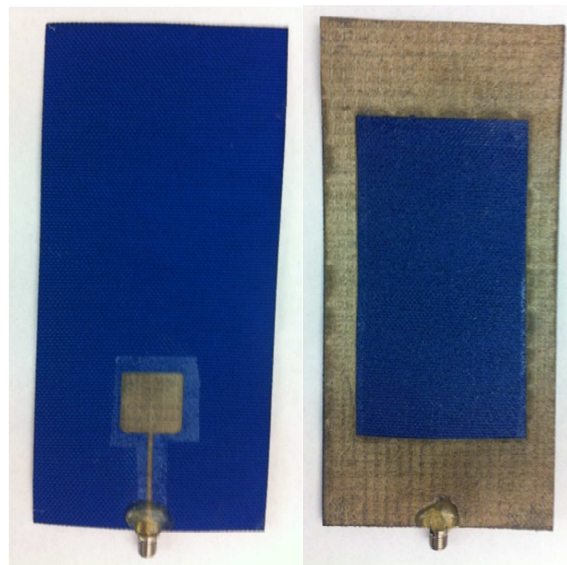
Figure 58: Fabricated single-element wideband slot antenna.

The range of operation for the single-element slot antenna is shown to be approximately 1.5 GHz to 6 GHz. This range of operation is illustrated in the return loss plot of Figure 59. The general trend of the simulated return loss plot agrees well with the return loss measurements. The radiation patterns at discrete frequencies of 2 GHz, 3.5 GHz, and 5 GHz are presented in Figure 60 through Figure 62 with comparison between the E and H planes as well as between simulation and measurement. The radiation pattern shapes correspond well with simulation. The primary difference between the measured radiation patterns and those simulated occur in the Phi = 90° plane. In these plots, the simulation suggests a squeezing of the pattern in the horizontal plane, whereas this is not evident to the same degree in measurement. These anomalies could be a result of improper alignment with the horn antenna as the textile antenna revolves in the anechoic chamber. These differences, however, are acceptable as the goal of
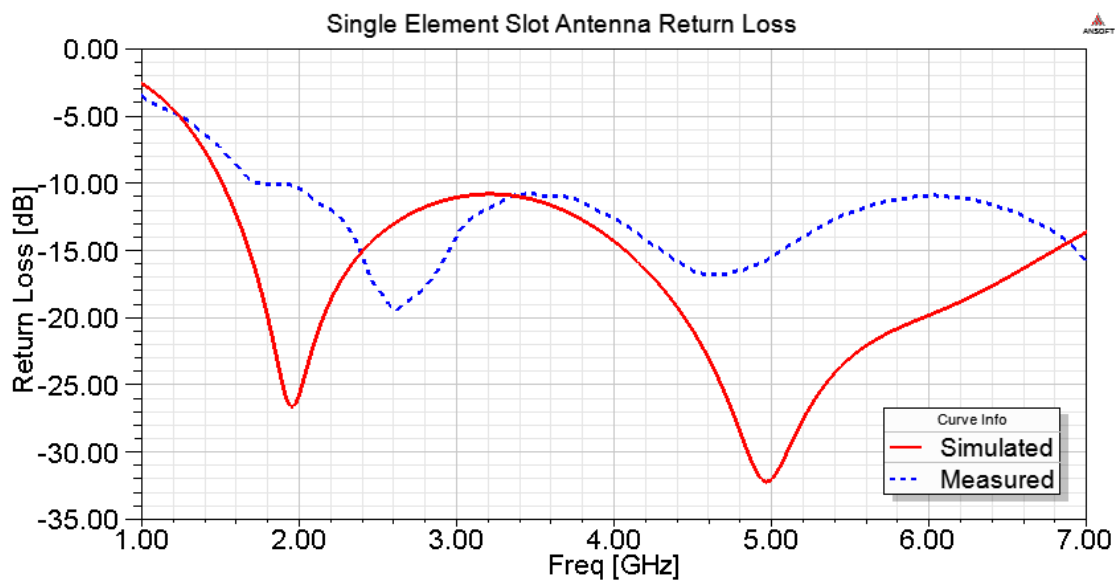
Figure 59: Single-element slot antenna return loss.

Single Element Slot 2GHz Phi=0deg

Single Element Slot 2GHz Phi=90deg

(a)

(b)

Figure 60: Radiation patterns at 2 GHz. (a) Phi = 0°; (b) Phi = 90°. Red, simulation; blue, measured.

Single Element Slot 3.5GHz Phi=0deg

Single Element Slot 3.5GHz Phi=90deg

(a)

(b)

Figure 61: Radiation patterns at 3.5 GHz. (a) Phi = 0°; (b) Phi = 90°. Red, simulation; blue, measured.

Single Element Slot 5GHz Phi=0deg

Single Element Slot 5GHz Phi=90deg

(a)

(b)

Figure 62: Radiation patterns at 5 GHz. (a) Phi = 0°; (b) Phi = 90°. Red, simulation; blue, measured.

simulation is to provide an estimation of the actual antenna performance. If all losses were accurately taken into account in addition to the antenna being placed in an appropriate simulation environment, the measurements and simulation results could better agree with one another. The second difference appears in the radiation pattern null locations. The measured nulls are not always as deep as the simulated nulls. This discrepancy is attributed to the difficulty in exactly aligning the center of the horn antenna with the center of rotation and the central radiating point of the antenna under test. Slight misalignments suggest that the exact Phi = 90° plane is not being measured. Waviness of the antenna under test as it is revolved in the anechoic chamber can also be a source of error during measurements.

Following the development and validation of a single-element slot antenna, a two-element slot antenna array was developed to demonstrate the fabrication capability for relatively larger fabric areas. A picture of this fabricated antenna can be seen in Figure 63. Difficulty was encountered in the fabrication process of this antenna owing to the intricate feed structure seen in Figure 63. The spacing and straightness of the feed lines are important parameters for antenna design. Discrepancies existing between simulation and measurement are likely a result of these inaccuracies. The return loss of the two-element slot array is shown in Figure 64. There is good agreement between the simulation and measurement for this antenna design over the frequency range of operation, from approximately 1.5 GHz to 6 GHz. To correlate with the single-element slot results, the radiation patterns are again presented at 2 GHz, 3.5 GHz, and 5 GHz and are shown in Figure 65, Figure 66, and Figure 67, respectively.

Figure 63: Fabricated two-element slot antenna array.
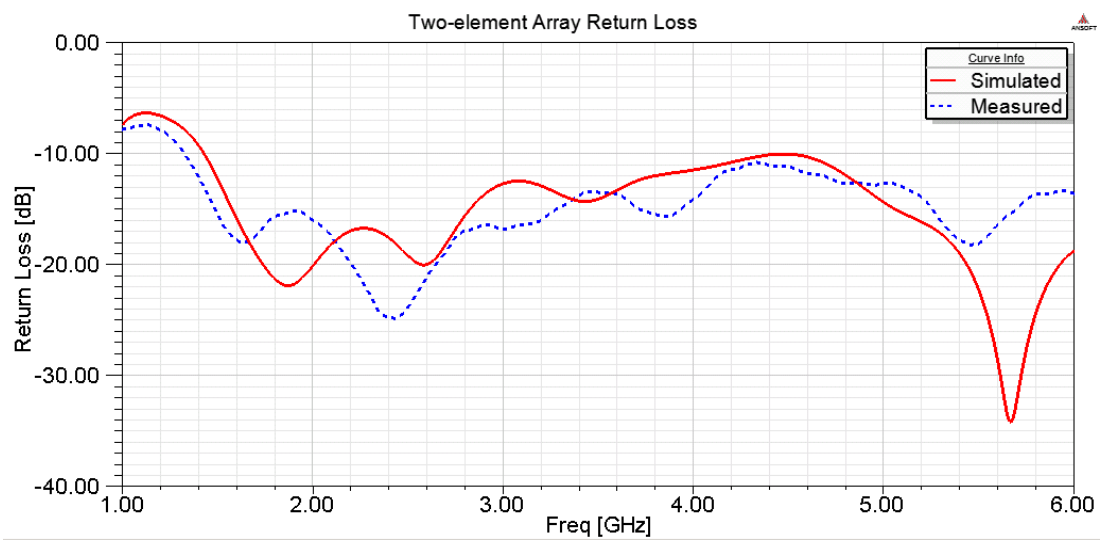
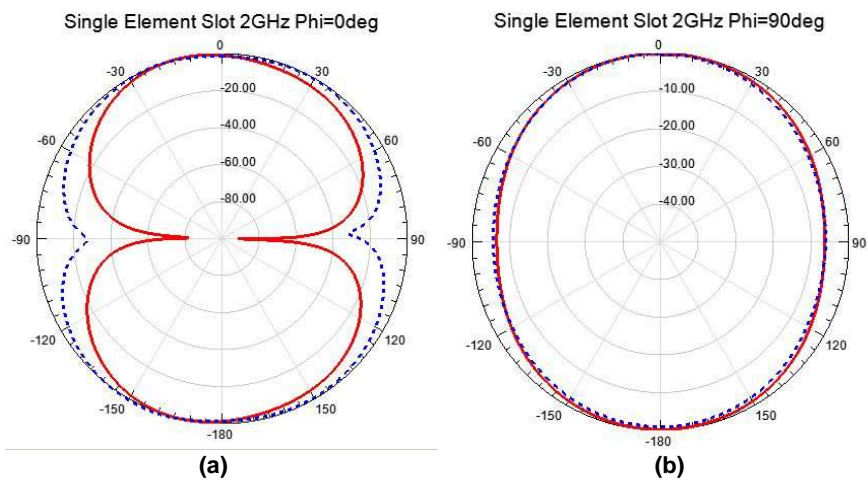**Figure 64: Return loss of two-element slot antenna array.**
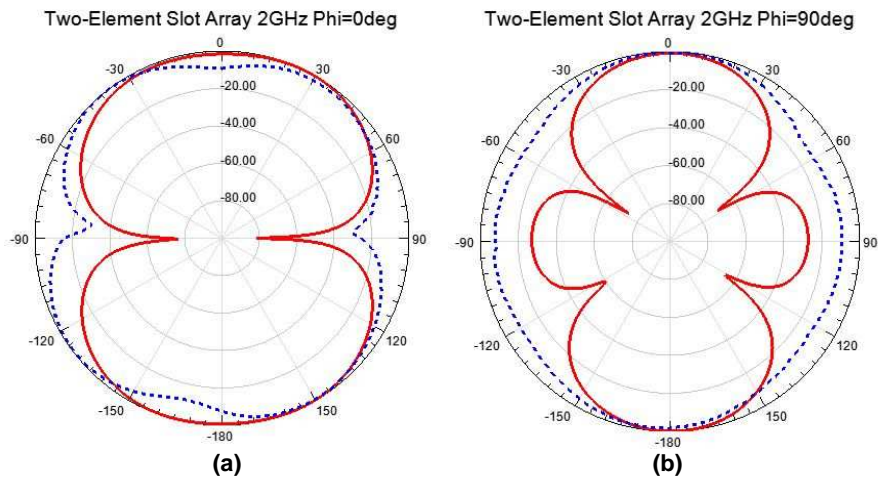
Figure 65: Radiation patterns at 2 GHz. (a) Phi = 0°; (b) Phi = 90°. Red, simulation; blue, measured.
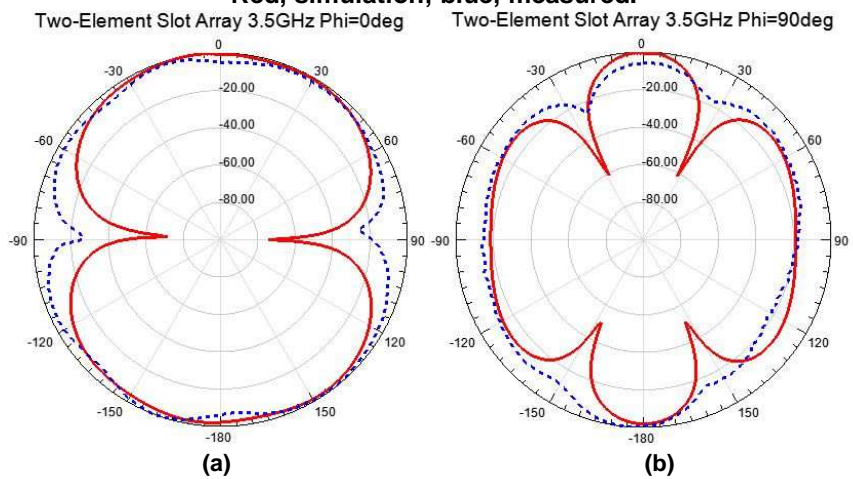
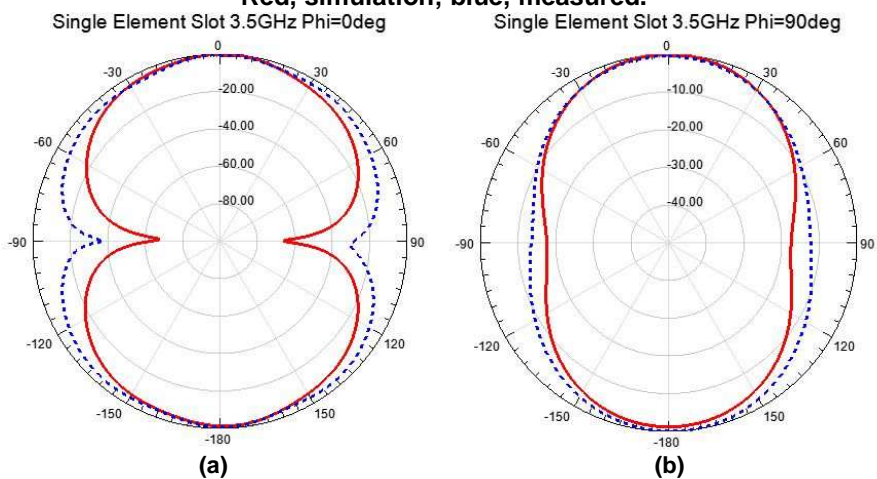**Figure 66: Radiation patterns at 3.5 GHz. (a) Phi = 0°; (b) Phi = 90°. Red, simulation; blue, measured.**

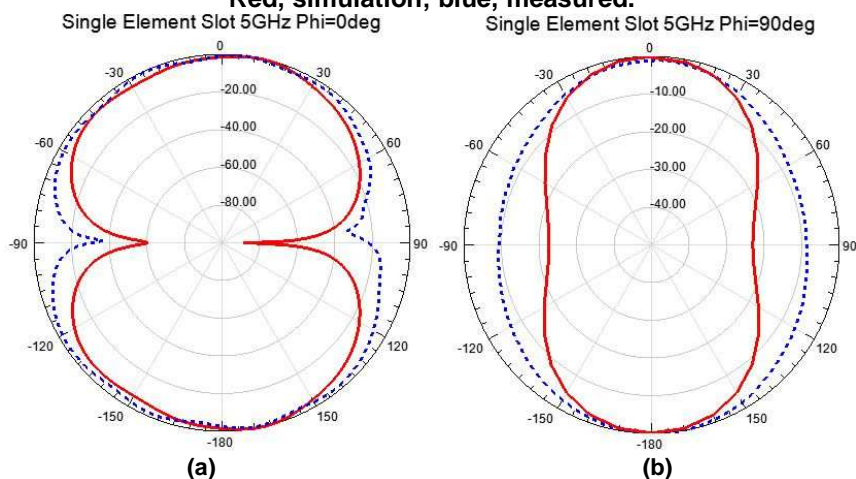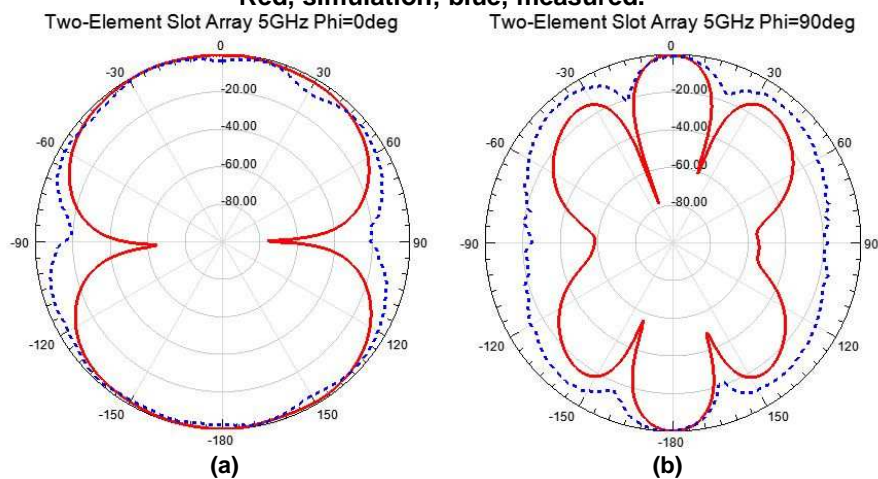**Figure 67: Radiation patterns at 5 GHz. (a) Phi = 0°; (b) Phi = 90°. Red, simulation; blue, measured.**

As with the single-element slot antenna, the two-element slot array differs from the simulated results in some areas. In each case, these differences are a result of the null location and magnitude. Due to misalignment in the chamber between the horn antenna and the textile antenna as the radiation pattern is being measured, the magnitude of these nulls as well as their location can be altered. The flexibility of the textile antennas creates difficulty in ensuring proper alignment as these patterns are measured. The Phi = 90° plane shows greater discrepancy because the size of the two-element slot antenna prohibits it from rotating about the center of the slot antenna feed. Instead, it rotates about the end of the antenna, generating further error.

Ideally, the gain increase resulting from doubling the number of antenna elements is 3 dB. In practice, a gain increase greater than 2 dB is practical for array development when including the feedline insertion loss. Due to the difficulty in the fabrication process, the gain increase illustrated by the two-element slot array did not meet these standards over the frequency range of interest. At 5 GHz, there was a reduction in gain as opposed to an increase. Similarly, the gain increase at 3.5 GHz was only around 0.5 dB. At 2 GHz, the gain increase was more acceptable, increasing by approximately 1.2 dB. More precision in the fabrication process might allow for better results to be obtained in the array comparison. Error in fabrication can lead to mismatched slot antennas. That is to say that the two-element slot antenna may not be a doubled reproduction of the single-element antenna. Barring this certainty, accurate array development and results may not be possible. In simulation, the gain increases between 1 dB and 2 dB for the textile antenna when the conductor boundaries are a

perfect electric conductor and the dielectric loss of the cordura textile is considered. The above investigation validated our capability to fabricate multilayer fabric structures. Better alignment schemes are still required to improve the overall performance of such structures.

Data Transmission

In anticipation of allocating many sensors with different capabilities and functions across the fabric, lots of data can be collected. Processing of these data will require their transmission using wireless links to some central computational centers. Various types of antennas can be used for wireless transmission—for example a patch antenna or a slot antenna can be used for low data rate transmission or ultra wide-band antennas for high data rates transmission.

UWB systems are being used increasingly in a variety of applications. Fortunately, many advances are being made in the realm of conductive textiles and flexible electronics. These textiles can be used as a sensing system as illustrated in Chapter IV or used to implement wearable antennas as discussed in Chapter II. Combining these two applications is attractive for a number of reasons. First, wearable antennas constructed entirely from fabric offer a cost-effective, flexible solution when compared to rigid antennas. UWB technology is similarly attractive for body area network applications due to the low-power operation and low radiated power inherent in its system design.

For demonstration, an UWB textile antenna for wearable applications was developed and tested in an indoor localization system at the University of Tennessee. A monopole antenna was developed using the precision laser cutting capability discussed above in a similar manner to the slot and patch antennas presented. To the best of the author's knowledge, applying textile antennas for use in indoor localization systems has not yet been implemented in research. Much of the previous research relates UWB and textile antennas with body area network applications but not for localization. The developed monopole operates from 1 to 15 GHz according to simulation. This design complies with the Federal Communications Commission UWB frequency band allocation of 3.1–10.6 GHz. Following the development and initial testing of this monopole, it was applied to the indoor localization system at UT to ascertain whether textile antennas cold be used as a means for localization.

Monopole Antenna Design

Many papers have been written on the design of wideband antennas constructed from fabrics. Wideband antenna design approaches and those taken by Zhang [60] are considered to develop a wideband textile monopole antenna for use in UWB localization applications. Figure 68 illustrates this antenna design and the sizing parameters associated with the design. The entire antenna is realized on a fabric patch measuring 60 mm × 70 mm with a total thickness of less than 1 mm for the three layers. With the laser precision cutting machine discussed above and the iron-on adhesive, the monopole antenna is fabricated as shown in Figure 69. This antenna, due to its fabric

Parameter	Size (mm)
L (mm)	70
W (mm)	60
Lms (mm)	32
Lg (mm)	28
R (mm)	14
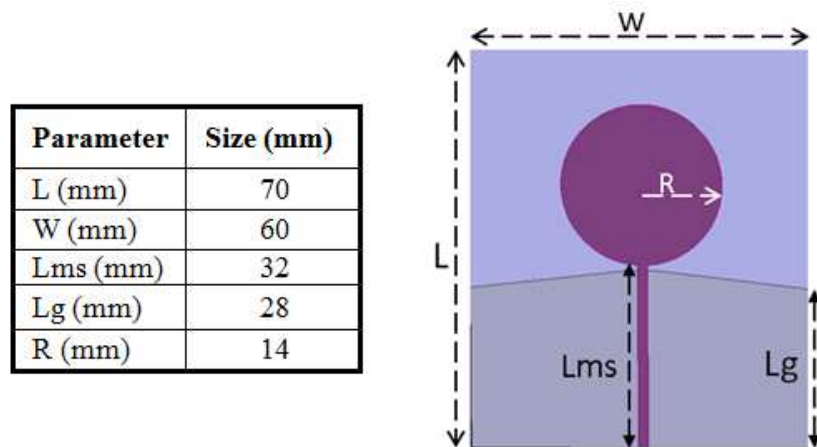
Figure 68: Textile monopole dimensions.
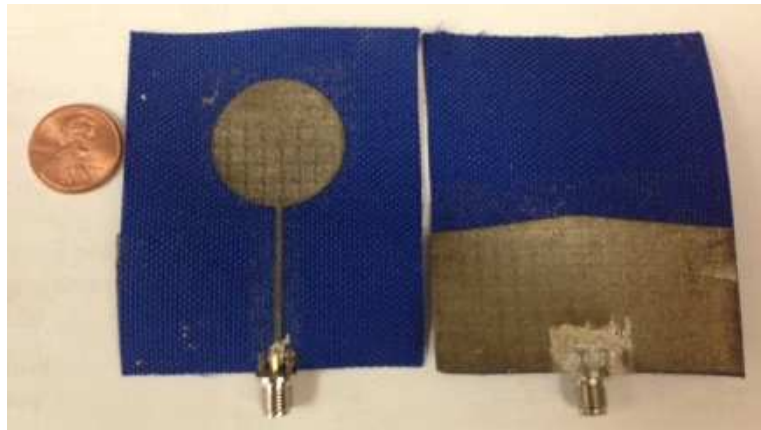
Figure 69: Fabricated UWB textile monopole.

composition and small size can be easily integrated into clothing of a fire-fighter or a soldier, for example.

The measured return loss for this antenna provides acceptable bandwidth for use in the localization experiment. The current localization system functions in a frequency

range of 5–9 GHz. As shown in Figure 70, this monopole design has acceptable return loss over the range 2–11GHz. This agrees well with the bandwidth of the simulated antenna from 1–15 GHz. Figure 71 and Figure 72 compare the radiation patterns of the monopole antenna at 3 GHz and 6 GHz.
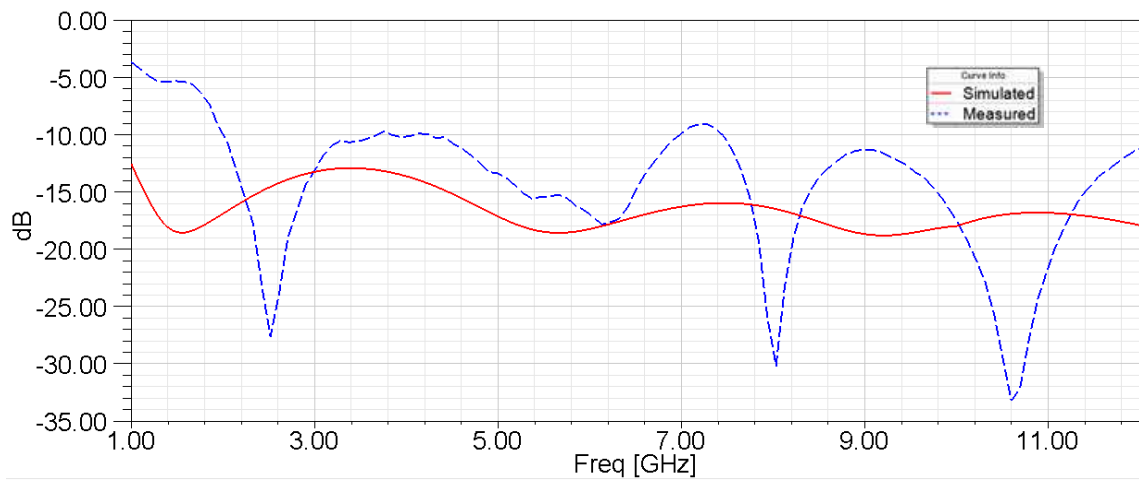
Figure 70: Simulated and measured monopole return loss.
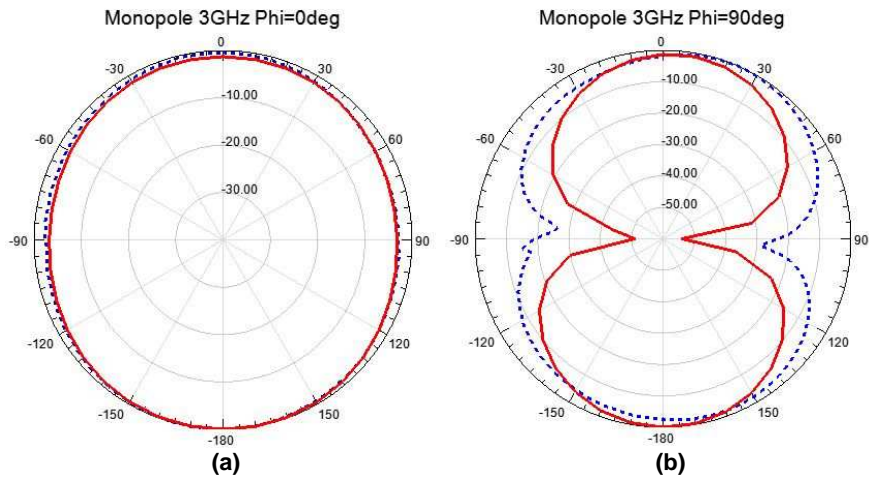
**Figure 71: Radiation patterns at 3 GHz. (a) Phi = 0°, (b) Phi = 90°.
Red, simulation; blue, measured.**
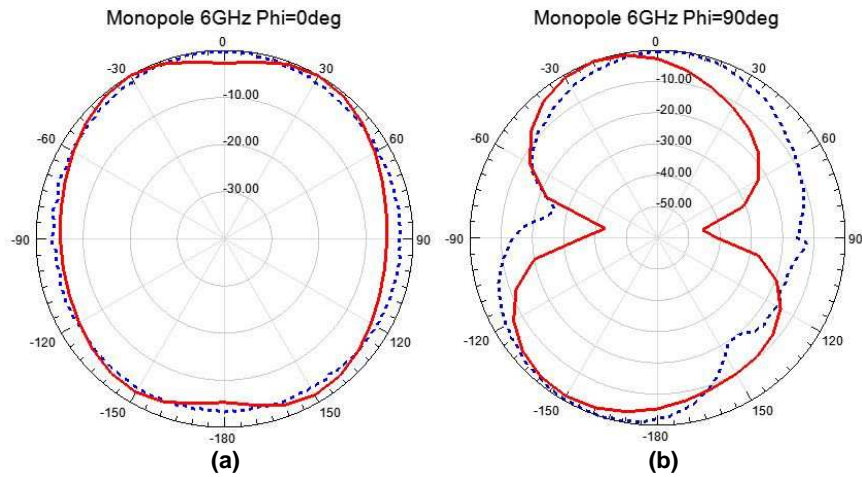
**Figure 72: Radiation patterns at 6 GHz. (a) Phi = 0°, (b) Phi = 90°.
Red, simulation; blue, measured.**

Monopole Localization Experiment

After fabricating and testing the functionality of the monopole design, the antenna was applied to an indoor localization system employing this fabric antenna as a part of a transmitting tag. The goal of this experiment was to analyze the potential of textile antennas for human movement tracking. The localization system discussed by Kuhn [61] uses a tag that transmits a UWB pulse with full-width at half-amplitude (FWHA) of 300 ps and modulated at a center frequency of 8 GHz. The pulse is received by N base stations and uses the difference in time of arrival to triangulate the tag position. A leading edge algorithm and subsampling is used to recreate the transmitted pulse for localization. Using four antennas, we can track the tag in three dimensions; using more base stations improves signal-to-noise ratio and provides redundancy in localization information. The measurements are verified through comparison to an optical tracking system that has an accuracy of 0.3 mm. A simplified block diagram of the localization system can be seen in Figure 73. The fidelity of the fabric monopole in producing the pulse was first analyzed and compared to the original copper omnidirectional monopole printed on RT/Duroid substrate usually used by the system. This original antenna can be seen in Figure 74.
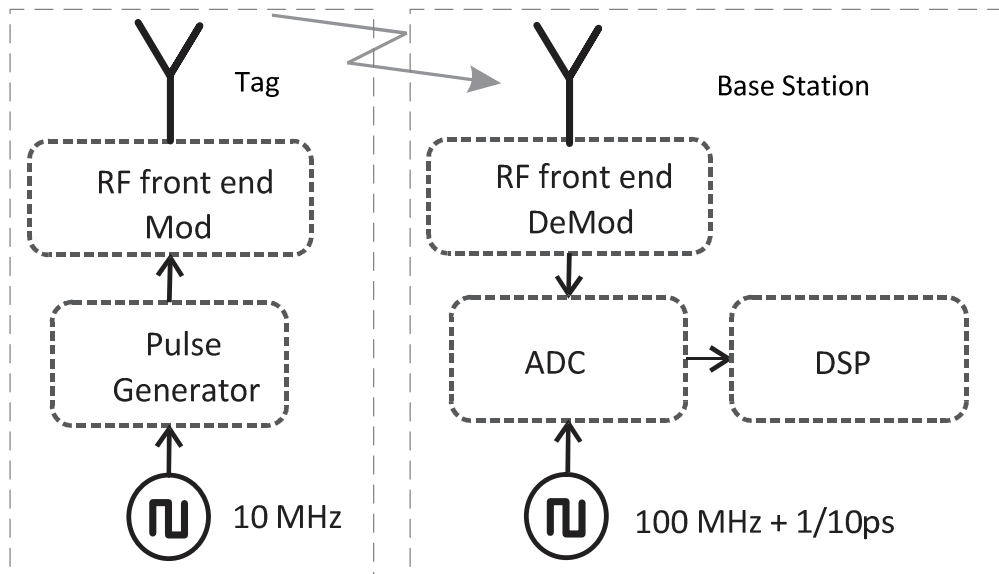
Figure 73: Indoor localization system block diagram.
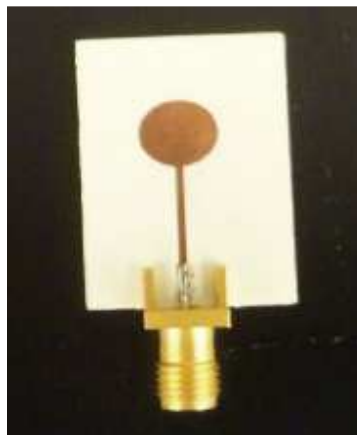
Figure 74: Omnidirectional monopole antenna used in the indoor localization system.

Figure 75 shows three received and down converted pulses: that of the original tag antenna, the fabric monopole, and the fabric monopole placed near the body. We can see the pulses are similar as they have approximately the same width and shape. However, the pulse produced by the fabric antenna in free space is relatively lower. This amplitude drop is expected due to the relatively high loss of the cordura substrate and the moderate conductivity of the conductive fabric. The figure also shows how the pulse is affected when placed against the body. The pulse shape remains similar and has higher amplitude as a result of the constructive interference from the back reflection of the body. The sharpness of the pulse's leading edge, a critical factor for the localization leading edge algorithm, is acceptable for all three cases.
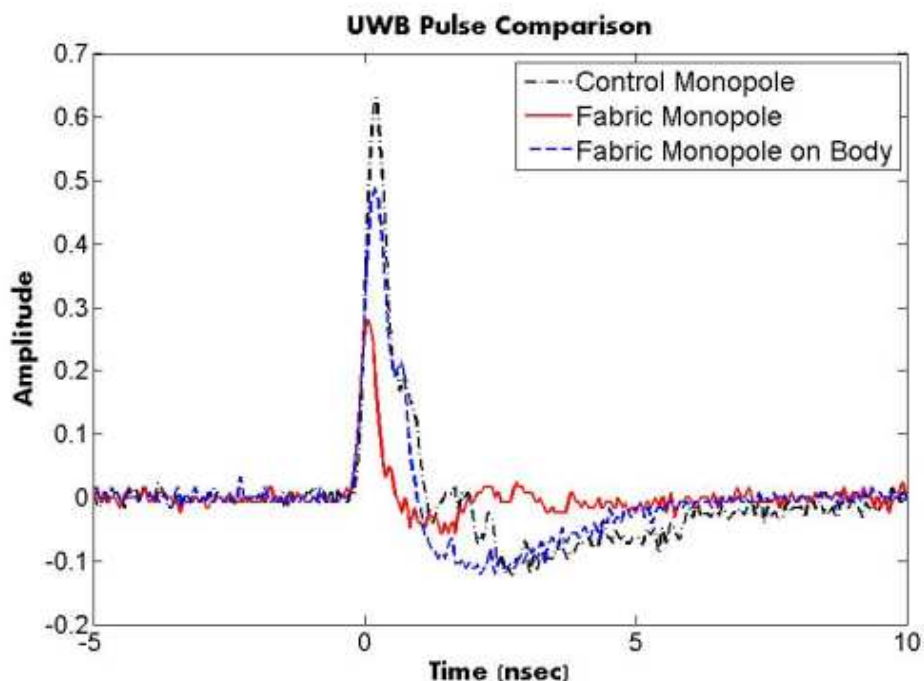
Figure 75: Down converted UWB pulse comparison between the omnidirectional monopole (black dot-dash), the fabric monopole (red solid), and the fabric monopole placed in close proximity to the shoulder (blue dash).

This experiment tracked the tag by use of two base stations for one-dimensional localization. The tag used the fabric monopole as the transmitting antenna. An optical probe was also attached to the tag for use as a reference in comparing the two tracking positions. Calibration was performed to account for the offset distance between the fabric antenna and the optical probe.

The experiment performed real-time tracking to compare the optical sensing system with our fabric monopole. If the distance from the transmitting tag to base station 1 is A and the similar distance to base station 2 is B as shown in Figure 76, Figure 77 shows the difference in distance, B – A, versus the time difference of arrival of base stations A and B. After performing a calibration between the transmitting textile antenna and the optical tracker, the tag was slowly moved so that a comparison between localization systems could be performed. The figure shows a total agreement of the UWB and optical probe with error less than few centimeters. This error becomes more visible as the distance from the base stations increases beyond 5 feet. This can be attributed to a diminishing signal-to-noise ratio with increasing distance due to an
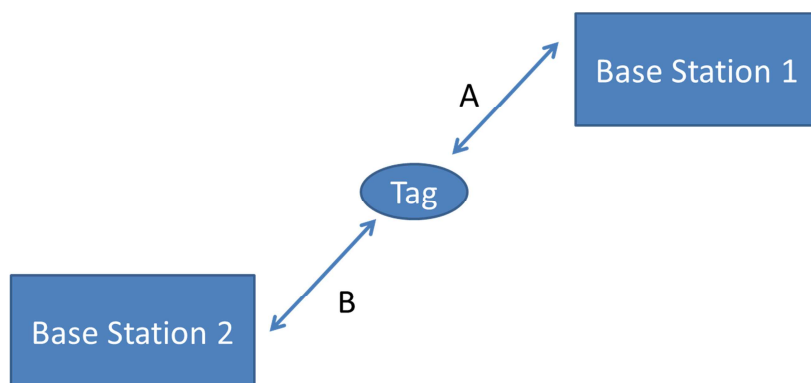
Figure 76: Simplified diagram of indoor localization experiment.
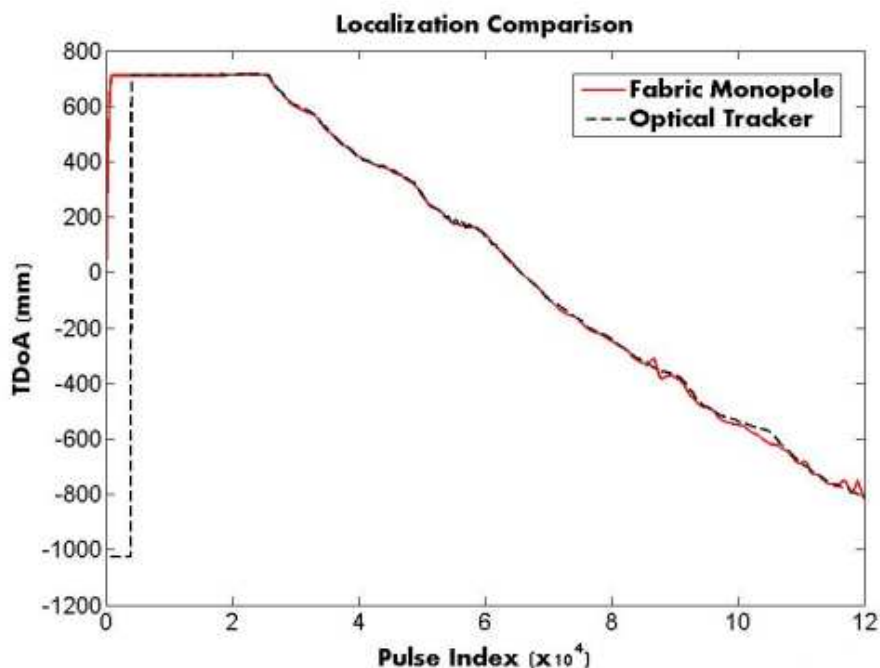
Figure 77: Comparison of optical tracker and fabric monopole accuracy.

input pulse power well below the FCC mask. Further techniques can be applied to further increase this range, including increasing the transmitting power, but still within the FCC power mask. Meter distances can be achieved if we allow for less precision. These results encourage the use of textile antennas in human movement sensing in combat wound detection applications. If appropriate considerations are included, this technology could be expanded and usefully applied to locate victims in the wake of a natural disaster for example.

Conductive Vias Implementation

This thesis also investigates the ability to implement conductive vias in textiles. To maintain the flexibility of the textiles, it is desirable to implement these vias using

conductive threads as opposed to introducing eyelets as suggested by Moro et al. [47]. These vias can be implemented with a sewing machine, which has the added benefit of variable stitch type as well as the stitch width and spacing. These parameters become paramount as the capability of textile substrate integrated waveguides are explored. The capability of the SIW to function properly is entirely dependent on minimizing the spacing between adjacent vias to reduce leakage. The technique presented permits the ability to sew multiple lines, thereby reducing leakage by offsetting the rows of vias. Confirmation that these textile vias accurately connect the top and bottom layers electrically was verified with a digital multi-meter measuring continuity.

Figure 78 illustrates a constructed dog-bone slot antenna with the vias included. Figure 79 better depicts these vias by zooming into the corner of the dog-bone slot antenna. The return loss plot of this antenna is included in Figure 80 followed by the radiation pattern in Figure 81 corresponding to the resonant frequency of the antenna at 2 GHz. As can be seen, the Phi = 90° radiation patt ern squints off the broadside direction. The front-to-back ratio for this antenna is decent with a value of approximately 10 dB. Showing that the inclusion of conductive vias is feasible, this thesis leaves the implementation of SIW technology for future publications.
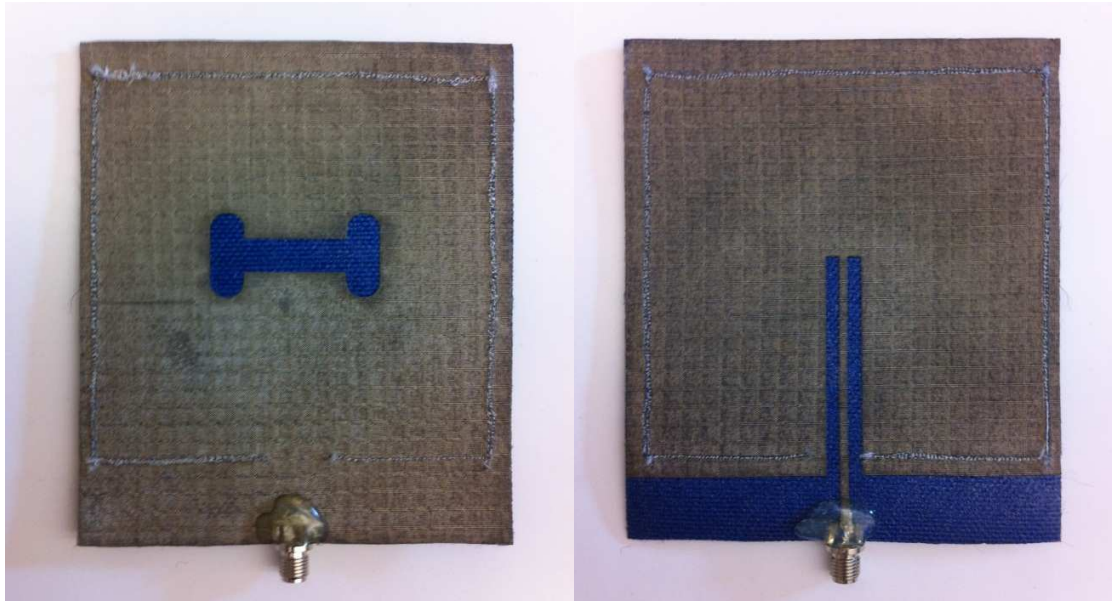
Figure 78: Dog-bone slot antenna implementing conductive vias with conductive thread.

Figure 79: Conductive vias implemented with two rows of closely stitched conductive thread.
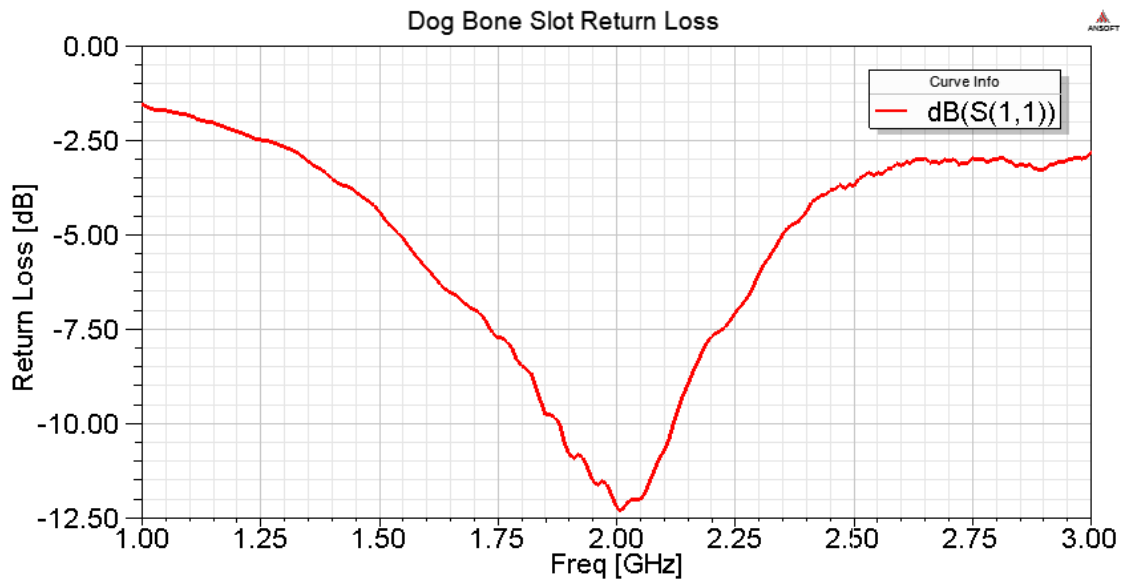
Figure 80: Return loss of the fabricated dog-bone slot antenna.
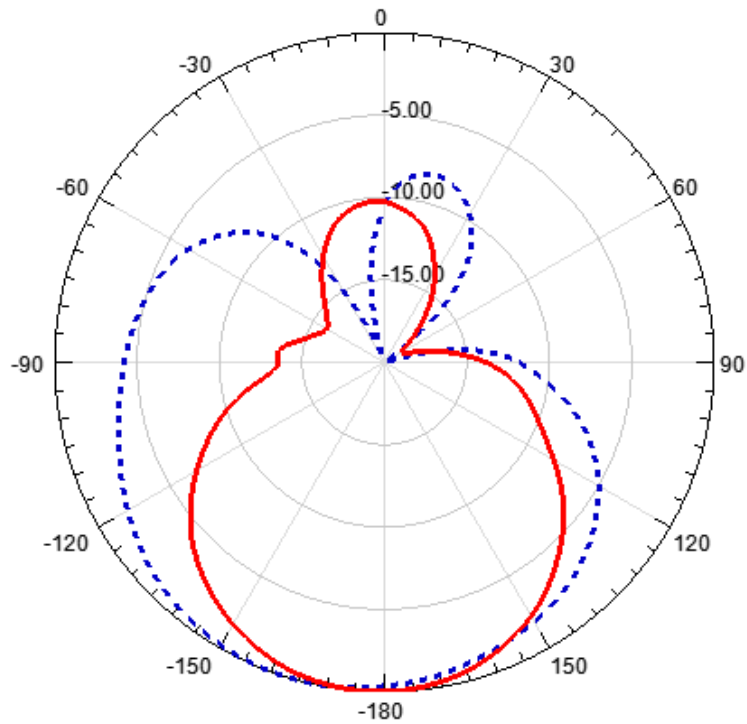
Figure 81: Radiation patterns of the dog-bone slot antenna.

CHAPTER VI: Future Work

Prior to application of conductive textile technology in various fields, further research must still be conducted. Combat wound detection systems must be reliable, lightweight, and durable to survive in the harsh environments in which they are active and necessary. Steps must be taken to meet these various system requirements. This chapter offers suggestions for system development utilizing the technology presented in this thesis with the goal of meeting these requirements.

Distributed Sensor Development

As shown from the development of the distributed textile sensor presented in Chapter IV, the current system has some limitations. For this system to be easily applicable to the uniforms of deployed soldiers, the cables leading to the resistance probing points must be eliminated. Additionally, the sensing electronics must be reduced to an acceptable size, with power concentrations being a primary concern. Soldiers cannot be expected to carry additional large batteries to power this system. A potential solution to this challenge is to employ a multilayer textile structure. This structure could be composed of the sensing textile on one layer with textile traces placed on the opposite side. To avoid shorting these layers together, they would be spaced by a lightweight, thin dielectric material. As illustrated with the dog-bone slot antenna presented in Chapter V, conductive vias can be implemented by sewing conductive thread in the desired pattern. These vias can be placed at the probing locations to offer electrical connection between the two conductive textile layers.

Routing these textile traces to the edge of the fabric and then utilizing a cable bundle to connect to the sensing electronics will provide a good alternative to the problem presented.

In addition to being simplified through the reduction of cables, the system must also ensure accuracy. This can, in theory, be achieved rather easily. Currently, the system utilizes the "one-to-many" technique for resistive sensing. That is to say that one point is held constant while the resistance between that point and each other point is measured. To achieve redundancy in data collection and therefore confirmation as to the location of penetration, a "many-to-many" technique can be implemented. This system, created by multiplexing the multiplexers, is a simple hardware alternative for offering redundancy.

A second idea is to utilize the "many-to-many" sensing technique in a more consolidated manner. Here, each resistive measurement would only be taken between a stationary point and its closest neighbors. Minute changes in resistance should be more obvious with this technique. In the current system, the resistance change directly next to penetration and the resistance change some distance away from the cut are much different. It is the goal of this "magnifying glass" technique to expound on this phenomenon to produce a closer look as to the location of penetration within the system. Depending on the application, this technique may be too complex. While the hardware is no more difficult to implement than the "many-to-many" technique, the data processing could be a challenge to accurately and effectively portray the system as small cells of resistive changes.

Multiple textile sensing layers spaced apart by some distance can also be of potential use in this application. Here, information can be gleaned as to the trajectory of penetration as well as to the existence of penetration. This knowledge can be coupled with effective signal processing to determine the approximate location of impact with the body by calculating the angle of arrival of the bullet partnered with the location of penetration on the sensing system. This idea is illustrated in Figure 82. By placing one layer outside the protective vest shown in Figure 82 and one layer inside, it is even possible to determine if a soldier is encountering fire that is not penetrating the protective ballistic layer. The key to this application is the easy and inexpensive replacement of the distributed sensors if they are compromised.
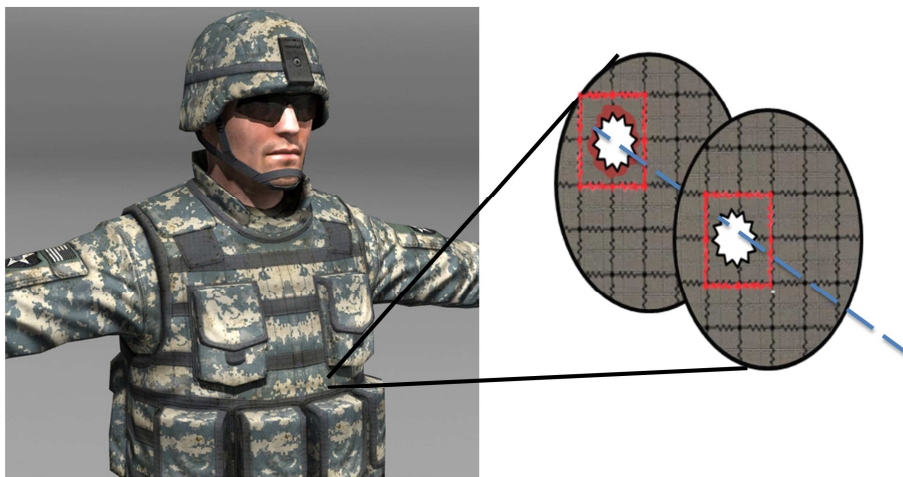
Figure 82: Multilayer distributed fabric sensor.

Antenna and Signal Transmission Development

In addition to the distributed sensor system development discussed above, further research must be conducted for antenna and signal transmission. Primarily, questions must be answered regarding the necessary range as well as the antenna gain requirements and size restraints. Additionally, it must be decided whether to continue implementation of the multilayer textile antenna or to explore better opportunities for antenna development. Depending on the application, it may be necessary to implement antenna arrays to provide better gain for extending range or to reduce the size of the antenna while still maintaining specific gain requirements or radiation patterns.

While the gain and range requirements are application specific, it is possible to initially decide whether to continue the implementation of multilayer textile antennas or to move towards developing technology that could promote the use of only one textile layer. The difficulty in producing multilayer antennas is seen through fabrication. While laser cutting capabilities can accurately define the conductive layers, it is difficult to place the layers in their exact position during the iron-on process. A potential work-around to this challenge is to print metal layers on the textiles, similar to the idea of printed circuit boards. Applied Nanotech, a small company in Texas, has the ability to print on a variety of surfaces through both a screen printing process and an inkjet printing process. Each of these options creates tradeoffs with the current multilayer approach. Chief among these is the ability to ensure accurate alignment between top and bottom layers. Given a fiducial reference point, it is theoretically possible to ensure

alignment between the top and bottom layers. A comparison between potential antenna fabrication methods can be found in Table 4.

The benefits of utilizing the printing technique come in the form of enhanced conductivity. Since the conductor thickness is much smaller than that of the conductive textile, a much lower resistivity can be achieved. According to the printing company, the textile remains very flexible after printing. A primary concern with this is how far the material can flex without severing electrical connections along printed layers. The obvious tradeoff to utilizing the printing methods is to sacrifice the maximum size capability for increased conductivity. Depending on the application, this sacrifice may be acceptable. As this technology becomes more widespread, the size limitations associated with the printing process will likely be addressed. If larger sizes could be obtained, it may become a valid option for larger system development.

In addition to antenna development, the use of conductive vias as illustrated by the dog-bone slot antenna fabrication brings rise to the capability of implementing substrate integrated waveguide (SIW) designs entirely from textile materials. The challenge with these designs is again in the fabrication process. While the metal layers

Table 4: Comparison of potential conductive layer candidates

Method	Conductor Thickness (µm)	Resistivity (µΩ-cm)	Size Constraints (in.)
Conductive Textile	100	500	24 × 12
Inkjet Printing	1	5	8 × 8
Screen Printing	4	50	15 × 15

are easy to adhere to the dielectric material with only one layer having intricate designs, the challenge comes in sewing the vias. Here, the difficulty exists in sewing a straight line so that the waveguide maintains the same effective width throughout. Various SIW designs have been simulated, including a T-junction power divider, a GCPW-SIW transition, and a Y-junction power divider. Simulation results suggest that it is possible to create SIW technology using conductive textiles. The fabrication and measurement of this technology is left for future work. The base of knowledge produced throughout this thesis provides a basis for this work.

System Development

Figure 83 illustrates a system concept for combat wound detection which allows the textile antennas to communicate in a small cell with a centrally located communications soldier. From here, the sensor data transmitted by each soldier in the
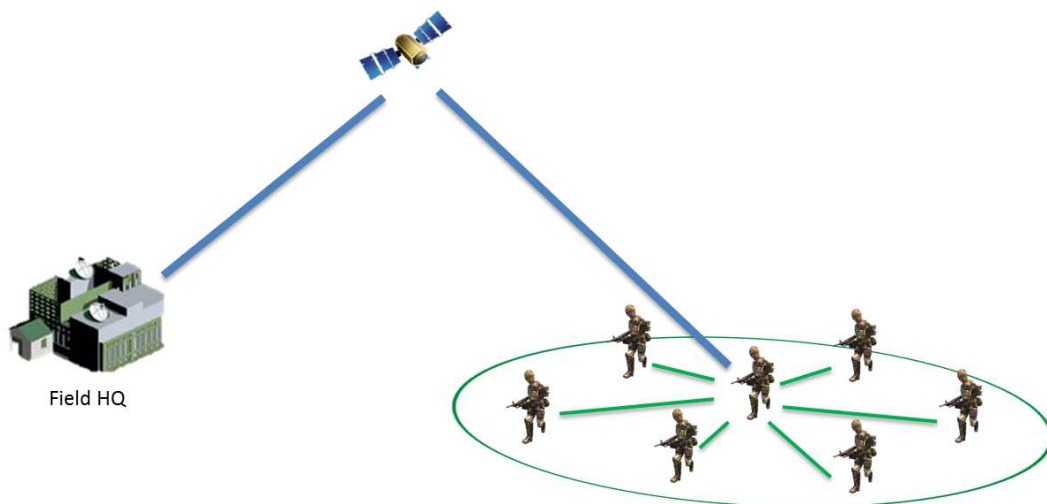
Figure 83: Combat wound detection system concept.

group can be compiled and transmitted over longer distances to headquarters. It is expected that this information will allow medical staff to be better prepared to treat combat wounds. Additionally, this technology can be implemented in human movement tracking scenarios, as presented on a small scale by the indoor localization experiment with the textile monopole antenna. With proper equipment, the range of this system can be ideally expanded to a range between 10 and 100 meters. If this range could be achieved with localization accuracy of about a meter, the technology could be applied to localization in harsh environments. A potential application for this scenario would be the successful localization and tracking of emergency response firefighters as they work their way through a burning building in search of survivors. The base system would allow the crew members outside of harm's way to keep tabs on the safety of each of the firefighter crew members.

System development in each of these cases is not trivial. Each system has its own requirements that make it a challenging task. The emergency response application, for example, requires that accurate tracking be performed from a safe location. This means that the signal must accurately propagate and return through a noisy, unpredictable environment. In the case of combat wound detection, multilayer textile sensing devices must be easily and accurately developed. There is potential that printing techniques as discussed in this chapter could be used to eliminate the need for multiple textile layers. However, this is dependent on the ability to introduce conductive vias after the printing is completed so that the two sides can be electrically connected in a desired location.

CHAPTER VII: Conclusion

The research documented in this thesis has successfully demonstrated the capability of conductive textiles in both remote sensing and microwave applications. Novel approaches were taken to improve the current level of knowledge in each of these applications. The distributed textile sensor has the advantage of being a low-cost option for many applications including combat wound detection. The discrete resistive grid measurement approach allows the collected data to accurately predict the presence of cuts and penetrations within the fabric. This prediction is achieved through visual analysis of the results gathered. The visualization technique also provides estimation as to the location of penetration. Location information, in conjunction with the incorporation of sensors to measure vital signs, can be utilized to predict the severity of penetrations within the fabric. Simulation has shown that the size of the cut is directly correlated to the density of the probing locations. From probing 32 locations in experiments, a limitation on the minimum detectable cut size was evident. However, when cuts exceeded this size, the location of the cut as well as the cut's approximate length was evident through visual analysis.

The research also suggested means for improving accuracy through periodic calibration as a result of the drift in textile point-to-point resistance over time. The frequency of calibration is described as application specific as a result of allowing resistive variation in sensing. This proof-of-concept remote sensing system compares well with the simulation profiles created in MATLAB to model the variation in resistance of a discrete resistive grid. These simulation models also permit the introduction of cuts

and tears within the discrete grid. A comparison between simulation and experimental results also suggests good correlation.

In addition to the remote sensing capabilities for the detection of penetration and cuts in conductive textiles as demonstrated in this thesis, this research also built upon the use of conductive textiles for flexible antenna design as a component of communication systems. The antennas designed by use of these textiles were accurately defined with a laser cutting system, an approach not yet presented by other researchers. Generally, these antennas have been fabricated manually by use of a sharp blade followed by an iron-on process to adhere the textile layers together. This research, instead, precedes the iron-on adhesion process with an accurate conductive layer definition using an Epilog Zing 24 laser cutter system. The development of the dog-bone slot antenna presented in Chapter V promotes the investigation of substrate integrated waveguide technology in textiles. With the improved manner for via implementation, as opposed to inserting metal eyelets in the fabric, substrate integrated waveguide technology can accurately be developed.

Significant potential exists for the further development of these antennas and communication system components through metal printing processes as well as through application specific designs such as ultra-wideband tracking systems. Chapter VI indicates numerous opportunities for future research tailored to system development for deployed soldier localization and combat wound detection. In addition to fabrication advancements, these opportunities will drive the future development of this technology. In addition to antenna development, textiles can be used as a medium for

communication system component integration. The potential for this can also be explored.

Some technical challenges were faced during the completion of this research. The successful navigation of these challenges allowed for novel developments to be made in the areas previously discussed in this chapter. Some of the difficulties encountered included the ability to sense large textile samples and the visualization of the resistance grid results. The implementation of electrodes to sample the discrete resistance locations allowed for large, configurable textile samples to be accurately sensed. The analysis and inclusion of the second order discrete Laplacian mask provided an effective means for visualization of the resistance grid results. Without this mask, it proved difficult to accurately sense the location of resistance perturbations and potential textile penetrations. Challenges were also faced in the development of textile antennas. Finding an effective means for fabric layer adhesion was a challenge. Initially, a spray-on adhesive was used which did not allow for ample time to accurately align the top and bottom textile layers. As soon as the layers made contact with one another, the position of the layer was final. Using the iron-on fabric adhesive proved to be a much more effective technique to accurately align the top and bottom textile layers before they were adhered to the dielectric material. The development of large microstrip feeding networks also proved difficult initially. The thin, complex fabric microstrip lines would easily tear during the adhesion process or from handling. To solve this issue, support bars were included in the design to provide extra durability during layer placement. These bars could be easily cut apart after the layers were placed on the dielectric fabric.

Solving the various technical challenges encountered during this research led to the completion of promising research for sensing and localization systems and in particular for combat wound detection. Investigation as to the uses of conductive textiles in combat wound detection systems provided a number of promising results and conclusions. The inexpensive nature and effective sensing ability of conductive textiles make them an attractive option for incorporation into existing protective vests for military personnel. While advances in metallic printing may prove to be a future solution for textile sensor and antenna development, conductive textiles are currently at the forefront. The accuracy and effectiveness of metallic printing must still be investigated before it can be employed in combat wound detection systems. Table 5 summarizes the contributions of this research.

Table 5: List of Contributions with a Brief Description

Contribution	Description
1. **Bullet, cuts, impact and penetration through wounded soldier body localization**	*Used MATLAB to model conductive textiles as a large resistor network. Then models were used to predict the result of penetrations of a bullet and cuts within the textile.*
2. **Developed and validated a novel distributed Resistance Sensing Network**	*A large area sensing network based on implementing a distributed resistance sensing network was developed; verified and validated using MATLAB simulation models with LabView Data Acquisition Program*

Table 5: Continued.

Contribution	Description
3. **Developed a very adaptive reconfigurable, Large-Scale Penetration Detection Network**	*Implemented a unique adaptive sensing solution using electrodes to provide reconfigurable resistance sensing capabilities that would allow zooming capabilities in certain region.*
4. **Enhanced the sensing accuracy using Redundant Sensing – "Magnification" and differential resistance grid state change**	*Developed models to magnify the effect of localized changes in resistance by measuring resistance between adjacent nodes for the entire resistance grid thus avoiding aging effects and false detection.*
5. **Developed relatively low cost fabrication technique combining laser-definition with iron-on process to realize metalized textile patterns**	*Utilized Epilog Zing 24 Laser Cutting System to accurately define textile antennas instead of manually defining with a sharp knife. Simple iron-on methods were implemented for precise metalized patterns definition and allocation on the fabrics.*
6. **Developed a practical method for implementing conductive vias in textiles**	*Showed the potential for conductive via implementation using a sewing machine and conductive thread. The sewing machine allows for variation in stitch type, stitch width and stitch length to create various types of conductive vias.*
7. **Proposed a simple, low profile, low cost, accurate Integrated Textile Systems for combat wound detection**	*Provided a basis for integrated systems using textiles by discussing the development of sensing technology coupled with communication system development.*

REFERENCES

1. Nathan C. Rowe, et al., "Radio-Frequency (RF) Devices for Safeguards: Where We Are and Where We Need to Go," Proc. Of the Institute of Nuclear Materials Management, 2011.

2. Nathan C. Rowe, et al, "Activated Ultra-Wideband (UWB) Tagging for Use in Secure Environments," Proc. Of the Institute of Nuclear Materials Management, 2010.

3. B. J. Stinson, et al, "Application for Automated Inventory Management of Weapons and Related Assets," Proc. Of the Institute of Nuclear Materials Management, 2008.

4. Chris A. Pickett, et al, "Continuous Automated Vault Inventory System (CAVIS)," Proc. Of the Institute of Nuclear Materials Management, pp. 256-262, 1994.

5. Upper Arm Blood Pressure Cuff EW3106W, Panasonic Inc., (2012, May 15), [Online], Available: http://www.us.panasonic.com/.

6. "Avant® 4000 wireless tabletop pulse oximeter," Nonin Medical, Inc., Plymouth, MN, (2012, May 13), [Online], Available: http://www.nonin.com/.

7. Zephyr Inc., (2012, May 13), [Online], Available: http://www.zephyr-technology.com/.

8. EPOC Neuroheadset, Emotiv, (2012, May 16), [Online], Available: http://www.emotiv.com/.

9. LifeSync Wireless ECG System, LifeSync Corp., (2012, May 15), [Online], Available: http://www.lifesynccorp.com/products/wireless-system.html.

10. 1100/1101 Wireless Probes, Neoprobe, (2012, May 13), [Online], Available: http://www.neoprobe.com/Bluetooth-Wireless-Probe.html

11. Body Media FIT On-Body Monitoring System, Body Media Inc., Pittsburgh, PA, (2012, May 15), [Online], Available: http://www.bodymedia.com.

12. Basis Band, Basis Science Inc., San Francisco, CA, (2012, May 15), [Online], Available: http://en.mybasis.com/.

13. C. Zysset, K. Cherenack, T. Kinkeldei and G. Tröster, "Weaving Integrated Circuits into Textiles," 2010 International Symposium on Wearable Computers, pp. 1-8, October 2010.

14. "Textile Metallization," Swicofil, (2013, January 15), Available: http://www.swicofil.com/textile_metallization.html.

15. B. K. Little, Y. Li, V. Cammarata, R. Broughton and G. Mills, "Metallization of Kevlar Fibers with Gold," ACS Applied Materials and Interfaces, vol. 3, pp. 1965-1973, 2011.

16. M. Chedid, I. Belov and P. Leisner, "Experimental analysis and modeling of textile transmission line for wearable applications," International Journal of Clothing Science and Technology, vol. 19, no. 1, pp. 59-71, 2007.

17. "Conductive Fabrics," How to Get What You Want, (2013, March 20), [Online], Available: http://www.kobakant.at/DIY/?p=376.

18. F. Carpi and D. De Rossi, "Electroactive Polymer-Based Devices for e-Textiles in Biomedicine," IEEE Transactions on Information Technology in Biomedicine, vol. 9, no. 3, pp. 295-318, September 2005.

19. S. Park and S. Jayaraman, "Enhancing the quality of life through wearable technology," IEEE Transactions on Eng. Med. Biol., vol. 22, no. 3, pp. 41-48, March 2003.

20. P. F. Binkley, "Predicting the potential of wearable technology," IEEE Transactions on End. Med. Biol., vol. 22, no. 3, pp.23-27, March 2003

21. J. M. Winters, Y. Wang and J. M. Winters, "Wearable sensors and telerehabilitation," IEEE Transactions on End. Med. Biol., vol. 22, no. 3, pp. 56-65, March 2003.

22. D. De Rossi, F. Carpi, F. Lorussi, A. Mazzoldi, E. P. Scilingo and A. Tognetti, "Electroactive fabrics for distributed, conformable and interactive systems," IEEE Sensors Conference, October 2002.

23. R. Paradiso, "Wearable health care system for vital signs monitoring," Proceedings of the 4th Annual IEEE Conference on Information Technology Applications in Biomedicine, pp. 283-286, April 2003.

24. R. Paradiso, A. Gemignani, E. P. Scilingo and D. De Rossi, "Knitted bio-clothes for cardiopulmonary monitoring," Proceedings in the 25th Annual International Conference IEEE Eng. Med. Biol. Soc., pp. 3720-3723, September 2003.

25. K. Kifayat, P. Fergus, S. Cooper and M. Merabti, "Body Area Networks for Movement Analysis in Physiotherapy Treatments," 2010 IEEE 24th International Conference on Advanced Information Networking and Applications Workshops, pp. 866-872, April 2010.

26. N. Kiss, G. Patai, P. Hanák, T. Lipic, P. Skoda, L. Gjenero, A. Dubravic and I. Michieli, "Vital fitness and health telemonitoring of elderly people," 2011 Proceedings of the 34th International Convention MIPRO, pp. 279-284, May 2011.

27. A. Tognetti, N. Carbonaro, G. Zupone and D. De Rossi, "Characterization of a Novel Data Glove Based on Textile Integrated Sensors," Proceedings of the 28th IEEE EMBS Annual International Conference, pp. 2510-2513, August 2006.

28. R. Wijesiriwardana, K. Mitcham, W. Hurley and T. Dias, "Capacitive Fiber-Meshed Transducers for Touch and Proximity-Sensing Applications," IEEE Sensors Journal, vol. 5, no. 5, pp. 989-994, October 2005.

29. E. Wade and H. H. Asada, "Cable-Free Wearable Sensor System Using a DC Powerline Body Network in a Conductive Fabric Vest," Proceedings of the 26th Annual International Conference of the IEEE EMBS, pp. 5376-5379, September 2004.

30. D. De Rossi, F. Carpi, F. Lorussi, A. Mazzoldi, R. Paradiso, E. P. Scilingo and A. Tognetti, "Electroactive Fabrics and Wearable Biomonitoring Devices," AUTEX Research Journal, vol. 3, no. 4, pp. 180-185, December 2003.

31. R. DeVaul, M. Sung, J. Gips and A. Pentland, "MIThril 2003: Applications and Architecture", Available: http://www.media.mit.edu/wearables/papers.html

32. "Need for an Intelligent Wearable Motherboard," Georgia Tech Wearable Motherboard: The Intelligent Garment for the 21st Century. Available: http://www.gtwm.gatech.edu/

33. "LifeShirt". Vivonoetics. 2012. Available:

    http://vivonoetics.com/products/sensors/lifeshirt/

34. D. L. Paul, M. Klemm, C. J. Railton and J. P. McGeehan, "Textile Broadband E-Patch Antenna at ISM Band," IET Seminar on Antennas and Propagation for Body-Centric Wireless Communications, pp.38-43, April 2007.

35. C. Hertleer, H. Rogier, L. Vallozzi and L. Van Langenhove, "A Textile Antenna for Off-Body Communication Integrated Into Protective Clothing for Firefighters," IEEE Transactions on Antennas and Propagation, vol. 57, no. 4, pp. 919-925, April 2009.

36. H. Sugiyama, H. Goto, H. Iwasaki, "Wearable Dual Band Antenna Made of Fabric Cloth for BAN Use," Asia Pacific Microwave Conference 2012, December 2012.

37. A. Galehdar and D. V. Thiel, "Flexible, Light-Weight Antenna at 2.4GHz for Athlete Clothing," IEEE Antennas and Propagation Society International Symposium, pp. 4160-4163, June 2007.

38. H. Shimasaki and M. Komeya, "Studies on a Cavity-Backed Slot Antenna Made of a Conductive Textile Bent along a Spherical Surface," Technical Committee on Microwave Engineering, pp. 115-118, October 2012.

39. H. Shimasaki and M. Tanaka, "Measurement of the roundly bending characteristics of a cavity-backed slot antenna for microwave energy transmission," IEICE Trans. Communications, vol.J82-B, no. 10, pp. 1905-1914, October 1999.

40. S. E. Morris, Y. Bayram, L. Zhang, Z. Wang, M. Shtein and J. L. Volakis, "High-Strength, Metalized Fibers for Conformal Load Bearing Antenna Applications,"

IEEE Transactions on Antennas and Propagation, vol. 59, no. 9, pp. 3458-3462, September 2011.

41. Z. Wang, L. Zhang, Y. Bayram, and J. L. Volakis, "Embroidered E-Fiber-Polymer Composites for Conformal and Load Bearing Antennas," IEEE Antennas and Propagation Society International Symposium, pp. 1-4, July 2010.

42. M. Klemm and G. Troester, "Textile UWB Antennas for Wireless Body Area Networks," IEEE Transactions on Antennas and Propagation," vol. 54, no. 11, pp. 3192-3197, November 2006.

43. H. Giddens, D. L. Paul, G. S. Hilton and J. P. McGeehan, "Influence of Body Proximity on the Efficiency of a Wearable Textile Patch Antenna," 6th European Conference on Antennas and Propagation, pp. 1353-1357, March 2012.

44. S. Zhu and R. Langley, "Dual-band wearable antennas over EBG substrate," IEEE Transactions on Antennas as Propagation, vol. 57, no. 4, pp. 926-935, April 2009.

45. M. Klemm and G. Troster, "Textile UWB antenna for on-body communications," 1st European Conference on Antennas and Propagation, pp. 1-4, November 2006.

46. W. Thompson, R. Cepeda, G. S. Hilton, M. A. Beach and S. Armour, "An Improved Antenna Mounting for Ultra-Wideband On-Body Communications and Channel Characterization," IEEE Transactions on Microwave Theory and Techniques, vol. 59, no. 4, pp. 1102-1108, April 2011.

47. R. Moro, S. Agneessens, H. Rogier and M. Bozzi, "Wearable textile antenna in substrate integrated waveguide technology," Electronics Letters, vol. 48, no. 16, pp. 985-987, August 2012.

48. Q. L. Guo, F. H. Zhi and X. D. Lin, "Planar slot antenna backed by substrate integrated waveguide cavity," IEEE Antennas and Wireless Propagation Letters, vol. 7, pp. 236-239, 2008.

49. R. Salvado, C. Loss, R. Gonçalves and P. Pinho, "Textile Materials for the Design of Wearable Antennas: A Survey," Sensors Journal, no.12, pp.15841-15857, 2012.

50. Y. Ouyang and W. J. Chappell, "High Frequency Properties of Electro-Textiles for Wearable Antenna Applications," IEEE Transactions on Antennas and Propagation, vol. 56, no. 2, February 2008.

51. S. Sankaralingam and B. Gupta, "Determination of Dielectric Constant of Fabric Material and Their Use as Substrates for Design and Development of Antennas for Wearable Applications," IEEE Transactions on Instrumentation and Measurement, vol. 59, no. 12, December 2010.

52. F. Y. Wu, "Theory of Resistor Networks: The Two-Point Resistance," Journal of Physics, vol. A, no. 37, pp. 6653-6673, 2004.

53. R. Grothmann, "Resistance of a Grid," [Online], Available: http://euler.rene-grothmann.de/Programs/Examples/Resistance%20of%20a%20Grid.html.

54. J. Cserti, G. David and P. Attila, "perturbation of Infinite Networks of Identical Resistors," American Journal of Physics, vol. 70, no. 2, pp. 153, 2002.

55. J. H. Asad, R. S. Hijjawi, A. Sakaj and J. M. Khaliefah, "Remarks on Perturbation of Infinite Networks of Identical Resistors," International Journal of Theoretical Physics, vol. 44, no. 4, pp. 471-483, 2005.

56. D. Atkinson and F. J. van Steenwijk, "Infinite Resistive Lattices," American Journal of Physics, vol. 67, no. 6, pp. 486, 1999.

57. G. Venezian, "On the Resistance between Two Points on a Grid," American Journal of Physics, vol. 62, no. 11, pp. 1000, 1994.

58. A. Mitra, "Finite Difference Method for the Solution of Laplace Equation," Department of Aerospace Engineering, Iowa State University, Lecture Notes.

59. Y. F. Liu, K. L. Lay, Q. Xue and C. H. Chan, "Experimental Studies of Printed Wide-Slot Antenna for Wide-Band Applications," IEEE Antennas and Wireless Propagation Letters, vol. 3, pp. 273-275, 2004.

60. C. Zhang and A. E. Fathy, "Development of an Ultra-wideband Elliptical Disc Planar Monopole Antenna with Improved Omni-Directional Performance Using a Modified Ground," *2006 IEEE Antennas and Propagation Society Intl. Symp.*, pp. 1689-1692, July 2006.

61. M. J. Kuhn, M. R. Mahfouz, C. Zhang, B. C. Merkl and A. E. Fathy, "A System-Level Simulation Framework for UWB Localization," *IEEE Trans. on Microwave Theory and Techniques*, pp. 3527-3537, December 2010.

APPENDIX

Appendix A: Conductive Textiles on the Market

Table 6: Conductive Textiles Available from LessEMF.com

LessEMF.com						
	Product	Fabric Type	Metallic Coating	Thickness (mm)	Shielding Effectiveness	Resistivity (Ω/sq.)
	Radioscreen	Polyester	Cu-Ni plated	0.09	>50dB 10MHz-3GHz	<0.1
	Argenmesh	Nylon	Ag threads	-	50dB 100MHz-3GHz	<0.1
	Soft&Safe Shielding Fabric	Bamboo	Ag threads	-	>50dB 10MHz-3GHz	<1
	Staticot	Polyester /Cotton	Stainless Steel threads	-	40dB up to 10GHz	1000
	VeilShield	Polyester	ZnNiCu plated	0.018	>40dB	0.1
	RipStop Silver Fabric	Nylon	Ag plated	0.0508	>50dB 20MHz-4GHz	<0.25

Table 6: Continued.

	Product	Fabric Type	Metallic Coating	Thickness (mm)	Shielding Effectiveness	Resistivity (Ω/sq.)
	Cu Polyester Taffeta Fabric	Taffeta	Cu plated	0.08	>75dB 10MHz-3GHz	0.05
	Ni/Cu Ripstop Fabric	Polyester	Ni-Cu plated	0.08	>75dB 10MHz-3GHz	<0.03
	Microwave Absorbing Sheet	Carbon	-	0.445	>25dB 1GHz-10GHz	~3
	SaniSilver	Cotton	Ag	-	>50dB 30MHz-1.5GHz	<1
	ShieldIt Super	Polyester	Ni-Cu plated	0.1143	>60dB 10MHz-3+GHz	1
	Stretch Conductive Fabric	Nylon	Ag	0.4	>30dB 1GHz-10GHz	<0.5

Table 7: Conductive Textiles Available from Marktek, Inc.

	Product	Fabric Type	Metallic Coating	Thickness (mm)	Shielding Effectiveness	Resistivity (Ω/sq.)
				Marktek, Inc.		
	ALFS204	Foil/polyester	Al	0.58	>90dB at 1GHz	<0.05
	CSR68	Nylon	Cu-Ag	0.0762	90dB at 1GHz	0.02
	NCPB15	Non-woven	Ni-Cu	0.254	80dB at 1GHz	<0.09
	NCPT2	Taffeta/polyester	Ni-Cu	0.1524	80dB at 1GHz	<0.09
	NCSM65	Nylon	Ni-Cu	0.1	80dB at 1GHz	0.02
	NCS72R-FR	Nylon	Ni-Cu-Ag	0.0762	85dB at 1GHz	<0.02
	SBAL317	Nylon	Ag	0.23	>40dB at 1GHz	<3
	TCPB15	Nylon nonwoven	Sn-Cu	0.254	85dB at 1GHz	<0.05

Table 8: Conductive Textiles Available from Metal Textiles Corporation

	Product	Fabric Type	Metallic Coating	Thickness (mm)	Shielding Effectiveness	Resistivity (Ω/sq.)
				Metal Textiles Corporation		
	Taffeta	Polyester	Cu	0.11	68dB 30MHz-1GHz	0.05-0.08
	Taffeta	Polyester	Ni	0.11	68dB 30MHz-1GHz	0.05-0.08
	Taffeta	Polyester	Cu-Ni	0.12	68dB 30MHz-1GHz	0.05-0.08
	Ripstop	Polyester	Cu	0.12	68dB 30MHz-1GHz	0.05-0.08
	Ripstop	Polyester	Ni	0.12	68dB 30MHz-1GHz	0.05-0.08
	Ripstop	Polyester	Cu-Ni	0.12	68dB 30MHz-1GHz	0.05-0.08
	Non-woven	Polyester	Cu-Ni	0.10	60dB 30MHz-1GHz	0.06-0.10
	Mesh	Polyester	Cu-Ni	0.09	48dB 30MHz-1GHz	0.15-0.20

Table 9: Conductive Textiles Available from Swift Textile Metalizing, LLC.

	Product	Fabric Type	Metallic Coating	Thickness (mm)	Shielding Effectiveness	Resistivity (Ω/sq.)
	Continuous Loop	Nylon	Ag	0.86	50-55dB at 1GHz	<1.5
	Knit 48x21	Nylon	Ag	0.18	-	<1
	Tricot Knit 55x40-2	Nylon	Ag	0.23	50-55dB at 1GHz	<0.5
	Knit 55x40	Nylon	Ag	0.18	50-55dB at 1GHz	<1
	Knit 13x26	Nylon	Ag	0.15	-	<5
	Point Bonded 10	Non-woven	Ni-Ag	0.23	60dB at 1GHz	<1
	Point Bonded 20	Non-woven	Ni-Ag	0.38	75-80dB at 1GHz	<0.1

Table 9: Continued.

	Product	Fabric Type	Metallic Coating	Thickness (mm)	Shielding Effectiveness	Resistivity (Ω/sq.)
	Ripstop	Nylon	Ni-Ag	0.10	70-75dB	<0.1
	Ripstop	Nylon	3Ni-Ag	0.10	-	<0.05
	Ripstop	Nylon	Ag	0.10	65dB at 1GHz	<1
	Heavy Ripstop	Nylon	Ag	0.18	40dB at 1GHz	<1
	Taffeta	Nylon	Ni-Ag	0.13	70-80dB at 1GHz	<0.1
	Spandex	Polyester	Ag	0.57	-	<1.5

Appendix B: Conductive Textile Simulation Model

MATLAB Code

TopLevelResistanceMatrix.m

```matlab
%%%%%%%%%%%%%%%%%%%%%%%%%%%%%%%%%%%%%%%%%%%%%%%%%%%%%%%%%%%%%%%%%%%%%%
%Simulate Resistance Matrix Model of Conductive Fabric
%
% This is the top level of the resistance matrix simulation model.
% Using this model, you can choose the type of cut, size of
% resistance matrix, and whether to include measurement results.
%
%The function inputs are as defined:
%   x => number of side data points in the x dimension of
%       grid
%   y => number of side data points in the y dimension of
%       grid
%   cut => either a sheet (void), vertical, diagonal or point
%       cut.
%   meas => choice to include measurement data to plot
%%%%%%%%%%%%%%%%%%%%%%%%%%%%%%%%%%%%%%%%%%%%%%%%%%%%%%%%%%%%%%%%%%%%
clear all; close all; clc;

% Select the resistance grid size.
x = 16;
y = 32;

% Choose cut type, if any.
%   None -> 'void'              Point -> 'point'
%   Vertical -> 'vertical'      Diagonal -> 'diagonal'
cut = 'vertical';

% Are you validating with measurements?
%   Yes -> '1'      No -> '0'
meas = '0';

% Create Simulated Resistance Matrix
[R, V, Vdrop] = Simulate_Resistance_Matrix (x, y, cut);
R_error = R; % Hold value for error comparison.
R_norm = R./max(max(R)); % Normalize matrix to maximum value.

R_lap = del2(R_norm); % Perform 2D Discrete Laplacian.

% Create Measured Resistance Matrix
if meas == '1'
```

```matlab
    Rmeas =
Read_Labview_Data(64,'C:\Users\s49\Documents\MATLAB\ResistanceMatrixModel\Mod
ifiedScripts\LabViewData\64PortData_','.lvm',11);
    Rmeas_norm = Rmeas./max(max(Rmeas));

    Rmeas_lap = del2(Rmeas_norm);
end

figure;
surf(R_norm);
title(['Simulated Sheet', char(10), 'Cut: ', cut],'FontSize',18);
xlabel('X Grid Location','FontSize',12);
ylabel('Y Grid Location','FontSize',12);
axis([1 size(R,2)  1 size(R,1)]); axis ij;
colorbar; colormap jet;

figure;
surf(abs(R_lap));
title(['Simulated Sheet Laplacian', char(10), 'Cut: ', cut],'FontSize',18);
xlabel('X Grid Location','FontSize',12);
ylabel('Y Grid Location','FontSize',12);
axis([1 size(R,2)  1 size(R,1)]); axis ij;
colorbar; colormap jet;

if meas == '1'
figure;
surf(Rmeas_norm);
title(['Simulated Sheet', char(10), 'Cut: ', cut],'FontSize',18);
xlabel('X Grid Location','FontSize',12);
ylabel('Y Grid Location','FontSize',12);
axis([1 size(Rmeas,1)  1 size(Rmeas,2)]); axis ij;
colorbar; colormap jet;

figure;
surf(abs(Rmeas_lap));
title(['Simulated Sheet Laplacian', char(10), 'Cut: ', cut],'FontSize',18);
xlabel('X Grid Location','FontSize',12);
ylabel('Y Grid Location','FontSize',12);
axis([1 size(Rmeas,1)  1 size(Rmeas,2)]); axis ij;
colorbar; colormap jet;
end
```

Simulated_Resistance_Matrix.m

```matlab
%%%%%%%%%%%%%%%%%%%%%%%%%%%%%%%%%%%%%%%%%%%%%%%%%%%%%%%%%%%%%%%%%%%
%Simulate Resistance Matrix Model of Conductive Fabric
%
%This code implements the resistive matrix technique to
%simulate a square sheet of fabric.  The user can define a cut
%type to see the impact in resistance tomography that results.
%
%The function inputs are as defined:
%   x => number of side data points in the x dimension of
%        grid
%   y => number of side data points in the y dimension of
%        grid
%   cut => either a sheet (void), vertical, diagonal or point
%        cut.
%%%%%%%%%%%%%%%%%%%%%%%%%%%%%%%%%%%%%%%%%%%%%%%%%%%%%%%%%%%%%%%%%%%
function [R,V,Vdrop] = Simulate_Resistance_Matrix(x,y,Ctype)
n = x*y;

scale = 1;

% Set edge matrices

[topedge,leftedge,rightedge,bottomedge] = edgeMatrices(n,y);

% Calls function to make incidence matrix

[A] = makeIncidence(n,y,x,topedge,leftedge,rightedge,bottomedge);

% Select node connections to remove
if strcmp(Ctype,'vertical') == 1
   remove_node = [ceil(x/2)+1:x:floor(x/2)*x]; %vertical cut
elseif strcmp(Ctype,'horizontal') == 1
   remove_node = [floor(x/2)*x+1:floor(x/2)*x+floor(x/2)+1];%horizontal cut
elseif strcmp(Ctype,'diagonal') == 1
   remove_node = [x:x-1:floor(x/2)*x+floor(x/2)+1]; %diagonal cut
elseif strcmp(Ctype,'point') == 1
   remove_node = [54];
%else Ctype is void
end

% Remove Connections in Incidence Matrix
if strcmp(Ctype,'void') == 0
    for i = 1:length(remove_node)
        if strcmp(Ctype,'vertical') == 1
            %Vertical Cut
            A(remove_node(i),remove_node(i)-1) = 0;
            A(remove_node(i)-1,remove_node(i)) = 0;
        elseif strcmp(Ctype,'horizontal') == 1
            %Horizontal Cut
             A(remove_node(i),remove_node(i)-y) = 0;
```

```matlab
                A(remove_node(i)-y,remove_node(i)) = 0;
        elseif strcmp(Ctype,'diagonal') == 1
            %Diagonal Cut
            if i ==1
                A(remove_node(i),remove_node(i)-1) = 0;
                A(remove_node(i)-1,remove_node(i)) = 0;
            else
                A(remove_node(i),remove_node(i)-1) = 0;
                A(remove_node(i)-1,remove_node(i)) = 0;
                A(remove_node(i),remove_node(i)-y) = 0;
                A(remove_node(i)-y,remove_node(i)) = 0;
            end
        else %Point remove
            A(remove_node(i),remove_node(i)-1) = 0;
            A(remove_node(i)-1,remove_node(i)) = 0;
        end
    end
end
% Build Resistance Matrix
[R,j,V,Vdrop] = buildResistanceVector(A,scale);
V = V;
R = reshape(R,x,y);
R = R'; %correct the orientation of the matrices to match notation
end
```

edgeMatrices.m

```matlab
%%%%%%%%%%%%%%%%%%%%%%%%%%%%%%%%%%%%%%%%%%%%%%%%%%%%%%%%%%%%%%%%%%%%
%Find the Edge Vectors
%
%This code uses the side dimension and number of internal data
%points to assign vectors containing the top, left, right, and bottom
%node positions.
%
%The function inputs are defined as follows:
%   n => total number of internal matrix points
%   x => number of side data points in the x dimension of
%       grid
%
%The function outputs are defined as follows:
%   topedge => vector of top node positions
%   bottomedge => vector of bottom node positions
%   leftedge => vector of left node positions
%   rightedge => vector of right node positions
%%%%%%%%%%%%%%%%%%%%%%%%%%%%%%%%%%%%%%%%%%%%%%%%%%%%%%%%%%%%%%%%%%%%
function [topedge,leftedge,rightedge,bottomedge] = edgeMatrices(n,x)

    topedge = zeros(1,n); leftedge = zeros(1,n);
    rightedge = zeros(1,n); bottomedge = zeros(1,n);

    j = 1;
    for i = 2:1:n/x-1
        topedge(j) = i;
        j = j + 1;
    end
    topedge(:,j:end) = []; j = 1;

    for i = n/x+1:n/x:(x-2)*n/x+1
        leftedge(j) = i;
        j = j + 1;
    end
    leftedge(:,j:end) = []; j = 1;

    for i = 2*n/x:n/x:(x-1)*n/x
        rightedge(j) = i;
        j = j + 1;
    end
    rightedge(:,j:end) = []; j = 1;

    for i = (x-1)*n/x+2:1:n-1
        bottomedge(j) = i;
        j = j + 1;
    end
    bottomedge(:,j:end) = [];

    return
end
```

makeIncidence.m

```matlab
%%%%%%%%%%%%%%%%%%%%%%%%%%%%%%%%%%%%%%%%%%%%%%%%%%%%%%%%%%%%%%%%%
% Creating the Incidence Matrix
%
%This code implements the mathematics and patern recognition
%needed to develop an incidence matrix outlining a grid of
%resistors.
%
%The function inputs are defined as follows:
%   n => total number of internal matrix points
%   x => number of side data points in the x dimension of
%       grid
%   y => number of side data points in the y dimension of
%       grid
%   topedge => vector of top node positions
%   bottomedge => vector of bottom node positions
%   leftedge => vector of left node positions
%   rightedge => vector of right node positions
%
%The function outputs are defined as follows:
%   A => incidence matrix of the grid
%%%%%%%%%%%%%%%%%%%%%%%%%%%%%%%%%%%%%%%%%%%%%%%%%%%%%%%%%%%%%%%%%
function [A] = makeIncidence(n,x,y,topedge,leftedge,rightedge,bottomedge)
    A = zeros(n,n);
    for i = 1:n
        % Corners
        if i == 1
            A(i,2) = 1;
            A(i,n/x+1) = 1;
        elseif i == n/x
            A(i,y-1) = 1;
            A(i,2*n/x) = 1;
        elseif i == (x-1)*n/x + 1
            A(i,(x-1)*n/x + 2) = 1;
            A(i,(x-2)*n/x + 1) = 1;
        elseif i == n
            A(i,(x-1)*n/x) = 1;
            A(i,n-1) = 1;
        % Edges
        elseif intersect(i,topedge)  % Top Edge
            A(i,i-1) = 1;
            A(i,i+1) = 1;
            A(i,i+n/x) = 1;
        elseif intersect(i,leftedge)  % Left Edge
            A(i,i+1) = 1;
            A(i,i-n/x) = 1;
            A(i,i+n/x) = 1;
        elseif intersect(i,rightedge)  % Right Edge
            A(i,i-1) = 1;
            A(i,i-n/x) = 1;
            A(i,i+n/x) = 1;
        elseif intersect(i,bottomedge)  % Bottom Edge
```

```matlab
            A(i,i-1) = 1;
            A(i,i+1) = 1;
            A(i,i-n/x) = 1;
        % Center points
        else
            A(i,i-1) = 1;
            A(i,i+1) = 1;
            A(i,i-n/x) = 1;
            A(i,i+n/x) = 1;
        end
    end
return
end
```

buildResistanceVector.m

```matlab
%%%%%%%%%%%%%%%%%%%%%%%%%%%%%%%%%%%%%%%%%%%%%%%%%%%%%%%%%%%%%%
% Build Resistance Vector
%
% This uses code similar to that supplied by R. Grothmann to
% calculate the point to point resistance matrix by implementing
% the predefined incidence matrix of the grid.
%
%The function inputs are defined as follows:
%   A => the incidence matrix of the network grid
%   scale => scaling factor for the interconnecting resistance
%       value in the grid
%
%The function outputs are defined as follows:
%   R => the resistance vector corresponding to every node
%       point
%   j => number of nodes in the matrix
%   V => the voltage at each node in the grid
%   V => the voltage drop between the origin node and the
%       measurement node.
%%%%%%%%%%%%%%%%%%%%%%%%%%%%%%%%%%%%%%%%%%%%%%%%%%%%%%%%%%%%%
function [R,j,V,Vdrop] = buildResistanceVector(A,scale)
    B = A;
    C = -sum(B);
    n = size(A); n = n(1);
    for i = 1:n
        B(i,i) = C(i);
    end

    B_loop = B;
    R = zeros(1,n);
    I = R;
    Vout = zeros(n,n);
    Voutdrop = Vout;
    nodes = 1:1:n;


    % Builds Resistance Matrix
    port1 = 1; R(1) = 0;
    B_loop(port1,:) = 0; B_loop(port1,port1) = 1;
    Vdrop = zeros(n,1);
    Vdrop(port1) = 1; %1V drop between terminals of Req;
    B = B_loop;

    for j = 1:length(nodes)

        port2 = nodes(j);
        B_loop(port2,:) = 0; B_loop(port2,port2) = 1;
        V = pinv(B_loop)*Vdrop; % Returns least squares solution

        I(j) = sum(A(port1,:)) * V(port1) - dot(A(port1,:),V);
```

```
        I(j) = I(j)/scale;

        R(j) = (V(port1)-V(port2))/I(j);
        Voutdrop(j,1:n) = Vdrop;
        Vout(j,1:n) = V;
        %Need to set B back to original matrix.
        B_loop = B;
    end
    V = Vout;
    Vdrop = Voutdrop;
return
end
```

VITA

Stephen Holland was born in East Ridge, Tennessee, to Thomas and Mary Holland. He has one older brother, Matthew. Stephen attended Spring Creek Elementary in East Ridge and continued to Hunter Middle School and Ooltewah High School in Ooltewah, Tennessee. After graduation in 2008, he moved north to Knoxville, Tennessee, to pursue his Bachelors of Science in Electrical Engineering at the University of Tennessee. During his time as an undergraduate, Stephen was blessed with an opportunity to complete undergraduate research with Dr. Aly Fathy as well as summer internships with Tennessee Valley Authority and Oak Ridge National Laboratory. It is through these experiences that he discovered and honed an interest in microwave engineering and its applications. In May 2012, Stephen received his Bachelors of Science and graduated *summa cum laude*. In pursuit of a Master of Science in Electrical Engineering, Stephen accepted a graduate research assistantship at the University of Tennessee, Knoxville in the Electrical Engineering Department under the guidance of Dr. Aly Fathy. This position allowed Stephen to work with both Dr. Fathy's Microwave and Antenna group and the Safeguards and Security Technology group at the Oak Ridge National Laboratory under the supervision of Dr. Michael Kuhn. Stephen graduated with a Master of Science degree in Electrical Engineering in May 2013.